J. metamorphic Geol., 1998, **16,** 309–343

An internally consistent thermodynamic data set for phases of petrological interest

T. J. B. HOLLAND[1] AND R. POWELL[2]
[1]*Department of Earth Sciences, University of Cambridge, Cambridge CB2 3EQ, UK (email: tjbh@esc.cam.ac.uk)*
[2]*School of Earth Sciences, University of Melbourne, Parkville, Victoria 3052, Australia*

ABSTRACT The thermodynamic properties of 154 mineral end-members, 13 silicate liquid end-members and 22 aqueous fluid species are presented in a revised and updated data set. The use of a temperature-dependent thermal expansion and bulk modulus, and the use of high-pressure equations of state for solids and fluids, allows calculation of mineral–fluid equilibria to 100 kbar pressure or higher. A pressure-dependent Landau model for order–disorder permits extension of disordering transitions to high pressures, and, in particular, allows the alpha–beta quartz transition to be handled more satisfactorily. Several melt end-members have been included to enable calculation of simple phase equilibria and as a first stage in developing melt mixing models in NCKFMASH. The simple aqueous species density model has been extended to enable speciation calculations and mineral solubility determination involving minerals and aqueous species at high temperatures and pressures. The data set has also been improved by incorporation of many new phase equilibrium constraints, calorimetric studies and new measurements of molar volume, thermal expansion and compressibility. This has led to a significant improvement in the level of agreement with the available experimental phase equilibria, and to greater flexibility in calculation of complex mineral equilibria. It is also shown that there is very good agreement between the data set and the most recent available calorimetric data.

Key words: *P–T*; thermodynamic data.

INTRODUCTION

The need for reliable internally consistent thermodynamic data continues to grow, in part because the availability of such data has been the driving force for research into increasingly complex equilibria relating to natural rocks. Such equilibria may be found only via calculation, given the extremely sluggish reaction kinetics which apply to determining directly the greatest majority of such equilibria in the laboratory, especially at lower temperatures, as well as the difficulty of establishing reversals of reactions involving solid solutions. The levels of precision and accuracy required of thermodynamic data in order to be able to forward-model synthetic and natural mineral assemblages mean that the continuing upgrading and expansion of the data set by incorporation of new phase equilibrium constraints, calorimetry and new measurements of molar volume, thermal expansion and compressibility are more than justified.

Earlier work on mineral thermodynamic data sets for rock-forming minerals includes compilations of calorimetrically derived data such as those of Robie *et al.* (1978) and Robie & Hemingway (1995) on the one hand, and tabulations based largely upon analyis of phase equilibrium data, such as those of Helgeson *et al.* (1978), Holland & Powell (1985), Powell & Holland (1985), Berman (1988), Holland & Powell (1990) and, most recently, Gottschalk (1997). Although there is a tendency for convergence in the data sets, unsurprising given that they are based on the same corpus of experimental and calorimetric data, and a steady improvement in the ability of such sets to reproduce the experimental brackets, some major differences will continue to remain because of the different methods and philosophy used in the data analysis in the various works. The present data set has an expanded breadth (more end-members, particularly for forming solid solutions, and inclusion of aqueous and silicate melt species), and provides uncertainties allowing the likely uncertainties on the results of thermodynamic calculations to be estimated. This is a critical issue in that calculations using data sets should always involve uncertainty propagation to help evaluate the results. Because the experimental phase equilibria involve overlapping subsets of compositional space, the derived thermodynamic data are highly correlated, and it is only the inclusion of the correlations which enables the reliable calculation of uncertainties on mineral reactions to be performed.

The thermodynamic data extraction involves using weighted least squares on the different types of data (calorimetric, phase equilibria, natural mineral partitioning) to determine enthalpies of formation of the end-members of the phases. Entropies, volumes, heat capacities, thermal expansions and compressibilities are not derived by regression, but are taken as known in this process. Other parameters intimately involved,

for example regular solution parameters in exchange equilibria, are also taken as known, having been determined separately by pre-processing the data. The entropies of the end-members in the data set are not determined along with the enthalpies by regression because, in most circumstances, they are determined more reliably by estimation techniques (e.g. Holland, 1989) than by fitting to experimental brackets. Where appropriate, such estimated entropies have been adjusted, within their likely uncertainties, to improve agreement with the experiments. The regression involves determination of the enthalpies of 189 end-members using 319 reaction equilibria, 82 direct calorimetric constraints on the end-member enthalpies of formation at 298K, and 30 constraints from enthalpies of reaction and high-temperature calorimetry. Thus the total number of degrees of freedom in the regression is 242 ($319+82+30-189$), and the value for σ_{fit} is 1.14. This represents a considerable improvement over the smaller data set (123 end-member enthalpies and 208 reaction equilibria) in which σ_{fit} was 1.71 (Holland & Powell, 1990).

With regard to the earlier data set of Holland & Powell (1990), hereafter referred to as HP90, there have been many changes to the thermodynamic data themselves and to the equations of state used. These changes require documentation so that their quality may be assessed by those making use of such data in calculations. Otherwise the philosophy and methods are the same as used in HP90, and as modified in Powell & Holland (1993b).

A list of the chemical compositions of the phases and end-members considered in this study may be found in Table 1. The end-members are listed under the headings ortho- & ring silicates (garnets, olivines, etc.), chain silicates (pyroxenes & pyroxenoids, amphiboles, etc.), sheet silicates (micas, chlorites, etc.), framework silicates, oxides & hydroxides, carbonates, elements, gas species, and melt species. Within each subgroup the end-members are arranged alphabetically. Aqueous species are listed separately. Much of the considerable volume of tabulated data needed to represent and summarize the generation of this internally consistent thermodynamic data set is available from the *Journal of Metamorphic Geology's* Web site at http://www.gly.bris.ac.uk/www/jmg.html or equivalent USA or Australian sites. This includes a table of all of the experimentally determined mineral equilibrium brackets used in the least squares analysis, and the calculated fit to them (Table 7b). This is in the form of full computer output from the data extraction program LSQDS.

CHANGES TO METHODOLOGY

The principal differences in methodology from the data set of HP90 are briefly outlined before the details of the new data set are discussed.

Thermal expansion. The temperature dependence of the thermal expansion, α_T, of solid phases drops rapidly above the Debye

Table 1a. The formulae of the end-members of the phases in the internally consistent data set (aqueous and melt end-members are in (b) below).

Group	End-member	Symbol	Formula
Ortho- & ring silicates	akermanite	ak	$Ca_2MgSi_2O_7$
	almandine	alm	$Fe_3Al_2Si_3O_{12}$
	andalusite	and	Al_2SiO_5
	andradite	andr	$Ca_3Fe_2Si_3O_{12}$
	clinohumite	chum	$Mg_9Si_4O_{16}(OH)_2$
	clinozoisite	cz	$Ca_2Al_3Si_3O_{12}(OH)$
	cordierite	crd	$Mg_2Al_4Si_5O_{18}$
	epidote (ordered)	ep	$Ca_2FeAl_2Si_3O_{12}(OH)$
	fayalite	fa	Fe_2SiO_4
	Fe–chloritoid	fctd	$FeAl_2SiO_5(OH)_2$
	Fe–cordierite	fcrd	$Fe_2Al_4Si_5O_{18}$
	Fe–epidote	fep	$Ca_2Fe_2AlSi_3O_{12}(OH)$
	Fe–osumilite	fosm	$KFe_2Al_5Si_{10}O_{30}$
	Fe–staurolite	fst	$Fe_4Al_{18}Si_{7.5}O_{48}H_4$
	forsterite	fo	Mg_2SiO_4
	gehlenite	geh	$Ca_2Al_2SiO_7$
	grossular	gr	$Ca_3Al_2Si_3O_{12}$
	hydrous cordierite	hcrd	$Mg_2Al_4Si_5O_{18}{\cdot}H_2O$
	hydroxy–topaz	tpz	$Al_2SiO_4(OH)_2$
	kyanite	ky	Al_2SiO_5
	larnite–bredigite	larn	Ca_2SiO_4
	lawsonite	law	$CaAl_2Si_2O_7(OH)_2{\cdot}H_2O$
	merwinite	merw	$Ca_3MgSi_2O_8$
	Mg–chloritoid	mctd	$MgAl_2SiO_5(OH)_2$
	Mg–staurolite	mst	$Mg_4Al_{18}Si_{7.5}O_{48}H_4$
	Mn–chloritoid	mnctd	$MnAl_2SiO_5(OH)_2$
	Mn–cordierite	mncrd	$Mn_2Al_4Si_5O_{18}$
	Mn–staurolite	mnst	$Mn_4Al_{18}Si_{7.5}O_{48}H_4$
	monticellite	mont	$CaMgSiO_4$
	osumilite(1)	osm1	$KMg_2Al_5Si_{10}O_{30}$
	osumilite(2)	osm2	$KMg_3Al_3Si_{11}O_{30}$
	phase A	phA	$Mg_7Si_2O_8(OH)_6$
	pumpellyite	pump	$Ca_4MgAl_5Si_6O_{21}(OH)_7$
	pyrope	py	$Mg_3Al_2Si_3O_{12}$
	rankinite	rnk	$Ca_3Si_2O_7$
	sillimanite	sill	Al_2SiO_5
	spessartine	spss	$Mn_3Al_2Si_3O_{12}$
	sphene	sph	$CaTiSiO_5$
	spurrite	spu	$Ca_5Si_2O_8(CO_3)$
	tephroite	teph	Mn_2SiO_4
	tilleyite	ty	$Ca_5Si_2O_7(CO_3)_2$
	vesuvianite	vsv	$Ca_{19}Mg_2Al_{11}Si_{18}O_{69}(OH)_9$
	zircon	zrc	$ZrSiO_4$
	zoisite	zo	$Ca_2Al_3Si_3O_{12}(OH)$
Pyroxenes & pyroxenoids	acmite	acm	$NaFeSi_2O_6$
	Ca–Tschermak pyroxene	cats	$CaAl_2SiO_6$
	diopside	di	$CaMgSi_2O_6$
	enstatite	en	$Mg_2Si_2O_6$
	ferrosilite	fs	$Fe_2Si_2O_6$
	hedenbergite	hed	$CaFeSi_2O_6$
	jadeite	jd	$NaAlSi_2O_6$
	Mg–Tschermak pyroxene	mgts	$MgAl_2SiO_6$
	pseudowollastonite	pswo	$CaSiO_3$
	pyroxmangite	pxmn	$MnSiO_3$
	rhodonite	rhod	$MnSiO_3$
	wollastonite	wo	$CaSiO_3$
Amphiboles	anthophyllite	anth	$Mg_7Si_8O_{22}(OH)_2$
	cummingtonite	cumm	$Mg_7Si_8O_{22}(OH)_2$
	Fe–anthophyllite	fanth	$Fe_7Si_8O_{22}(OH)_2$
	Fe–glaucophane	fgl	$Na_2Fe_3Al_2Si_8O_{22}(OH)_2$
	ferroactinolite	fact	$Ca_2Fe_5Si_8O_{22}(OH)_2$
	gedrite (Na-free)	ged	$Mg_5Al_4Si_6O_{22}(OH)_2$
	glaucophane	gl	$Na_2Mg_3Al_2Si_8O_{22}(OH)_2$
	grunerite	grun	$Fe_7Si_8O_{22}(OH)_2$
	pargasite	parg	$NaCa_2Mg_4Al_3Si_6O_{22}(OH)_2$
	riebeckite	rieb	$Na_2Fe_5Si_8O_{22}(OH)_2$
	tremolite	tr	$Ca_2Mg_5Si_8O_{22}(OH)_2$
	tschermakite	ts	$Ca_2Mg_3Al_4Si_6O_{22}(OH)_2$
Other chain silicates	deerite	deer	$Fe_{18}Si_{12}O_{40}(OH)_{10}$
	Fe–carpholite	fcar	$FeAl_2Si_2O_6(OH)_4$
	Fe–sapphirine (793)	fspr	$Fe_{3.5}Al_9Si_{1.5}O_{20}$
	Mg–carpholite	mcar	$MgAl_2Si_2O_6(OH)_4$

Table 1a. (*continued*).

Group	End-member	Symbol	Formula
	sapphirine (442)	spr4	$Mg_4Al_8Si_2O_{20}$
	sapphirine (793)	spr7	$Mg_{3.5}Al_9Si_{1.5}O_{20}$
Micas	annite	ann	$KFe_3AlSi_3O_{10}(OH)_2$
	celadonite	cel	$MgAlSi_4O_{10}(OH)_2$
	eastonite	east	$KMg_2Al_3Si_2O_{10}(OH)_2$
	Fe–celadonite	fcel	$KFeAlSi_4O_{10}(OH)_2$
	margarite	ma	$CaAl_4Si_2O_{10}(OH)_2$
	Mn–biotite	mnbi	$KMn_3AlSi_3O_{10}(OH)_2$
	muscovite	mu	$KAl_3Si_3O_{10}(OH)_2$
	Na–phlogopite	naph	$NaMg_3AlSi_3O_{10}(OH)_2$
	paragonite	pa	$NaAl_3Si_3O_{10}(OH)_2$
	phlogopite	phl	$KMg_3AlSi_3O_{10}(OH)_2$
Chlorites	Al-free chlorite	afchl	$Mg_6Si_4O_{10}(OH)_4$
	amesite (14 Ang)	ames	$Mg_4Al_4Si_2O_{10}(OH)_4$
	clinochlore (ordered)	clin	$Mg_5Al_2Si_3O_{10}(OH)_4$
	daphnite	daph	$Fe_5Al_2Si_3O_{10}(OH)_4$
	Fe–sudoite	fsud	$Fe_2Al_4Si_3O_{10}(OH)_4$
	Mn–chlorite	mnchl	$Mn_5Al_2Si_3O_{10}(OH)_4$
	sudoite	sud	$Mg_2Al_4Si_3O_{10}(OH)_4$
Other sheet silicates	antigorite	atg	$Mg_{48}Si_{34}O_{85}(OH)_{62}$
	chrysotile	chr	$Mg_3Si_2O_5(OH)_2$
	Fe–talc	fta	$Fe_3Si_4O_{10}(OH)_2$
	kaolinite	kao	$Al_2Si_2O_5(OH)_4$
	prehnite	pre	$Ca_2Al_2Si_3O_{10}(OH)_2$
	pyrophyllite	prl	$Al_2Si_4O_{10}(OH)_2$
	talc	ta	$Mg_3Si_4O_{10}(OH)_2$
	tschermak–talc	tats	$Mg_2Al_2Si_3O_{10}(OH)_2$
Framework silicates	albite	ab	$NaAlSi_3O_8$
	analcite	anl	$NaAlSi_2O_6{\cdot}H_2O$
	anorthite	an	$CaAl_2Si_2O_8$
	coesite	coe	SiO_2
	cristobalite	crst	SiO_2
	heulandite	heu	$CaAl_2Si_7O_{18}{\cdot}6H_2O$
	high albite	abh	$NaAlSi_3O_8$
	kalsilite	kals	$KAlSiO_4$
	laumontite	lmt	$CaAl_2Si_4O_{12}{\cdot}4H_2O$
	leucite	lc	$KAlSi_2O_6$
	meionite	me	$Ca_4Al_6Si_6O_{24}(CO_3)$
	microcline	mic	$KAlSi_3O_8$
	nepheline	ne	$NaAlSiO_4$
	quartz	q	SiO_2
	sanidine	san	$KAlSi_3O_8$
	stilbite	stlb	$CaAl_2Si_7O_{18}{\cdot}7H_2O$
	stishovite	stv	SiO_2
	tridymite	trd	SiO_2
	wairakite	wrk	$CaAl_2Si_4O_{12}{\cdot}H_2O$
Oxides	baddeleyite	bdy	ZrO_2
	corundum	cor	Al_2O_3
	geikielite	geik	$MgTiO_3$
	hematite	hem	Fe_2O_3
	hercynite	herc	$FeAl_2O_4$
	ilmenite	ilm	$FeTiO_3$
	lime	lime	CaO
	magnesioferrite	mft	$MgFe_2O_4$
	magnetite	mt	Fe_3O_4
	manganosite	mang	MnO
	nickel oxide	NiO	NiO
	periclase	per	MgO
	pyrophanite	pnt	$MnTiO_3$
	rutile	ru	TiO_2
	spinel	sp	$MgAl_2O_4$
	ulvospinel	usp	Fe_2TiO_4
Hydroxides	brucite	br	$Mg(OH)_2$
	diaspore	dsp	$AlO(OH)$
	goethite	gth	$FeO(OH)$
Carbonates	ankerite	ank	$CaFe(CO_3)_2$
	aragonite	arag	$CaCO_3$
	calcite	cc	$CaCO_3$
	dolomite	dol	$CaMg(CO_3)_2$
	magnesite	mag	$MgCO_3$
	rhodochrosite	rhc	$MnCO_3$
	siderite	sid	$FeCO_3$

Table 1a. (*continued*).

Group	End-member	Symbol	Formula
Elements	diamond	diam	C
	graphite	gph	C
	iron	iron	Fe
	nickel	Ni	Ni
Gas species	carbon dioxide	CO2	CO_2
	carbon monoxide	CO	CO
	hydrogen	H2	H_2
	methane	CH4	CH_4
	oxygen	O2	O_2
	water fluid	H2O	H_2O

Table 1b. End-members in melts and solutions.

Group	End-member	Symbol	Formula
Melt species	albite liquid	abL	$NaAlSi_3O_8$
	anorthite liquid	anL	$CaAl_2Si_2O_8$
	diopside liquid	diL	$CaMgSi_2O_6$
	enstatite liquid	enL	$Mg_2Si_2O_6$
	fayalite liquid	faL	Fe_2SiO_4
	Fe-liquid (in KFMASH)	fliq	$K_3Fe_{0.5}Al_4Si_{19.5}O_{47}$
	forsterite liquid	foL	Mg_2SiO_4
	H_2O liquid	h2oL	H_2O
	H_2O liquid (in KFMASH)	hliq	H_2O
	K-feldspar liquid	kspL	$KAlSi_3O_8$
	Mg-liquid (in KFMASH)	mliq	$K_3Mg_{0.5}Al_4Si_{19.5}O_{47}$
	silica liquid	qL	SiO_2
	sillimanite liquid	silL	Al_2SiO_5
Aqueous Species	H^+ (aq)	H+	H^+
	Cl^- (aq)	Cl−	Cl^-
	OH^- (aq)	OH−	OH^-
	Na^+ (aq)	Na+	Na^+
	K^+ (aq)	K+	K^+
	Ca^{2+} (aq)	Ca++	Ca^{2+}
	Mg^{2+} (aq)	Mg++	Mg^{2+}
	Fe^{2+} (aq)	Fe++	Fe^{2+}
	Al^{3+} (aq)	Al+++	Al^{3+}
	CO_3^{2-} (aq)	CO3−	CO_3^{2-}
	$Al(OH)_3^\circ$ (aq)	AlOH3	$Al(OH)_3$
	$Al(OH)_4^-$ (aq)	AlOH4−	$Al(OH)_4^-$
	KOH° (aq)	KOH	KOH
	HCl° (aq)	HCl	HCl
	KCl° (aq)	KCl	KCl
	$NaCl^\circ$ (aq)	NaCl	NaCl
	$CaCl_2^\circ$ (aq)	CaCl2	$CaCl_2$
	$CaCl^+$ (aq)	CaCl+	$CaCl^+$
	$MgCl_2^\circ$ (aq)	MgCl2	$MgCl_2$
	$MgCl^+$ (aq)	MgCl+	$MgCl^+$
	$FeCl_2^\circ$ (aq)	FeCl2	$FeCl_2$
	aqueous silica	aqSi	SiO_2

temperature, and various simple expressions have been used in the literature to handle this behaviour. Here the arguments of Holland *et al.* (1996b) and Pawley *et al.* (1996) are followed in using the simplest possible expression that allows the thermal expansion to rise to a limiting value at very high temperatures. The expressions used here are

$$\alpha_T = a^\circ \left(1 - \frac{10}{\sqrt{T}}\right)$$

$$V_{1,T} = V_{1,298}\ [1 + a^\circ\ (T - 298) - 20a^\circ(\sqrt{T} - \sqrt{298})]$$

so that α_T tends to a° at high temperatures. In defence of such simplicity, it is noted that (a) the data measured at high temperature do not warrant more complexity (Pawley *et al.*, 1996) and (b) the simplification has generally negligible effects on calculated molar volumes and molar Gibbs energies at higher temperatures at elevated pressures. In addition, handling the thermal expansion via a single parameter allows simpler and more robust estimation of thermal expansion for phases with unknown properties.

Compressibility. The volume behaviour of solid phases as a function of pressure is now handled via the Murnaghan equation of state (EOS). The background and choice of the expressions used are more fully discussed in Holland *et al.* (1996b). The Murnaghan EOS can be expressed as

$$P = \frac{\kappa}{\kappa'}\left[\left(\frac{V^\circ}{V}\right)^{\kappa'} - 1\right]$$

in which V is the volume, V° the volume at ambient (1 bar) pressure, P the pressure, κ the bulk modulus and κ' the pressure derivative of the bulk modulus. A value of $\kappa' = 4$ is commonly assumed in cases where the data are insufficiently precise to determine this parameter and is justified on the basis that for many geologically relevant silicates and oxides, κ' is close to 4 (e.g. Poirier, 1991); in this study κ' will be set at 4.0 for all end-members. From fitting a large number of high-pressure volume data by a non-linear regression technique, it was found that setting $\kappa' = 4$ can fit almost all the data within their stated uncertainties, especially when the room pressure volume is allowed to vary within its measured uncertainty. Setting $\kappa' = 4$ and rearranging gives

$$V_{P,T} = V_{1,T}\left[1 - \frac{4P}{\kappa_T + 4P}\right]^{1/4}$$

$$\int_1^P V dP = \frac{V_{1,T}\kappa_T}{3}\left[\left(1 + \frac{4P}{\kappa_T}\right)^{3/4} - 1\right].$$

The value for the bulk modulus at high temperatures is taken to be $\kappa_T = \kappa_{298}$ $(1 - 1.5 \times 10^{-4}\ (T - 298))$. The arguments leading to use of this are given in Holland *et al.* (1996b) except that the term $-3a^\circ\kappa_{298}$ has been replaced by $-1.5 \times 10^{-4}\kappa_{298}$ for simplicity.

Extrapolation of heat capacity. Extrapolation of heat capacities to high temperature, where measurements exist only up to modest temperatures, is frequently needed. Examples include those carbonates or hydrates that become unstable at modest temperatures at low pressures, but that are stable to considerable temperatures at elevated pressures. Substituting the equations above for thermal expansion and compressibility into the thermodynamic relationship $C_p = C_v + TV\alpha^2\kappa$, the values of heat capacity at very high temperatures have been estimated from a Debye model for C_v, using the known C_p at a temperature where measurements are available. Alternatively constraints have been placed on the heat capacity by assuming that at very high temperatures C_v has reached its limiting value of $3n$R J/K and evaluating C_p from $C_p = C_v + TV\alpha^2\kappa$.

EOS for fluid phases. In this study the CORK equations from Holland & Powell (1991) are used for CO_2 and H_2O, in which the molar volumes at high pressures and temperatures are expressed in terms of the Modified Redlich Kwong equation with an additional virial-like term, $V = V_{MRK} + V_{vir}$. For H_2O the volumes of Rice & Walsh (1957) were used as high-pressure constraints, and for CO_2 the original expressions of Holland & Powell (1991) are used, which yield almost identical molar volumes at high pressures to those from the recent study of Sterner & Pitzer (1994). The fugacities and volumes of CO_2 and H_2O from the CORK equations are tabulated over the range 0–120 kbar and 200–140 °C in Tables 2(a)–2(d), with Table 2(a) here, and the remainder on the Web. Only the virial-like terms require changing, relative to the expressions in Holland & Powell (1991), where the extra contribution to the volumes is given by $V_{vir} = a(P - P_\circ) + b(P - P_\circ)^{1/2} + c(P - P_\circ)^{1/4}$. The new terms are, for H_2O, $a = 1.9853\ 10^{-3}$, $b = -8.9090\ 10^{-2}$, $c = 8.0331\ 10^{-2}$, $P_\circ = 2.0$, and for CO_2, $a = 5.40776\ 10^{-3} - 1.59046\ 10^{-6}T$, $b = -1.78198\ 10^{-1} + 2.45317\ 10^{-5}T$, $c = 0$, $P_\circ = 5.0$, with all units in kilojoules, kilobars, Kelvins.

Pressure dependence in Landau theory disordering. Phases which undergo order–disorder transitions or show lambda heat capacity anomalies were modelled using a tricritical Landau model in HP90. The approach has been extended here to include a pressure dependence, so that the order–disorder transition temperature can be a function of pressure. Adding a pressure dependence allows the behaviour of quartz to be modelled in a much more natural way, so that alpha and beta quartz do not require separate thermodynamic data. The method is outlined below using quartz as an example.

A baseline heat capacity is taken from the high-temperature data for beta quartz, and the lambda anomaly below 847K is added to it using tricritical Landau theory, as outlined in HP90,

$$C_p = a + bT + cT^{-2} + dT^{-1/2} + \frac{S_{max}T}{2\sqrt{T_c}\sqrt{T_c - T}}$$

where the critical temperature T_c now is required to be a function of pressure. The last term is not added at temperatures above T_c. Following the simple exposition in Putnis (1992), T_c is taken to be linear in pressure, a consequence of assuming that the excess volume of disordering mirrors the excess entropy of disordering, $V_{excess}^{Landau} = V_{max}\ (1 - Q^2)$, and $V_{max} = S_{max}\ dT_c/dP$. Although this limits the boundary for alpha and beta quartz to be linear in P–T, this limitation is not severe as the experimental boundary is quite close to being a straight line up to the pressure of the quartz–coesite reaction. Using α and β quartz as an example, it is simplest to convert all properties to the totally disordered form (β) and then to add the equilibrium Landau free energy of ordering: $G_{equil} = G_\beta + \Delta G_{Land}$. The equilibrium properties may then be found by adding the excess energies onto the basic properties for the ordered α form.

$$G_{excess} = G_{equil} - G_\alpha$$
$$= h'_{298} - Ts'_{298} + \int \nu'_T dP + \Delta G_{Land}$$

where

$$h'_{298} = S_{max}T_c^\circ(Q_{298}^2 - \frac{1}{3}Q_{298}^6)$$

$$s'_{298} = S_{max}Q_{298}^2$$

$$\nu'_T = V_{max}Q_{298}^2\ (1 + a^\circ(T - 298) - 20a^\circ(\sqrt{T} - \sqrt{298})$$

$$\int \nu'_T dP = \frac{1}{3}\nu'_T\kappa\left(\left(1 + \frac{4P}{\kappa}\right)^{3/4} - 1\right)$$

$$\Delta G_{Land} = S_{max}\ ((T - T_c)Q^2 + \frac{1}{3}T_cQ^6)$$

with

$$\kappa = \kappa_{298}\ (1 - 1.5\ 10^{-4}\ (T - 298))$$

$$T_c = T_c^\circ + \frac{V_{max}}{S_{max}}P$$

$$Q_{298}^4 = \left(1 - \frac{298}{T_c^\circ}\right)$$

$$Q^4 = \left(1 - \frac{T}{T_c}\right)$$

Properties given in the data set are the Landau critical temperature at 1 bar, T_c°; the thermal expansion parameter, a°; the bulk modulus at 298K, κ_{298}; the maximum entropy of disorder, S_{max}; and the maximum volume of disorder, V_{max}. The critical temperature at higher pressures, T_c, is then given as above.

Hydrous cordierite. The thermodynamic properties of hydrous cordierite have been updated to take account of the measured heat capacities of Carey (1993) and the enthalpy of hydration measured by Carey & Navrotsky (1992), as well as the new water content data of Skippen & Gunter (1996). Taking the heat capacity of hydrous cordierite as 8.3 J larger than anhydrous cordierite (Carey, 1993), together with the assumption of 1 mole of H_2O in the hydrous end-member, leads to $\Delta G = \Delta H - T\Delta S + 8.3\ (T - 298 - T\ln T/298) + RT\ln f_{H_2O}$ for the equilibrium hcrd = crd + H_2O. A least squares fit to the hydration data of Mirwald *et al.* (1979) and Skippen & Gunter (1996) yields an enthalpy of reaction which is within error of the value of 41.8 ± 1.6 kJ measured calorimetrically by Carey & Navrotsky (1992). It was therefore decided to accept the calorimetric enthalpy as a constraint and to retrieve the entropy from the hydration data. The resulting values used in the data set

Table 2. Fugacities of H_2O and CO_2 at crustal temperatures and pressures (in the range 200–1000 °C and 0.5–10 kbar). Further tables of fugacities and volumes to 1400 °C and 120 kbar may be found on the Web.

$RT\ln f_{H_2O}$ (kJ mol^{-1})

P/T	200	300	400	500	600	700	800	900	1000
0.5	11.48	20.93	30.10	37.36	43.35	49.04	54.57	60.02	65.40
1.0	12.48	22.06	31.44	39.52	46.83	53.60	60.06	66.34	72.50
1.5	13.45	23.14	32.66	41.03	48.84	56.20	63.23	70.04	76.69
2.0	14.40	24.18	33.81	42.38	50.46	58.17	65.57	72.75	79.75
2.5	15.34	25.20	34.92	43.64	51.92	59.86	67.53	74.98	82.25
3.0	16.26	26.19	35.99	44.83	53.26	61.39	69.26	76.91	84.40
3.5	17.17	27.16	37.03	45.97	54.53	62.80	70.83	78.65	86.31
4.0	18.06	28.11	38.04	47.07	55.73	64.12	72.29	80.26	88.06
4.5	18.93	29.03	39.02	48.13	56.89	65.39	73.66	81.76	89.69
5.0	19.80	29.95	39.99	49.17	58.01	66.60	74.98	83.17	91.22
5.5	20.66	30.85	40.93	50.18	59.09	67.77	76.23	84.53	92.67
6.0	21.50	31.74	41.87	51.17	60.15	68.90	77.45	85.82	94.05
6.5	22.34	32.61	42.78	52.15	61.19	70.00	78.62	87.08	95.38
7.0	23.17	33.48	43.69	53.10	62.20	71.08	79.77	88.29	96.67
7.5	23.99	34.34	44.58	54.05	63.20	72.13	80.88	89.47	97.91
8.0	24.80	35.19	45.47	54.97	64.18	73.16	81.97	90.62	99.12
8.5	25.61	36.03	46.34	55.89	65.14	74.17	83.03	91.74	100.30
9.0	26.41	36.86	47.20	56.79	66.09	75.17	84.08	92.83	101.45
9.5	27.20	37.68	48.06	57.69	67.02	76.15	85.10	93.91	102.58
10.0	27.99	38.50	48.90	58.57	67.94	77.11	86.11	94.97	103.68

$RT\ln f_{CO_2}$ (kJ mol^{-1})

P/T	200	300	400	500	600	700	800	900	1000
0.5	23.33	29.27	34.97	40.52	45.99	51.40	56.77	62.11	67.42
1.0	26.51	33.19	39.64	45.94	52.14	58.27	64.34	70.37	76.37
1.5	29.07	36.13	42.99	49.72	56.35	62.90	69.39	75.84	82.25
2.0	31.37	38.69	45.83	52.85	59.77	66.62	73.41	80.16	86.87
2.5	33.52	41.04	48.39	55.63	62.77	69.85	76.87	83.86	90.80
3.0	35.58	43.26	50.78	58.18	65.51	72.77	79.98	87.15	94.29
3.5	37.57	45.38	53.04	60.59	68.06	75.48	82.85	90.18	97.48
4.0	39.51	47.43	55.21	62.88	70.49	78.04	85.54	93.00	100.44
4.5	41.41	49.43	57.31	65.09	72.81	80.47	88.09	95.68	103.23
5.0	43.27	51.38	59.35	67.23	75.05	82.81	90.54	98.23	105.89
5.5	45.07	53.26	61.31	69.28	77.19	85.04	92.86	100.65	108.41
6.0	46.81	55.07	63.21	71.25	79.24	87.18	95.08	102.96	110.81
6.5	48.52	56.85	65.05	73.17	81.23	89.25	97.23	105.19	113.12
7.0	50.18	58.58	66.85	75.03	83.16	91.25	99.31	107.34	115.35
7.5	51.83	60.28	68.61	76.86	85.05	93.21	101.33	109.43	117.51
8.0	53.44	61.95	70.34	78.64	86.90	95.12	103.30	111.47	119.61
8.5	55.03	63.59	72.03	80.40	88.71	96.99	105.23	113.46	121.66
9.0	56.61	65.22	73.71	82.12	90.49	98.82	107.12	115.40	123.67
9.5	58.16	66.82	75.36	83.82	92.24	100.62	108.97	117.31	125.63
10.0	59.70	68.40	76.98	85.50	93.96	102.39	110.80	119.18	127.55

are $\Delta H = 41.8$ kJ, $\Delta S = 109.0$ J K^{-1} and $\Delta C_p = 8.3$ J for the reaction crd + H_2O = hcrd. The level of agreement between the calorimetric data and the measured water contents makes a satisfactory justification of the assumption of ideal mixing of cordierite and hydrous cordierite with one mole of H_2O, and lends weight to the model as a tool for calculating the thermodynamic properties of water-bearing cordierite.

Aqueous species. As a tool capable of simple extrapolation of thermodynamic properties of aqueous species, the density model of Anderson *et al.* (1991) appears to be remarkably successful. This density model has been extended to make it agree with not only the ambient-temperature solubility and calorimetric studies but also with the high-temperature and high-pressure mineral solubility experiments. According to the density model of Anderson *et al.* (1991) the apparent Gibbs energy of an aqueous species i is approximated by

$$G_i^\circ = \Delta_f H_i^\circ - TS_i^\circ + \frac{C_{p,i}^\circ}{298.15\left(\frac{\partial\alpha}{\partial T}\right)_P^\circ}\left(\alpha^\circ(T-298.15)+\ln\frac{\rho}{\rho^\circ}\right)$$

where $\Delta_f H$ is the enthalpy of formation, S is the entropy, C_p is the heat capacity, α is the thermal expansion of H_2O, $\left(\frac{\partial\alpha}{\partial T}\right)_P$ is the partial derivative of the thermal expansion of H_2O, and ρ is the density of H_2O. The superscript circles imply properties at the reference conditions of 1 bar and 298.15K. Three modifications have been made to this model which allow greater flexibility in reproducing experimental data on mineral solubilities and dissociation constants. Firstly, the logarithmic term is multiplied by a factor of T/T', where $T' = T$ below 500K and $T' = 500$ above 500K. A modification of this sort was suggested by Anderson *et al.* (1991) when considering the experimental data at high temperatures for the dissociation of NaCl. Secondly, the heat capacity of the aqueous species is augmented by a term linear in temperature, giving $C_p = C_p^* + bT$. Thirdly, the molar volumes of the aqueous species at the reference conditions are corrected for the density model contribution, $C_p^*\beta^\circ / 298.15\,(\partial\alpha/\partial T)_P^\circ$, to the volume at 1 bar and 298.15K. With these modifications, the revised density model becomes:

$$G_i^\circ = \Delta_f H_i^\circ - TS_i^\circ + PV_i^\circ + b_i\left(298.15T - \frac{298.15^2}{2} - \frac{T^2}{2}\right) + \frac{C_{p,i}^*}{298.15\left(\frac{\partial\alpha}{\partial T}\right)_P^\circ}\left[\alpha^\circ(T-298.15) - \beta^\circ P + \frac{T}{T'}\ln\frac{\rho}{\rho^\circ}\right]$$

where V_i° is the standard state molar volume of species i, β° is the compressibility of H_2O at the reference conditions, and $C_{p,i}^* = C_{p,i}^\circ - 298.15b_i$. The values for the various constants, $\alpha^\circ =$

25.93×10^{-5} K^{-1}, $\beta^\circ = 45.23 \times 10^{-6}$ bar^{-1}, and $(\partial\alpha/\partial T)^\circ_P = 9.5714 \times 10^{-6}$ K^{-2} are taken from the tables in Anderson *et al.* (1991). The modified density model leads to the following form for the behaviour of K at high temperatures and pressures:

$$\ln K = A + \frac{B}{T} + C\frac{P}{T} + \frac{D}{T}\ln\frac{\rho}{\rho^\circ} + ET.$$

Thus, by taking the standard state properties of aqueous species (C°_p, $\Delta_f H^\circ$, S°, V°, b), together with the modified density model equations above, reactions involving minerals and aqueous species may be calculated to high temperatures and pressures. Aqueous species include neutral complexes such as $NaCl^\circ$, $CaCl^\circ_2$ and aqueous silica (aqSi) in addition to charged ions and complexes such as Na^+ or $CaCl^+$. The properties of the aqueous species are not part of the least squares regression, having been processed separately and then added to the mineral data set.

Examples where experimental equilibria are compared with calculations using thermodynamic data for minerals and aqueous species in THERMOCALC are given in Figs 1 and 2. Figure 1 shows experimental Ca and Mg molalities for equilibria among the phases wollastonite, quartz, diopside, tremolite, talc and forsterite (Luce *et al.*, 1985) and calculated equivalents. Speciation calculations involved $CaCl^\circ_2$, $CaCl^+$, $MgCl^\circ_2$, $MgCl^+$, HCl°, H^+ and Cl^-. Agreement is quite good even at temperatures as high as 800 °C. In Fig. 2 the experimental data for a number of equilibria involving muscovite, quartz, pyrophyllite, kaolinite, andalusite and K-feldspar are compared with the calculated total K molality. The example has been selected for comparison with the study of Sverjensky *et al.* (1991). The calculations include speciation involving only KCl°, K^+, HCl°, H^+ and Cl^-. The agreement with experiment is generally quite good. It has been argued by Sverjensky *et al.* (1991), on the basis of such solubility studies, that the enthalpies of all Na and K silicates (paragonite, albite, muscovite and sanidine) should be made more stable by around 6 kJ mol^{-1} in order to fit the experiments. This study retains the calorimetrically derived enthalpies (as in Robie & Hemingway, 1995) for the following four reasons. (i) The enthalpies of formation for microcline and sanidine from low-temperature acid calorimetry have been revised by Robie & Hemingway (1995) and are coincidentally similar to the values proposed by Sverjensky *et al.* (1991). (ii) The high-temperature oxide melt calorimetry of Kiseleva *et al.* (1990) on microcline may be taken together with the calorimetry of Westrich & Navrotsky (1981) to yield -3979.6 ± 4.3 kJ mol^{-1} for the standard enthalpy of formation of microcline, using the reaction scheme $3KF + 2cor + 9q = AlF_3 + 3mic$, confirming the low-temperature data in Robie & Hemingway (1995). (iii) The calorimetry of Kiseleva *et al.* (1990) on the exchange reactions $ab + KCl = mic + NaCl$ and $ab + KF = mic + NaF$ together with the reaction $3NaF + 2\,cor + 9q = AlF_3 + 3ab$ yield a standard enthalpy of formation for low albite of -3936.7 ± 3.6 kJ mol^{-1}, in good agreement with the low-temperature acid-calorimetric data tabulated in Robie *et al.* (1978) and Robie & Hemingway (1995). (iv) The high-temperature oxide-melt calorimetry of Navrotsky *et al.* (1980) on jadeite, albite, nepheline, quartz and $NaAlO_2$ also provide estimates on the enthalpy of low albite which agree with the low-temperature acid calorimetry. From the three reactions $ab = NaAlO_2 + 3q$, $jd = NaAlO_2 + 2q$, and $ne = NaAlO_2 + q$, the standard enthalpies of albite (-3934.1 ± 2.9 kJ mol^{-1}), jadeite (-3028.8 ± 2.7 kJ mol^{-1}) and nepheline (-2092.6 ± 2.5 kJ mol^{-1}) may be derived. These are all in good agreement with the low-temperature calorimetry summarized in Robie & Hemingway (1995).

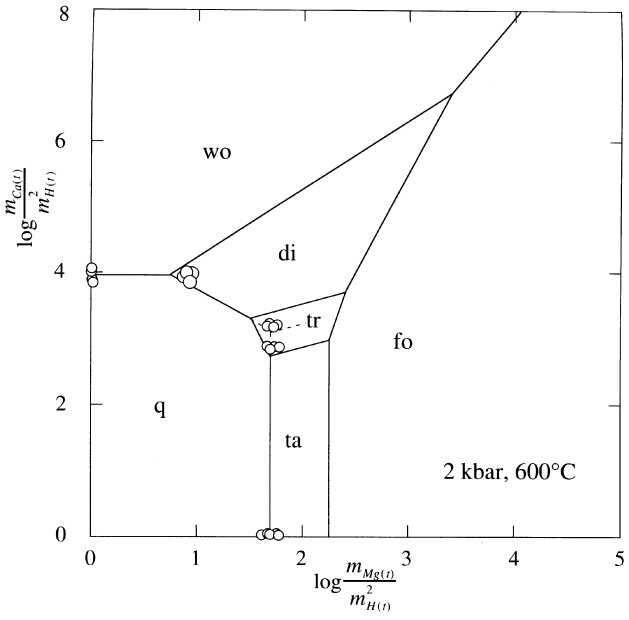

Fig. 1. Comparison of experimental and calculated mineral stability fields, in terms of molal total concentration ratios, in the system $CaO–MgO–SiO_2–H_2O–HCl$ at 2 kbar and 600 °C. The lines are calculated and the circles are experimental concentration ratios from Luce *et al.* (1985). See text for discussion.

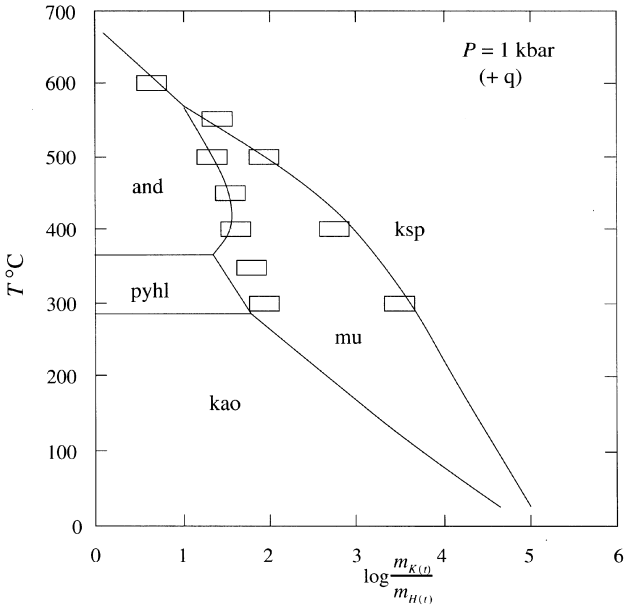

Fig. 2. Comparison of experimental and calculated mineral stability fields, in terms of molal total concentration ratios, in the system $K_2O–Al_2O_3–SiO_2–H_2O–HCl$ at 1 kbar. The boxes are experimental data listed in Sverjensky *et al.* (1991), and the lines are calculated. See text for discussion.

In marked contrast, the reversed experiments of Haselton & Cygan (1988) on the composition of fluids coexisting with and + mu + q and with san + mu + q at 1 kbar at 400 and 500 °C show fluids with systematically larger values of total K/H than those in Fig. 2. The uncertainties in such solubility studies may therefore have been underestimated, and the need to to make adjustments to enthalpies of muscovite and potassium feldspar is probably unwarranted until such discrepancies are resolved satisfactorily.

Melt species. A first attempt at building a set of melt end-member thermodynamic properties is made here, with the intention of expanding and improving it in the future. Much pioneering groundwork has already been done, and the reader is referred to Berman & Brown (1987), Ghiorso & Sack (1995) and Bottinga (1991) for further details and references. The basic volume and heat capacity data required for melt end-members may be estimated from Lange & Carmichael (1987, 1990), Kress & Carmichael (1991) and Stebbins *et al.* (1984). For the preliminary set of end-members, the

heat capacities are assumed to be temperature independent, and the volumes have been converted to the formulation outlined above for solids, including the constant $\kappa'=4$ in the Murnaghan equation for compressibility. While the $\kappa'=4$ assumption may appear to be overly simplistic, this approach nevertheless is even capable of fitting the partial molar volumes of H_2O in albite–H_2O melts measured by Burnham & Davis (1971, 1974); see Fig. 3(a). The data for bulk modulus, entropy and enthalpy are derived from the P–T experimental brackets on the relevant melting curves, constrained by entropy or enthalpy of fusion data, where available. For dry melts involving diopside, forsterite, fayalite, anorthite, albite, potassium feldspar, enstatite and quartz compositions, the melting curves are reproduced quite successfully to high pressures. For the H_2O component in melts, the heat capacity and entropy are not known, and preliminary estimates are based on the properties of liquid H_2O, adjusted on the basis of the wet melting of albite. Although the properties of the melt end-members are independent of any mixing model, unfortunately the H_2O end-member cannot be determined without recourse to mixing assumptions, and its properties are likely to need modification when the melt activity relations become better known. Initially, the activity of H_2O in simple melts, like those of albite, anorthite, sanidine, or quartz composition, is assumed to adhere to the simple model advocated by Nicholls (1980) such that

$$a_{H_2O}=X_h^2\gamma_h$$
$$a_i=X_i^2\gamma_i=(1-X_h)^2\gamma_i$$

where X_h is the mole fraction of H_2O in such simple melts, and X_i is the mole fraction of the simple silicate component i. The activity coefficients are then estimated using the simple regular solution model (Nicholls, 1980). Figure 3(b) shows calculated melting temperatures (wet and dry) of albite compared with the experimental data of Goldsmith & Jenkins (1985) and Clark (1966). For the mixing properties of hydrous melt, a regular solution parameter $W_{ab\ H_2O}=-9.4$ kJ was used.

The principal uncertainty involved in using melt end-members stems from the assumption of constant heat capacity for liquids. While this assumption may be reasonable at liquidus temperatures, the use of these thermodynamic data for calculating low-temperature solidus relations (e.g. the wet melting of quartz-saturated granitic melts) is not advised. In this respect, the regular solution parameter for albite–H_2O must be regarded as no more than a fitting parameter, because it almost certainly absorbs any errors introduced by assuming that the melt species have constant heat capacity.

In addition to these melt end-members with simple mineral stoichiometry, thermodynamic data are also provided for the KFMASH melt end-members mliq, fliq and hliq described and used in Holland *et al.* (1996a). These allow preliminary modelling of water-undersaturated melts under P–T conditions close to the dehydration-melting univariant equilibria in KFMASH in the range 4–10 kbar pressure.

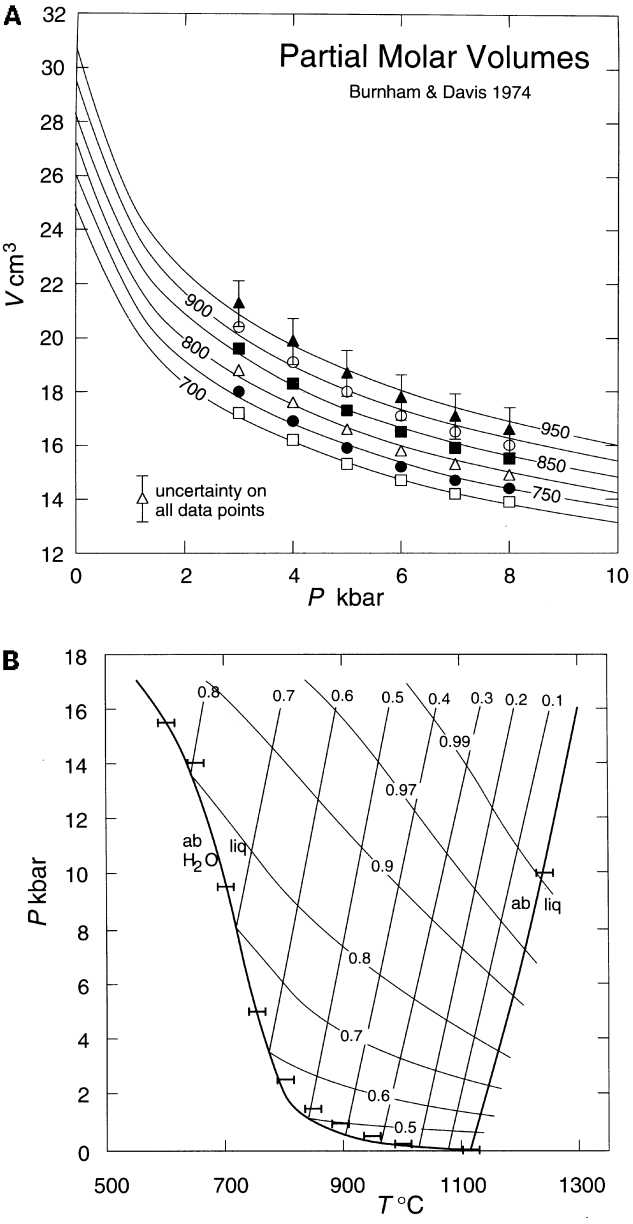

Fig. 3. (a) Partial molar volume of H_2O in albite melts. The symbols are data from Burnham & Davis (1974), with representative error bars, and the curves are calculated using the simple Murnaghan equation of state with $\kappa'=4$ (see text). (b) Calculated melting relations for albite compared with experimental melting curves. The steeper isopleth set gives the composition of H_2O-undersaturated melt coexisting with albite, and the flatter isopleth set gives the composition of H_2O-saturated albitic melt. The contours are for X_{H_2O}.

ACTIVITY MODELS IN SOLID SOLUTIONS

In this work the thermodynamic properties of end-members have been derived, as far as possible, from equilibria involving pure end-members, avoiding the added uncertainty which arises from using mixing models in solid solutions. However, certain end-member enthalpies may only be derived from equilibria in which those end-members occur as part of a solid solution rather than as stoichiometric phases, and therefore the derived enthalpies are tied to the chosen activity model. In this work, the end-members which depend on solution models fall into three categories: (a) those requiring one of the simple mixing models described below (eastonite, celadonite, magnesium tschermak's pyroxene, the osumilites, the sapphirines, epidote, Fe–epidote, hydrous cordierite, acmite, cummingtonite, tschermakite, the chlorites, and tschermak's talc); (b) those end-members derived through cation exchange equilibria with other phases (Fe–osumilite, spessartine, hedenbergite, Fe–anthophyllite, Fe–carpholite, Fe–sapphirine, annite, Fe–celadonite, daphnite, Fe–sudoite, Fe–talc, magnesioferrite, and ankerite); and (c) Mn end-members derived by Mg–Mn exchange between phases at assumed P–T from natural assemblages (Mahar *et al.*, 1997). Those in this last category (Mn–biotite, Mn–chlorite, Mn–cordierite, Mn–staurolite, and Mn–chloritoid) are therefore to be regarded as fictive Mn end-members which mix ideally with their Fe and Mg counterparts in the low Mn concentration range usually found in natural pelitic minerals. Of those in category (b) above, Fe–talc is derived from very Fe–poor compositions and should also be regarded as a fictive end-member. In the following discussion, where non-ideality is involved it is represented in terms of a macroscopic regular solution model (symmetric formalism; Powell & Holland, 1993).

Phengite. The ideal mixing model used in HP90 involved mixing of octahedral Al and Mg on the two M2 sites in the dioctahedral mica structure, M1 being vacant. This may be unrealistic given that Mg–Al ordering is such a strong control on the behaviour of octahedral site distributions (e.g. in omphacite and chlorite). Thus it is anticipated that each Mg entering the dioctahedral sheet will tend to be placed such that its nearest neighbours are all Al. This short range order situation is not easy to model satisfactorily, but energetically this would be much more like a hypothetical fully ordered mica in which Al and Mg can only mix on one (M2A) of the two sites, such that each M2A is surrounded by three M2B sites and vice versa as shown in Fig. 4. The mixing of tetrahedral Al and Si is restricted to just two of the four T sites to maintain Al-avoidance, as also argued in HP90. Thus the activity model for muscovite–celadonite micas is

$$a_{\mathrm{mu}}^{\mathrm{ideal}} = 4X_{\mathrm{K}}^{\mathrm{A}}X_{\mathrm{Al}}^{\mathrm{M2A}}X_{\mathrm{Al}}^{\mathrm{T1}}X_{\mathrm{Si}}^{\mathrm{T1}} = y^2\,(2-y)$$

$$a_{\mathrm{cel}}^{\mathrm{ideal}} = X_{\mathrm{K}}^{\mathrm{A}}X_{\mathrm{Mg}}^{\mathrm{M2A}}\,(X_{\mathrm{Si}}^{\mathrm{T1}})^2 = \frac{1}{4}\,(1-y)\,(2-y)^2$$

where $y = X_{\mathrm{Al}}^{\mathrm{M2A}}$ is the mole fraction, or proportion, of muscovite in the white mica. Fitting the Si contents of phengite in the experiments of Massonne & Schreyer (1987, 1989) with a non-ideal regular solution model yielded values for $W_{\mathrm{mu\ cel}} = 0$ within error, and so phengitic micas are taken to be approximately ideal for the above mixing activities. The derived enthalpy of celadonite depends upon this mixing model, whereas that of the muscovite end-member does not depend on any mixing model.

Biotite. As for phengite, the Mg–Al ordering in trioctahedral micas leads to mixing of Al and Mg on only one of the three octahedral sites, such that each Al is surrounded by six Mg nearest neighbours in the octahedral sheet (see Fig. 4). Again, the mixing of tetrahedral Al and Si is restricted to just two of the four T sites to maintain Al-avoidance, and the ideal mixing activities in the phlogopite–eastonite solid solution are given by

$$a_{\mathrm{phl}}^{\mathrm{ideal}} = 4X_{\mathrm{K}}^{\mathrm{A}}X_{\mathrm{Mg}}^{\mathrm{M3}}X_{\mathrm{Al}}^{\mathrm{T1}}X_{\mathrm{Si}}^{\mathrm{T1}} = (1-y)^2\,(1+y)$$

$$a_{\mathrm{east}}^{\mathrm{ideal}} = X_{\mathrm{K}}^{\mathrm{A}}X_{\mathrm{Al}}^{\mathrm{M3}}\,(X_{\mathrm{Al}}^{\mathrm{T1}})^2 = \frac{1}{4}\,y\,(1+y)^2$$

where $y = X_{\mathrm{Al}}^{\mathrm{M3}}$ is the mole fraction, or proportion, of eastonite in the biotite. Non-ideal mixing is implied for this system by the calorimetric study of Circone & Navrotsky (1992) where a significant heat of mixing, equivalent to $W_{\mathrm{phl\ east}} = 22.8 \pm 18$ kJ, was demonstrated. Extrapolation of the calorimetric data enabled Circone & Navrotsky to estimate the enthalpies of formation of phlogopite and eastonite as -6218 ± 5.6 and -6358 ± 8.4 kJ mol^{-1} (corrected by -6 kJ for the revised enthalpy of sanidine in Robie & Hemingway (1995)). The values from the phase equilibria in this study are -6219.4 ± 3.1 and -6348.9 ± 4.7 kJ mol^{-1} respectively, showing excellent agreement for phlogopite, but less good agreement for eastonite. However, the value and uncertainty in $W_{\mathrm{phl\ east}}$ can be reduced to 10.0 ± 4 kJ by removing the most aluminous biotite data point. Significantly, rejection of this apparent outlier alters the extrapolated enthalpy of formation of the eastonite end-member to -6351 kJ mol^{-1}, in good agreement with the value from this study (-6348.9 ± 4.7 kJ mol^{-1}). The smaller value of $W_{\mathrm{phl\ east}} = 10$ kJ is therefore used together with the ideal activities above in the form $a_{\mathrm{phl}} = a_{\mathrm{phl}}^{\mathrm{ideal}}\gamma_{\mathrm{phl}}$ etc. Although the enthalpy of phlogopite does not depend on any activity model, the enthalpy of the eastonite end-member does depend on this mixing model.

Tremolite–tschermakite amphibole. The reversed experimental determination of Al content of aluminous tremolite (Jenkins, 1994) provides powerful constraints on the mixing properties of amphibole in this system. Jenkins compared several ideal mixing models with his reversals and noted that random mixing on both octahedral and tetrahedral sites was not supported by his experiments, and that a much more ordered situation was implied. Several such models, including those used by Jenkins, have been fitted to his experiments and the one which best fits the data is a partial-order model outlined below. Although the coupled one-site and two-site models of Jenkins yield close fits to his quartz-saturated experiments, they did not fit the silica-undersaturated data so well (Jenkins, 1994). There is a logical inconsistency in using such models because they imply an ordered tschermakite end-member, yet the fits to the experiments demand a tschermakite entropy which is 40–50 J K^{-1} *higher* than estimates for ordered tschermakite. To resolve this, the new partial-order model assumes that Al and Mg mix on the M2 octahedral sites, but that there is less than maximal configurational entropy on the tetrahedral sites. Restricting the mixing of Al and Si to just the four T1 sites still yields too high an entropy to account satisfactorily for Jenkins' reversals, as he noted. Thus it will be assumed that the entropy contribution is half that for random mixing on the T1 sites, a situation which can be considered to correspond to charge-balanced coupling between an Al on M2 and one or other of the two nearest T1 site Al cations, rather than strict charge balance coupling to just one single tetrahedral neighbour. The activities of tremolite and tschermakite end-members in this model are just those of the random mixing model but with the square root of the tetrahedral site terms.

$$a_{\mathrm{tr}}^{\mathrm{ideal}} = \left(X_{\mathrm{Mg}}^{\mathrm{M2}}\right)^2\left(X_{\mathrm{Si}}^{\mathrm{T1}}\right)^2 = \frac{1}{4}\,(1-y)^2\,(2-y)^2$$

$$a_{\mathrm{ts}}^{\mathrm{ideal}} = 4\left(X_{\mathrm{Al}}^{\mathrm{M2}}\right)^2\left(X_{\mathrm{Al}}^{\mathrm{T1}}\right)\left(X_{\mathrm{Si}}^{\mathrm{T1}}\right) = y^3\,(2-y)$$

where $y = X_{\mathrm{Al}}^{\mathrm{M2}}$ is the mole fraction, or proportion, of the tschermakite end-member. The experimental data of Jenkins (1994) and Hoschek (1995) were used to determine the non-ideal mixing enthalpy, using

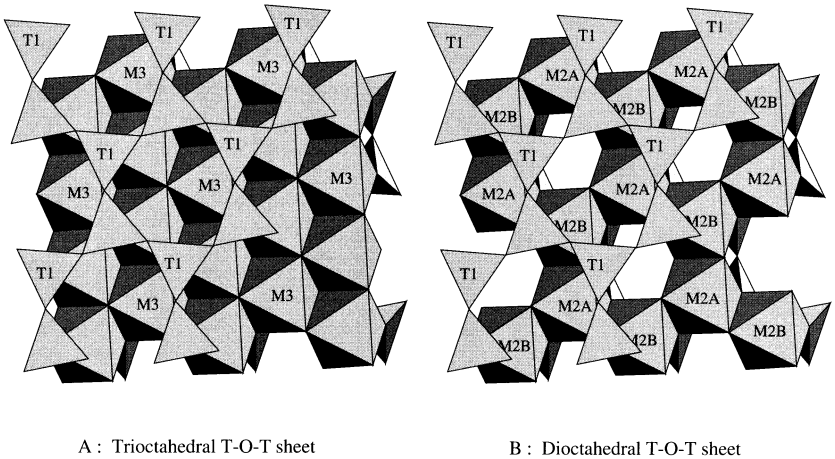

Fig. 4. Structure of dioctahedral and trioctahedral T–O–T sheets in mica and chlorite minerals, showing the site geometry to illustrate the activity models used. Al-avoidance, at least on a short range basis, is presumed to occur within the dioctahedral and trioctahedral sheets, as well as in the tetrahedral layers. Whether the mechanism is maximal dispersion of charges or of Mg–Al ordering, the entropy is greatly reduced over that of a random distribution, and in the model used here is taken to be that of a pseudo-ordered phase with Al occupying only one sort of the octahedral sites and one sort of tetrahedral site in such layered silicates. Diagram modified from the output of D. Palmer's program CrystalMaker.

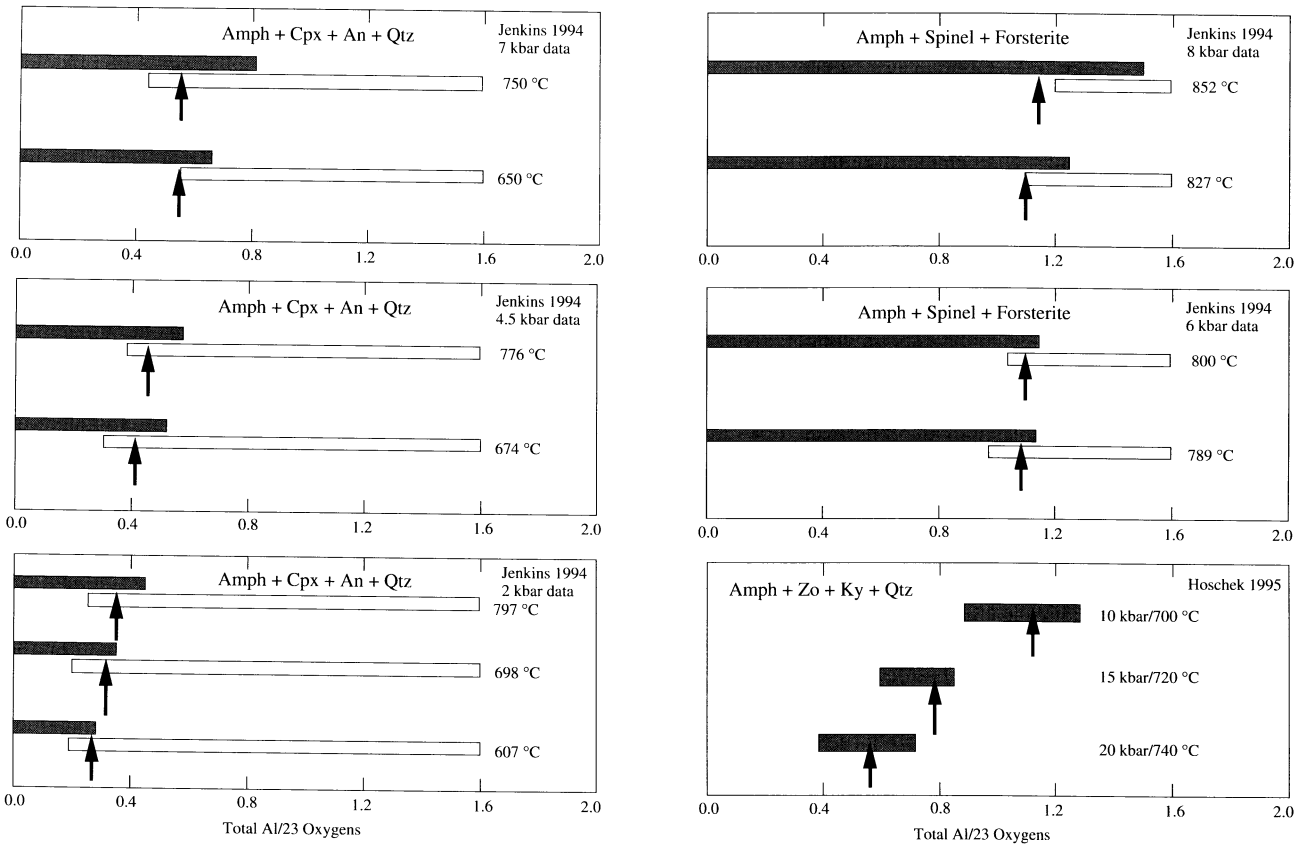

Fig. 5. Calculated (arrows) and experimentally reversed values for the alumina content of tremolite–tschermakite amphiboles in assemblages with diopside + anorthite + quartz, forsterite + spinel, and zoisite + kyanite + quartz. For the experiments of Jenkins (1994), the striped bars are the experimental compositions of amphibole from tremolite starting material and the empty bars are compositions grown from a tschermakitic starting material. For the experiments of Hoschek (1995), reversal intervals are shown as brackets of Al content. The non-ideal mixing model used for amphiboles is described in the text.

a simple regular solution model $a_{tr} = a_{tr}^{ideal}\gamma_{tr}$ with $RT\ln\gamma_{tr} = W_{tr\ ts}y^2$. The experimental reversals of Jenkins (1994) involving both silica-saturated and -undersaturated assemblages as well as those of Hoschek (1995) are well fitted, as may be seen in Fig. 5, with a value of $W_{tr\ ts} = 20$ kJ mol^{-1} in this reduced-entropy mixing model. The derived enthalpy of the tschermakite end-member depends on this mixing model.

Clinozoisite–epidote. The solid solution is treated as a ternary solution of clinozoisite, Fe–epidote and an ordered epidote solid solution, using the approach outlined in Holland & Powell (1996). Here, Al and Fe^{3+} are assumed to mix on only the M1 and M3 sites, with a strong tendency for Fe to order onto the M3 site. The model used is an extension of that used by Bird & Helgeson (1980) to incorporate non-ideal mixing. The activities of the three end-members are written

$$a_{cz}^{ideal} = X_{Al}^{M1}X_{Al}^{M3} = (1-p_{fep})p_{cz}$$
$$a_{fep}^{ideal} = X_{Fe}^{M1}X_{Fe}^{M3} = p_{fep}(1-p_{cz})$$
$$a_{ep}^{ideal} = X_{Al}^{M1}X_{Fe}^{M3} = (1-p_{fep})(1-p_{cz})$$

where p_{cz} is the proportion of the cz end-member etc. The activity coefficients are found from the simple regular solution expressions for the ternary solid solution among cz, fep and ep end-members. The degree of order, given by $Q = X_{Fe}^{M3} - X_{Fe}^{M1} = p_{ep}$, is found by substituting the activities into the equilibrium constant for the internal equilibrium cz + fep = 2ep. The enthalpy of this reaction is −26.1 kJ, and the values for $W_{cz\ fep}$, $W_{cz\ ep}$ and $W_{fep\ ep}$ are 15.4, 0.0 and 3.0 kJ mol^{-1} respectively, derived from the known values of the order parameter Q from Dollase (1973) and the experimental reversals of Liou (1973), Holdaway (1972) and Jenkins *et al.* (1983) as well as consideration of natural zoisite–clinozoisite partitioning data. While the derived enthalpies of ep and fep depend on this mixing model, that of cz does not.

Chlorite. The new experimental data of Baker & Holland (1996) pointed to the need for ordering around the clinochlore composition in the magnesium chlorites. The activity model used here is taken from Holland *et al.* (1998) and relies on the order–disorder models detailed in Holland & Powell (1996b). In magnesium chlorites the octahedral Al is taken as partitioning only into the M4 and M1 sites, with random mixing of Al and Si on two T2 sites. This was the assumption used in HP90, but it is now known that Al orders preferentially onto the M4 site at lower temperatures (Welch *et al.*, 1995). The parameters of the model are derived from the experimental study of Baker & Holland (1996) and the end-members used in this description are

chl	M1	M4	T2
afchl	Mg	Mg	Si_2
clin	Mg	Al	SiAl
ames	Al	Al	Al_2

$$X_{Al}^{T2} = y \qquad X_{Si}^{T2} = 1-y$$
$$X_{Al}^{M4} = y + \frac{Q}{2} \qquad X_{Mg}^{M4} = 1-y-\frac{Q}{2}$$
$$X_{Al}^{M1} = y - \frac{Q}{2} \qquad X_{Mg}^{M1} = 1-y+\frac{Q}{2}$$

where $y = \mathrm{Al(oct)}/2$, and the ideal activities are

$$a^{\mathrm{ideal}}_{\mathrm{afchl}} = \left(1-y+\frac{Q}{2}\right)\left(1-y-\frac{Q}{2}\right)(1-y)^2$$

$$a^{\mathrm{ideal}}_{\mathrm{clin}} = 4\left(1-y+\frac{Q}{2}\right)\left(y+\frac{Q}{2}\right)(1-y)y$$

$$a^{\mathrm{ideal}}_{\mathrm{ames}} = \left(y-\frac{Q}{2}\right)\left(y+\frac{Q}{2}\right)y^2$$

Therefore $y=0$ characterizes Al-free chlorite (afchl), $y=1$ denotes maximal-Al chlorite (ames), and clinochlore has $y=0.5$. The order parameter used is $Q = X^{\mathrm{M4}}_{\mathrm{Al}} - X^{\mathrm{M1}}_{\mathrm{Al}}$. The three end-members are assumed to mix according to a ternary regular solution. The degree of order Q is found by substituting the activities into the equilibrium constant for the internal equilibrium afchl + ames = 2clin. The enthalpy of this reaction is -63.0 kJ, and the values for $W_{\mathrm{afchl\ ames}}$, $W_{\mathrm{afchl\ clin}}$ and $W_{\mathrm{clin\ ames}}$ are 20.0, 18.0 and 18.0 kJ mol^{-1} respectively. Full details, together with an extension to Fe-bearing chlorites, may be found in Holland *et al.* (1998). The derived enthalpies of all the chlorite end-members depend on this mixing model.

Aluminous talc. The activity model for talc is the same as used in HP90. Talc having a similar structure to that of mica discussed above, the Al is assumed to order onto one of the octahedral sites (M3), and to enter only the two T1 sites. The ideal activities in MASH are given by

$$a_{\mathrm{ta}} = X^{\mathrm{M3}}_{\mathrm{Mg}}(X^{\mathrm{T1}}_{\mathrm{Si}})^2 = \tfrac{1}{4}(1-y)\,(2-y)^2$$

$$a_{\mathrm{tats}} = X^{\mathrm{M3}}_{\mathrm{Al}} X^{\mathrm{T1}}_{\mathrm{Al}} X^{\mathrm{T1}}_{\mathrm{Si}} = y^2\,(2-y)$$

where $y = X^{\mathrm{M3}}_{\mathrm{Al}}$ is the mole fraction, or proportion, of tats in the talc. While the derived enthalpy of aluminous talc depends on this mixing model, that of talc does not.

Sapphirine. Sapphirine compositions in the MAS system lie close to a solid solution $(\mathrm{Mg}_{4-y}\mathrm{Al}_{4+y})^{\mathrm{oct}}[\mathrm{Al}_{4+y}\mathrm{Si}_{2-y}]^{\mathrm{tet}}$ with common sapphirines lying between the 442 ($y=0$) and 793 ($y=0.5$) compositions (e.g. Higgins & Ribbe, 1979). These two compositions are used as end-members in this study, here called spr4 ($\mathrm{Mg_4Al_8Si_2O_{20}}$) and spr7 ($\mathrm{Mg_{3.5}Al_9Si_{1.5}O_{20}}$). According to Moore (1969), Higgins & Ribbe (1979) and Christy *et al.* (1992) there are high degrees of long and short range order on the eight octahedral and six tetrahedral sites, although the details are incompletely known. The consensus of these studies is that Mg resides on the M4, M5 and M6 sites with Al filling M7, leaving the remaining four octahedral sites (M1, M2, M3, M8) on which Mg and Al can both substitute. Of the six tetrahedral sites, T2 is occupied by Si while T5 is occupied by Al, leaving the four remaining tetrahedral sites (T1, T3, T4, T6) on which Al and Si can substitute. There is some suggestion that M1, M2 and M8 may be preferred by Al, and that the tetrahedral sites may similarly be more ordered, although it is not at all clear whether such ordering occurs in the high-temperature, short-duration experimental studies. Thus, as a first approximation, the mixing site distributions are

	M	T
spr4	$\mathrm{MgAl_3}$	$\mathrm{SiAl_3}$
spr7	$\mathrm{Mg_{0.5}Al_{3.5}}$	$\mathrm{Si_{0.5}Al_{3.5}}$

and the ideal activities are then given by

$$a_{\mathrm{spr4}} = 89.9(X^{\mathrm{M}}_{\mathrm{Mg}})\,(X^{\mathrm{M}}_{\mathrm{Al}})^3\,(X^{\mathrm{T}}_{\mathrm{Si}})\,(X^{\mathrm{T}}_{\mathrm{Al}})^3 = \frac{1}{729}(1-y)^2(3+y)^6$$

$$a_{\mathrm{spr7}} = 163(X^{\mathrm{M}}_{\mathrm{Mg}})^{0.5}\,(X^{\mathrm{M}}_{\mathrm{Al}})^{3.5}\,(X^{\mathrm{T}}_{\mathrm{Si}})^{0.5}\,(X^{\mathrm{T}}_{\mathrm{Al}})^{3.5} = \frac{1}{3217}(1-y)\,(3+y)^7.$$

The enthalpies of both these sapphirine end-members depend on this mixing model.

Osumilite. The activity models used are those of Holland *et al.* (1996a), where further details may be found. In the KMAS system, the two end-members used are osm1 $\mathrm{KMg_2Al_5Si_{10}O_{30}}$ and osm2 $\mathrm{KMg_3Al_3Si_{11}O_{30}}$. Mixing occurs on the T1 and T2 sites

	T1	T2	y
osm1	$\mathrm{Al_3}$	$\mathrm{Al_2}$	0
osm2	$\mathrm{MgAl_2}$	AlSi	1

where $y = 2X^{\mathrm{T2}}_{\mathrm{Si}}$, and the ideal activities are given by

$$a_{\mathrm{osm1}} = (X^{\mathrm{T1}}_{\mathrm{Al}})^3\,(X^{\mathrm{T2}}_{\mathrm{Al}})^2 = \frac{1}{108}(3-y)^3\,(2-y)^2$$

$$a_{\mathrm{osm2}} = 18X^{\mathrm{T1}}_{\mathrm{Mg}}\,(X^{\mathrm{T1}}_{\mathrm{Al}})^2\,X^{\mathrm{T2}}_{\mathrm{Al}}\,X^{\mathrm{T2}}_{\mathrm{Si}} = \frac{1}{4}(3-y)^2\,(2-y).$$

The derived enthalpies of both osumilite end-members depend on this mixing model.

Pyroxene. In this study, the activities of enstatite and Mg-tschermak's pyroxene are required in orthopyroxene, and also the activity of acmite in jadeite–acmite clinopyroxene. For orthopyroxene, the simplest model is chosen, that of assumed charge coupling, whereby the tetrahedral site distribution is fixed by the occupancy of the nearest octahedral site, which leads to the simple relation in the MAS system, $a^{\mathrm{opx}}_{\mathrm{en}} = X^{\mathrm{opx}}_{\mathrm{en}}$ and $a^{\mathrm{opx}}_{\mathrm{mgts}} = X^{\mathrm{opx}}_{\mathrm{mgts}}$. In the jadeite–acmite series, the mixing occurs only on the smaller M1 site, so the activities become $a^{\mathrm{cpx}}_{\mathrm{acm}} = X^{\mathrm{cpx}}_{\mathrm{acm}}$ and and $a^{\mathrm{cpx}}_{\mathrm{jd}} = X^{\mathrm{cpx}}_{\mathrm{jd}}$. The enthalpies of Mg–tschermak's pyroxene and acmite depend on these simple mixing models (the enthalpies of enstatite and jadeite do not depend on any mixing model).

Cummingtonite–grunerite. The order–disorder model in Holland & Powell (1996b) was used for cummingtonite–grunerite. In this model, the activities are close to being ideal with only a very small positive departure from ideality in the range 500–1000 °C. Parameterized as a regular solution, the cummingtonite–grunerite activities in this temperature range are characterized by the approximate regular solution parameter $W^{\mathrm{cumm}}_{\mathrm{Fe,Mg}} = 2.5$ kJ per mixing atom. The derived enthalpy of the cummingtonite end-member depends on this mixing model, the grunerite enthalpy being derived from experiments of Lattard & Evans (1992) on end-member grunerite breakdown (as discussed later).

Fe–Mg non-ideality. In many instances the mixing of Fe and Mg on octahedral sites in minerals requires treatment as a non-ideal solid solution. In most cases the Fe and Mg end-members are determined without recourse to solid solution reactions, and the magnitudes of any regular solution parameters used here are those needed for consistency between the stoichiometric end-member reactions and the partitioning equilibria. However, for end-members such as hedenbergite, annite and ankerite the only experimental data available for extracting enthalpies is Fe–Mg partitioning experiments. A self-consistent set of parameters derived from consideration of such partitioning and limited calorimetry yields $W^{\mathrm{ol}}_{\mathrm{FeMg}} = 4.2$, $W^{\mathrm{opx}}_{\mathrm{FeMg}} = 0.5$, $W^{\mathrm{cpx}}_{\mathrm{FeMg}} = 2.5$, $W^{\mathrm{gt}}_{\mathrm{FeMg}} = 0.8$, $W^{\mathrm{bi}}_{\mathrm{FeMg}} = 3.0$, $W^{\mathrm{sid}}_{\mathrm{FeMg}} = 4.0$, $W^{\mathrm{dol}}_{\mathrm{FeMg}} = 3.0$, and $W^{\mathrm{sp}}_{\mathrm{FeMg}} = 0.7$ (per atom in each case). In addition, the approach of Davies & Navrotsky (1983) may be used to estimate values for other Fe–Mg solid solution phases on the basis of their relative molar volumes.

RESULTS AND DISCUSSION

The sources for the volume, entropy, heat capacity, thermal expansivity and bulk modulus data for all the end-members are given in the appendix Table A1 (Appendix 2). Table 1 lists the compositions of all the end-members in the revised and updated data set. Table 2 lists calculated volumes and fugacities of H_2O and CO_2 from the CORK equations at crustal pressures and temperatures. Table 3 lists the refined enthalpies of formation of end-members for which data

Table 3. Regressed values for enthalpy of formation (kJ mol^{-1}) from the elements and their uncertainties compared with the compilation of Robie & Hemingway (1995), RH(95). The $\pm$ for this study is a 95% confidence interval, 1.97σ, with the multiplier coming from the 0.975 point of the Student's t distribution with 242 degrees of freedom. The $\pm$ from Robie & Hemingway is just two times the standard deviation on the mean of the observations (so it is somewhat smaller than a 95% confidence interval as the number of observations being averaged is usually small, so the multiplier should be larger). The difference in enthalpy is d, and the diagnostic d/s is d divided by the sum of the two uncertainties. Only merwinite, stishovite and geikielite are in serious disagreement ($d/s \gg 1$, say). Stishovite enthalpy, however, is in excellent agreement with the calorimetry of Liu *et al.* (1996). hat is the diagonal element of the hat matrix, and entries in this column signify that the end-member enthalpy from Robie & Hemingway was included in the regression.

Group	End-member	This study	±	RH(95)	±	d	d/s	hat
Ortho- & ring silicates	akermanite	−3866.20	2.1	−3864.8	2.0	−1.4	0.3	0.10
	almandine	−5263.65	2.6	−5264.7	3.0	1.1	0.2	0.15
	andalusite	−2588.77	1.4	−2589.9	2.0	1.1	0.3	0.09
	andradite	−5768.09	3.4	−5771.0	5.9	2.9	0.3	0.07
	cordierite	−9163.64	3.4	−9161.5	5.9	−2.1	0.2	0.06
	ayalite	−1478.22	1.4	−1478.2	1.3	0.0	0.0	0.20
	forsterite	−2171.85	1.4	−2173.0	2.0	1.2	0.4	0.10
	gehlenite	−3986.79	2.9	−3985.0	5.0	−1.8	0.2	0.06
	grossular	−6644.07	3.2	−6640.0	3.2	−4.1	0.6	
	kyanite	−2593.13	1.4	−2593.8	2.0	0.7	0.2	0.09
	larnite-bredigite	−2307.25	2.0	−2306.7	1.5	−0.6	0.2	0.08
	lawsonite	−4869.19	1.9	−4869.0	2.1	−0.2	0.1	
	merwinite	−4546.32	3.0	−4536.2	3.0	−10.1	**1.7**	
	monticellite	−2252.90	1.2	−2251.0	3.0	−1.9	0.5	
	pyrope	−6284.23	2.5	−6285.0	4.0	0.8	0.1	0.08
	rankinite	−3944.46	3.0	−3949.0	10.0	4.5	0.3	
	sillimanite	−2585.89	1.4	−2586.1	2.0	0.2	0.1	0.09
	sphene	−2595.55	2.1	−2596.6	3.0	1.1	0.2	0.09
	spurrite	−5849.69	4.9	−5840.2	5.7	−9.5	0.9	
	tephroite	−1732.15	2.6	−1731.5	3.0	−0.7	0.1	0.14
	tilleyite	−6368.33	4.9	−6372.0	2.0	3.7	0.5	
	zircon	−2031.85	3.4	−2034.2	3.1	2.4	0.4	0.24
	zoisite	−6898.57	2.8	−6901.1	3.3	2.5	0.4	
Chain silicates	Ca–tschermak pyroxene	−3306.96	1.9	−3306.3	2.5	−0.7	0.2	0.09
	anthophyllite	−12068.59	6.8	−12070.0	8.0	1.4	0.1	
	diopside	−3202.54	1.6	−3201.5	2.0	−1.0	0.3	0.12
	enstatite	−3090.26	1.8	−3090.8	3.0	0.5	0.1	0.07
	ferrosilite	−2388.75	1.8	−2390.0	6.0	1.7	0.2	0.02
	jadeite	−3027.83	3.9	−3029.3	3.6	1.5	0.2	0.20
	pseudowollastonite	−1627.67	1.1	−1627.6	1.4	−0.1	0.0	0.11
	pyroxmangite	−1322.50	1.6	−1322.3	2.0	−0.2	0.1	0.13
	rhodonite	−1321.72	1.6	−1321.6	2.0	−0.1	0.0	0.13
	tremolite	−12309.72	5.8	−12303.0	7.0	−6.7	0.5	
	wollastonite	−1634.04	1.0	−1634.8	1.4	0.8	0.3	0.11
Sheet silicates	chrysotile	−4358.46	2.5	−4360.0	3.0	1.5	0.3	0.14
	kaolinite	−4122.33	1.6	−4119.0	1.5	−3.3	1.1	0.03
	margarite	−6241.19	2.9	−6244.0	2.6	2.8	0.5	
	muscovite	−5984.12	6.1	−5990.0	4.9	5.9	0.5	
	paragonite	−5946.33	4.0	−5949.3	3.8	3.0	0.4	
	phlogopite	−6219.44	6.2	−6226.0	6.0	6.6	0.5	0.20
	prehnite	−6203.16	2.4	−6202.6	2.0	−0.6	0.1	
	pyrophyllite	−5640.85	2.3	−5640.0	1.5	−0.9	0.2	0.46
	talc	−5896.92	3.2	−5900.0	2.0	3.1	0.6	
Framework silicates	albite	−3934.60	3.8	−3935.0	2.6	0.4	0.1	0.40
	analcite	−3309.89	3.7	−3310.1	3.3	0.2	0.0	0.24
	anorthite	−4233.48	1.7	−4234.0	2.0	0.5	0.1	0.14
	coesite	−905.52	0.7	−907.8	2.1	2.3	0.8	0.02
	high albite	−3924.84	3.8	−3923.6	2.6	−1.2	0.2	
	kalsilite	−2121.72	6.1	−2124.7	3.1	3.0	0.3	
	leucite	−3029.04	5.9	−3037.8	2.7	8.8	1.0	
	microcline	−3975.05	5.8	−3974.6	3.9	−0.5	0.1	0.43
	nepheline	−2095.01	4.1	−2090.4	3.9	−4.6	0.6	0.22
	quartz	−910.88	0.7	−910.7	1.0	−0.2	0.1	0.10
	sanidine	−3964.90	5.9	−3965.6	4.1	0.7	0.1	0.39
	stishovite	−875.68	1.3	−861.3	2.1	−14.4	**4.2**	
Oxides	baddeleyite	−1101.31	3.4	−1100.6	1.7	−0.7	0.1	0.77
	corundum	−1675.19	1.7	−1675.7	1.3	0.5	0.2	0.32
	geikielite	−1567.42	2.1	−1572.8	1.2	5.4	**1.6**	
	hematite	−825.73	1.4	−826.2	1.3	0.5	0.2	0.23
	ilmenite	−1231.25	1.8	−1232.0	2.5	0.8	0.2	0.10
	lime	−634.94	1.1	−635.1	0.9	0.2	0.1	0.31
	magnesioferrite	−1440.55	4.3	−1441.5	3.0	1.0	0.1	0.39
	magnetite	−1115.55	2.0	−1115.7	2.1	0.2	0.0	0.17
	manganosite	−385.16	1.0	−385.2	0.5	0.0	0.0	0.84
	nickeloxide	−239.44	0.8	−239.3	0.4	−0.1	0.1	0.69
	periclase	−601.65	0.6	−601.6	0.3	−0.1	0.1	0.76
	pyrophanite	−1359.14	4.7	−1360.1	4.0	1.0	0.1	0.26
	rutile	−944.19	1.7	−944.0	0.8	−0.2	0.1	0.83
	spinel	−2300.31	1.9	−2299.1	2.0	−1.2	0.3	0.16
	ulvospinel	−1497.44	2.2	−1493.8	2.0	−3.6	0.9	
Hydroxides	brucite	−924.97	0.7	−924.5	0.4	−0.5	0.4	0.03
	diaspore	−999.40	0.8	−1001.3	2.2	1.9	0.6	0.01
	goethite	−561.66	0.7	−562.6	2.1	0.9	0.3	0.02
Carbonates & diamond	aragonite	−1207.65	1.0	−1207.4	1.4	−0.3	0.1	0.11
	calcite	−1207.54	1.0	−1207.4	1.3	−0.1	0.1	0.12
	dolomite	−2324.56	1.4	−2324.5	1.5	−0.1	0.0	0.17
	magnesite	−1111.59	0.7	−1113.3	1.3	1.7	1.0	
	rhodochrosite	−891.06	1.3	−892.9	0.5	1.8	1.0	
	siderite	−761.50	1.0	−755.9	5.5	−5.6	0.9	
	diamond	2.07	0.1	1.9	0.1	0.2	1.0	

are available in Robie & Hemingway (1995) for comparison. The level of agreement is very encouraging indeed, and shows that the calorimetric measurements and phase equilibrium approaches are becoming mutually compatible. Table 4 lists the high-temperature oxide-melt calorimetry used in this study. The hat values (a measure of the leverage, or degree of influence of each reaction) are all low, implying that these reactions are not contributing unduly to the regression results. In the second section in Table 4 are the reactions defining the enthalpies of formation of the gas species CO_2, H_2O, CH_4 and CO, which all have essentially unit hat values, showing that these enthalpies are entirely derived from these reactions. In the third and last section of Table 4 are various enthalpies of reaction, either calorimetric measurements, or constraints applied in this study for activity models and Landau ordering terms discussed above. The list of thermodynamic properties and final regressed Gibbs free energies and enthalpies of formation of mineral and fluid end-members is given in Table 5, while a list of the thermodynamic properties of aqueous species may be found in Table 6. Because these aqueous species are not involved in the regression, more species may be added to this list for use with the other mineral end-members by deriving values for their thermodynamic properties following the methods outlined in Anderson *et al.* (1991) and in this paper.

To enable readers to assess the regression results in greater detail, a complete listing of all equilibria used and the values of the fitted temperatures and pressures is provided in Table 7(b). A small sample of this table is given here as Table 7(a); the remaining 61 pages of this may be consulted via the World Wide Web (at http://www.gly.bris.ac.uk/www/jmg/jmg.html). New features introduced since HP90 as well as problems in fitting the experimental results are discussed below, where they are grouped under different chemical subsystems (all can include H_2O and/or CO_2).

SiO_2 and CaO–SiO_2

The new end-members in this subsystem are high tridymite, high cristobalite, stishovite and larnite–bredigite. High cristobalite and high tridymite are fitted to the experiments of Ostrovsky (1966) and Jackson (1976), while data for stishovite are derived from the experiments of Zheng *et al.* (1996) and constrained by the calorimetry of Liu *et al.* (1996). Data for larnite–bredigite have been retrieved from the experiments of Zharikov & Shmulovich (1969).

Coesite enthalpy is now fitted to the experiments of Bose & Ganguly (1995), which lie at slightly higher pressure than those of Bohlen & Boettcher (1982), but are similar to the new experimental data of Theye *et al.* (1997).

Table 4. Oxide and reaction calorimetry. Enthalpies (kJ), with uncertainty (σ), are given at T and 298K. e^* is the normalized enthalpy residual (e/σ) and hat is the diagonal element of the hat matrix.

	T (°C)	$H(T)$	σ	H (298K)	e^*	hat	Reference
Enthalpies from the oxides							
$MgO + CO_2 = mag$	25	−116.8	1.0	−116.8	−0.1	0.04	Chai & Navrotsky (1993)
$CaO + CO_2 = cc$	25	−178.3	1.2	−178.3	0.6	0.07	Chai & Navrotsky (1993)
$Al_2O_3 + SiO_2 = sill$	697	−2.4	1.2	−0.6	−0.6	0.00	Charlu *et al.* (1975)
$Al_2O_3 + SiO_2 = and$	697	−5.0	1.2	−3.3	−0.5	0.00	Anderson *et al.* (1977)
$Al_2O_3 + SiO_2 = ky$	697	−8.3	1.2	−6.9	0.1	0.00	Anderson & Kleppa (1969)
$3MnO + 3SiO_2 + Al_2O_3 = spss$	692	−97.2	5.9	−89.1	−1.0	0.17	Shearer (1973)
$2MgO + SiO_2 = fo$	750	−59.5	1.9	−57.7	0.0	0.05	Brousse *et al.* (1984)
$2MgO + 2SiO_2 = en$	697	−67.9	3.5	−66.3	−0.1	0.02	Brousse *et al.* (1984)
$CaO + MgO + SiO_2 = mont$	750	−104.8	1.7	−103.1	1.3	0.05	Brousse *ett. (1984)*
$2CaO + MgO + 2SiO_2 = ak$	750	−178.2	1.6	−171.9	0.6	0.17	Brousse *et al.* (1984)
$CaO + MgO + 2SiO_2 = di$	697	−146.4	1.7	−142.9	1.0	0.07	Charlu *et al.* (1978)
$2MgO + 2Al_2O_3 + 5SiO_2 = crd$	697	−68.1	3.0	−54.5	0.3	0.04	Charlu *et al.* (1975)
$CaO + SiO_2 = wo$	697	−89.9	1.5	−87.5	0.5	0.05	Charlu *et al.* (1975)
$CaO + SiO_2 = pswo$	697	−83.3	1.3	−80.0	1.4	0.07	Charlu *et al.* (1975)
$MnO + SiO_2 = rhod$	713	−26.4	1.3	−24.2	1.1	0.21	Navrotsky & Coons (1976)
Enthalpies from the elements							
$gph + O_2 = CO_2$	25	−393.5	0.1	−393.5	−0.0	0.99	Robie & Hemingway (1995)
$2H_2 + O_2 = 2H_2O$	25	−483.6	0.0	−483.6	−0.0	1.00	Robie & Hemingway (1995)
$gph + 2H_2 = CH_4$	25	−74.8	0.3	−74.8	−0.0	1.00	Robie & Hemingway (1995)
$2gph + O_2 = 2CO$	25	−221.1	0.3	−221.1	−0.0	1.00	Robie & Hemingway (1995)
Enthalpies of reaction							
3en + 2cor = 2py	700	55.5	8.6	61.0	1.0	0.00	Charlu *et al.* (1975)
cor + q + woll = an	1000	−13.5	1.5	−10.9	1.6	0.04	Zhu *et al.* (1994)
sill = ky	701	−6.2	1.2	−6.5	0.6	0.00	Holm & Kleppa (1966)
sill = and	701	−2.8	1.0	−3.0	−0.1	0.00	Holm & Kleppa (1966)
$crd + H_2O = hcrd$	25	−41.8	1.0	−41.8	−0.0	1.00	Carey & Navrotsky (1992)
afhl + ames = 2clin	25	−29.6	0.1	−29.6	0.1	0.99	This study
fep + cz = 2ep	25	−26.1	1.0	−26.1	0.0	1.00	This study
q = aqSi	25	25.3	0.3	25.3	−0.0	1.00	This study
abh = ab	25	−9.8	0.0	−9.8	0	1.00	This study
stv = coes	25	−29.9	0.8	−29.9	−0.0	0.39	Liu *et al.* (1996)

Table 5. Molar thermodynamic properties (units: kJ, K, kbar) of the end-members whose formulae can be found in Table 1. $\Delta_f G$ is the Gibbs free energy of formation from the elements, calculated from regressed values of $\Delta_f H$. σ_H is one standard deviation on the enthalpy of formation; S is the entropy; V the volume (all properties at 1 bar and 298K); a, b, c and d are the coefficients in the heat capacity polynomial $C_p = a + bT + cT^{-2} + dT^{-1/2}$; a° is the thermal expansion parameter; κ is the bulk modulus (incompressibility) at 298K; and T_c, S_{max}, and V_{max} are Landau parameters discussed in the text.

End-member	$\Delta_f G$ (kJ)	$\Delta_f H$ (kJ)	σ_H (kJ)	S (J K^{-1})	V (J bar^{-1})	a (kJ K^{-1})	$b(10^5)$ (kJ K^{-2})	c (kJ K)	d (kJ K$^{-1/2}$)	a$^\circ$ (K^{-1})	κ (kbar)	T_c (K)	S_{max} (J K^{-1})	V_{max} (J bar^{-1})
Ortho- & ring silicates														
akermanite	−3668.89	−3866.20	1.06	212.50	9.254	0.3854	0.3209	−247.5	−2.8899	5.08	1420			
almandine	−4939.80	−5263.65	1.32	340.00	11.511	0.6773	0	−3772.7	−5.0440	4.03	1690			
andalusite	−2440.97	−2588.77	0.70	92.70	5.153	0.2773	−0.6588	−1914.1	−2.2656	4.11	1334			
andradite	−5424.33	−5768.09	1.72	318.00	13.204	0.6386	0	−4955.1	−3.9892	3.93	1590			
clinohumite	−9062.78	−9637.84	3.13	418.00	19.740	1.0700	−1.6533	−7899.6	−7.3739	5.00	1200			
clinozoisite	−6502.98	−6898.11	1.43	301.00	13.630	0.5670	1.8063	−7034.0	−2.6030	4.60	1120			
epidote	−6076.41	−6463.20	1.39	328.00	13.910	0.5446	2.4781	−11230.0	−1.1921	5.05	1233			
fayalite	−1378.98	−1478.22	0.71	151.00	4.631	0.2011	1.7330	−1960.6	−0.9009	5.05	1330			
Fe–chloritoid	−2973.74	−3209.17	0.82	162.00	6.980	0.4846	−1.3808	−198.9	−4.7622	5.42	1465			
Fe–cordierite	−7949.44	−8436.51	1.72	475.00	23.710	0.8515	4.4724	−6645.0	−5.6234	0.76	810	1800	20.00	0.2000
Fe–epidote	−5624.34	−6002.19	1.38	357.00	14.190	0.5201	3.1499	−15426.0	0.2188	5.05	1294			
Fe–staurolite	−22282.23	−23753.88	6.56	1010.00	44.880	2.8800	−5.6595	−10642.0	−25.3730	1.20	1200			
ferrosumilite	−13424.60	−14248.96	4.21	762.00	38.320	1.6560	−3.4163	−6497.7	−14.1143	0.80	800			
forsterite	−2052.75	−2171.85	0.72	95.10	4.366	0.2333	0.1494	−603.8	−1.8697	6.13	1250			
gehlenite	−3784.82	−3986.79	1.43	202.00	9.024	0.4057	−0.7099	−1188.3	−3.1744	4.17	1080	700	11.00	0.0970
grossular	−6280.94	−6644.07	1.60	255.00	12.535	0.6260	0	−5779.2	−4.0029	3.93	1680			
hydrous cordierite	−8891.08	−9447.25	2.03	487.30	23.322	0.8697	5.1995	−7723.7	−5.2512	0.76	810	1800	20.00	0.2000
kyanite	−2442.59	−2593.13	0.70	83.50	4.414	0.2794	−0.7124	−2055.6	−2.2894	4.04	1590			
larnite	−2191.74	−2307.25	1.00	127.60	5.160	0.2475	−0.3206	0	−2.0519	5.05	1200	1710	10.03	0.0500
lawsonite	−4513.04	−4869.19	0.86	230.00	10.132	0.6878	0.1566	375.9	−7.1792	5.82	1014			
merwinite	−4317.73	−4546.32	1.50	253.10	9.847	0.4175	0.8117	−2923.0	−2.3203	6.15	1200			
Mg–chloritoid	−3313.56	−3559.53	0.85	132.00	6.875	0.4644	−1.2654	−1147.2	−4.3410	5.42	1465			
Mg–cordierite	−8653.24	−9163.64	1.68	407.50	23.322	0.8213	4.3339	−8211.2	−5.0000	0.76	810	1800	20.00	0.2000
Mg–staurolite	−23595.24	−25103.09	6.69	910.00	44.260	2.8205	−5.9366	−13774.0	−24.1260	1.20	1200			
Mn–chloritoid	−3095.30	−3330.93	1.71	166.00	7.175	0.4644	−1.2654	−1147.2	−4.3410	5.42	1465			
Mn–cordierite	−8191.83	−8681.71	3.63	475.00	24.027	0.8477	2.8490	−7668.2	−5.3114	0.76	810	1800	20.00	0.2000
Mn–staurolite	−22732.93	−24206.00	8.90	1024.00	45.460	2.8733	−8.9064	−12688.0	−24.7490	1.20	1200			
monticellite	−2134.63	−2252.90	0.59	108.10	5.148	0.2507	−1.0433	−797.2	−1.9961	5.63	1120			
osumilite(1)	−14122.73	−14968.47	4.06	701.00	37.893	1.6258	−3.5548	−8063.5	−13.4909	0.76	810			
osumilite(2)	−13973.34	−14810.69	4.46	724.00	38.440	1.6106	−3.4457	−8262.1	−13.1288	0.76	810			
phase A	−6609.65	−7129.87	2.22	350.00	15.442	0.9640	−1.1521	−4517.8	−7.7247	8.26	1450			
pumpellyite	−13448.33	−14390.45	2.60	629.00	29.550	1.7208	−2.4928	−5998.7	−14.6203	5.00	1615			
pyrope	−5933.62	−6284.23	1.26	266.30	11.318	0.6335	0	−5196.1	−4.3152	4.36	1737			
rankinite	−3743.35	−3944.46	1.51	210.00	9.651	0.3723	−0.2893	−2462.4	−2.1813	6.50	950			
sillimanite	−2438.93	−2585.89	0.70	95.50	4.986	0.2802	−0.6900	−1375.7	−2.3994	2.21	1320	2200	4.00	0.0350
spessartine	−5326.31	−5646.30	3.18	367.00	11.792	0.5846	−0.1593	−7516.7	−2.7501	4.62	1790			
sphene	−2454.15	−2595.55	1.04	131.20	5.565	0.2337	0.4043	−2306.5	−1.2076	4.20	1100			
spurrite	−5534.67	−5849.69	2.46	330.00	14.697	0.6141	−0.3508	−2493.1	−4.1680	6.50	950			
tephroite	−1631.58	−1732.15	1.30	155.90	4.899	0.2196	0	−1292.7	−1.3083	5.05	1200			
tilleyite	−6008.28	−6368.33	2.45	390.00	17.039	0.7417	−0.5345	−1434.6	−5.8785	6.50	950			
hydroxytopaz	−2689.97	−2905.00	0.97	100.50	5.339	0.3877	−0.7120	−857.2	−3.7442	4.04	1315			
vesuvianite	−39897.47	−42351.62	9.86	1890.00	85.200	4.4880	−5.7952	−22269.3	−33.4780	5.00	1670			
zircon	−1917.35	−2031.85	1.72	84.03	3.926	0.2370	−1.7880	−149.6	−2.2678	2.22	1160			
zoisite	−6502.25	−6898.57	1.40	297.00	13.575	0.5957	6.2297	−5921.3	−3.3947	6.70	1120			

Table 5. (*continued*).

End-member	$\Delta_f G$ (kJ)	$\Delta_f H$ (kJ)	σ_H (kJ)	S (J K^{-1})	V (J bar^{-1})	a (kJ K^{-1})	$b(10^5)$ (kJ K^{-2})	c (kJ K)	d (kJ K$^{-1/2}$)	a$^\circ$ (K^{-1})	κ (kbar)	T_c (K)	S_{max} (J K^{-1})	V_{max} (J bar^{-1})
Pyroxenes & pyroxenoids														
acmite	−2419.31	−2586.69	4.28	170.60	6.459	0.3071	1.6758	−1685.5	−2.1258	4.66	1060			
Ca–tschermak pyroxene	−3129.29	−3306.96	0.86	138.00	6.356	0.3476	−0.6974	−1781.6	−2.7575	4.43	1140			
diopside	−3027.80	−3202.54	0.78	142.70	6.619	0.3145	0.0041	−2745.9	−2.0201	5.70	1223			
enstatite	−2915.53	−3090.26	0.89	132.50	6.262	0.3562	−0.2990	−596.9	−3.1853	5.05	1070			
ferrosilite	−2234.53	−2388.75	0.90	190.60	6.592	0.3987	−0.6579	1290.1	−4.0580	6.32	1010			
hedenbergite	−2680.39	−2844.15	1.02	174.20	6.795	0.3402	0.0812	−1047.8	−2.6467	5.70	1200			
jadeite	−2849.10	−3027.83	1.86	133.50	6.040	0.3011	1.0143	−2239.3	−2.0551	4.66	1284			
Mg–tschermak pyroxene	−3012.12	−3188.83	0.79	131.00	5.890	0.3714	−0.4082	−398.4	−3.5471	5.08	1144			
pseudowollastonite	−1543.80	−1627.67	0.53	88.20	4.008	0.1578	0	−967.3	−1.0754	5.39	1050			
pyroxmangite	−1245.18	−1322.50	0.81	99.30	3.472	0.1384	0.4088	−1936.0	−0.5389	5.08	1250			
rhodonite	−1244.76	−1321.72	0.81	100.50	3.494	0.1384	0.4088	−1936.0	−0.5389	5.08	1250			
wollastonite	−1548.47	−1634.04	0.53	82.50	3.993	0.1593	0	−967.3	−1.0754	4.60	795			
Amphiboles														
anthophyllite	−11342.22	−12068.59	3.38	536.00	26.540	1.2773	2.5825	−9704.6	−9.0747	5.00	700			
cummingtonite	−11331.61	−12056.79	3.44	540.00	26.330	1.2773	2.5825	−9704.6	−9.0747	5.00	700			
Fe–glaucophane	−10186.06	−10890.01	4.75	624.00	26.590	1.7629	−11.8992	9423.7	−20.2071	5.30	890			
Fe–anthophyllite	−8968.90	−9627.76	9.28	725.00	27.870	1.3831	3.0669	−4224.7	−11.2576	5.00	700			
ferroactinolite	−9837.33	−10511.44	3.31	705.00	28.280	1.2900	2.9991	−8447.5	−8.9470	5.34	760			
gedrite	−11584.19	−12319.88	7.77	515.00	25.800	1.3077	2.3642	−9307.4	−9.7990	4.80	770			
glaucophane	−11233.99	−11969.26	4.07	535.00	26.050	1.7175	−12.1070	7075.0	−19.2720	5.30	883			
grunerite	−8956.27	−9613.64	3.44	730.00	27.840	1.3831	3.0669	−4224.7	−11.2576	5.00	648			
pargasite	−11986.81	−12719.60	2.67	601.00	27.190	1.2802	2.2997	−12359.5	−8.0658	5.34	912			
riebeckite	−9352.16	−10035.55	8.83	691.00	27.490	1.7469	−11.3572	9370.3	−19.4687	5.30	890			
tremolite	−11581.42	−12309.72	2.91	550.00	27.270	1.2602	0.3830	−11455.0	−8.2376	5.34	762			
tshermakite	−11807.73	−12540.57	2.91	545.00	26.800	1.2448	2.4348	−11965.0	−8.1121	5.34	760			
Other chain silicates														
deerite	−16902.08	−18348.40	6.92	1650.00	55.740	3.1644	−2.7883	−5039.1	−26.7210	5.00	630			
Fe–carpholite	−4080.26	−4433.85	1.12	223.00	10.690	0.6748	−1.0092	−715.8	−6.5545	5.00	525			
Fe–sapphirine	−9273.62	−9834.00	12.15	551.00	20.391	1.2578	−2.2171	−1664.0	−11.3484	4.90	1200			
Mg–carpholite	−4430.87	−4794.70	0.89	194.00	10.590	0.6678	−1.2559	−1167.1	−6.4400	5.00	525			
sapphirine(221)	−10415.77	−11014.08	3.33	440.00	19.870	1.1603	−2.4324	−7706.6	−8.9742	4.90	1200			
sapphirine(793)	−10469.45	−11067.02	3.73	445.00	19.775	1.1679	−2.4870	−7607.3	−9.1553	4.90	1200			
Micas														
annite	−4796.02	−5143.44	3.30	428.00	15.432	0.8157	−3.4861	19.8	−7.4667	5.79	513			
celadonite	−5464.11	−5844.48	3.04	287.00	14.040	0.7412	−1.8748	−2368.8	−6.6169	5.96	500			
eastonite	−5958.83	−6348.94	4.70	306.00	14.751	0.7855	−3.8031	−2130.3	−6.8937	5.79	513			
Fe–celadonite	−5127.78	−5497.32	3.08	318.00	14.250	0.7563	−1.9147	−1586.1	−6.9287	5.96	490			
margarite	−5856.99	−6241.19	1.47	267.00	12.964	0.7444	−1.6800	−2074.4	−6.7832	4.87	1300			
Mn–biotite	−5113.37	−5463.50	4.87	433.00	15.264	0.8099	−5.9213	−1514.4	−6.9987	5.79	513			
muscovite	−5603.71	−5984.12	3.04	292.00	14.083	0.7564	−1.9840	−2170.0	−6.9792	5.96	490			
Na–phlogopite	−5791.07	−6172.14	2.24	318.00	14.450	0.7735	−4.0229	−2597.9	−6.5126	5.79	513			
paragonite	−5565.09	−5946.33	1.99	276.00	13.211	0.8030	−3.1580	217.0	−8.1510	7.74	550			
phlogopite	−5837.42	−6219.44	3.08	328.00	14.964	0.7703	−3.6939	−2328.9	−6.5316	5.79	512			
Chlorites														
Al-free chlorite	−8078.47	−8744.20	2.34	408.00	21.660	1.1466	1.1225	−7855.9	−9.3288	3.98	472			
amesite	−8378.38	−9052.53	2.02	390.00	20.520	1.1770	0.9041	−7458.7	−10.0530	3.98	472			
clinochlore	−8263.35	−8929.86	1.85	410.50	21.090	1.1618	1.0133	−7657.3	−9.6909	3.98	472			
daphnite	−6535.56	−7153.99	3.33	545.00	21.340	1.2374	1.3594	−3743.0	−11.2500	3.98	472			
Fe–sudoite	−7275.66	−7912.77	2.31	457.00	20.400	1.4663	−4.7365	−1182.8	−14.3880	3.98	472			
Mn–chlorite	−7065.50	−7680.49	8.81	580.00	22.590	1.2278	−2.6990	−6299.8	−10.4694	3.98	472			
sudoite	−7976.77	−8634.36	1.86	399.00	20.300	1.4361	−4.8749	−2748.5	−13.7640	3.98	472			

Table 5. (*continued*).

End-member	$\Delta_f G$ (kJ)	$\Delta_f H$ (kJ)	σ_H (kJ)	S (J K^{-1})	V (J bar^{-1})	a (kJ K^{-1})	$b(10^5)$ (kJ K^{-2})	c (kJ K)	d (kJ K$^{-1/2}$)	a° (K^{-1})	κ (kbar)	T_c (K)	S_{max} (J K^{-1})	V_{max} (J bar^{-1})
Other sheet silicates														
antigorite	−70622.39	−71417.98	19.91	3591.00	175.480	9.6210	−9.1183	−35941.6	−83.0342	4.70	525			
chrysotile	−4030.75	−4358.46	1.26	221.30	10.746	0.6247	−2.0770	−1721.8	−5.6194	4.70	525			
Fe–talc	−4451.06	−4799.03	3.18	352.00	14.225	0.5797	3.9494	−6459.3	−3.0881	3.70	480			
kaolinite	−3801.72	−4122.33	0.82	203.70	9.934	0.4367	−3.4295	−4055.9	−2.6991	5.10	645			
prehnite	−5825.13	−6203.16	1.21	292.80	14.026	0.7249	−1.3865	−2059.0	−6.3239	5.10	835			
pyrophyllite	−5266.87	−5640.85	1.16	239.40	12.810	0.7845	−4.2948	1251.0	−8.4959	5.10	770			
talc	−5516.73	−5896.92	1.60	260.00	13.625	0.6222	0	−6385.5	−3.9163	3.70	480			
tschermaks talc	−5605.60	−5987.61	1.20	259.00	13.510	0.5495	3.6324	−8606.6	−2.5153	3.70	480			
Framework silicates														
albite	−3711.91	−3934.60	1.88	210.10	10.006	0.4520	−1.3364	−1275.9	−3.9536	4.56	593	950	16.00	0.1240
analcite	−3090.97	−3309.90	1.86	232.00	9.740	0.6435	−1.6067	9302.3	−9.1796	5.00	400			
anorthite	−4007.51	−4233.48	0.84	200.00	10.079	0.3716	1.2615	−4110.2	−2.0384	2.38	919	2300	11.00	0.0500
coesite	−850.89	−905.52	0.36	40.80	2.064	0.0965	−0.0577	−444.8	−0.7982	1.80	1000			
cristobalite	−853.12	−906.04	0.35	46.50	2.610	0.0979	−0.3350	−636.2	−0.7740	0.81	600			
heulandite	−9750.35	−1059.41	2.90	669.00	31.800	1.5048	−3.3224	−2959.3	−13.2972	2.38	1000			
high albite	−3706.12	−3924.84	1.88	223.40	10.109	0.4520	−1.3364	−1275.9	−3.9536	4.56	593			
kalsilite	−2005.98	−2121.72	3.05	134.00	6.040	0.2420	−0.4482	−895.8	−1.9358	5.76	590			
laumontite	−6707.45	−7268.61	1.19	457.00	20.370	1.0134	−2.1413	−2235.8	−8.8067	2.38	1000			
leucite	−2866.19	−3029.04	2.95	200.00	8.828	0.3698	−1.6332	684.7	−3.6831	3.67	630	938	18.00	0.4820
meionite	−13104.74	−13843.65	2.78	752.00	33.985	1.3590	3.6442	−8594.7	−9.5982	3.16	870			
microcline	−3750.19	−3975.05	2.92	216.00	10.892	0.4488	−1.0075	−1007.3	−3.9731	3.35	574			
nepheline	−1980.35	−2095.01	2.07	124.40	5.419	0.2727	−1.2398	0	−2.7631	8.10	600	467	10.00	0.0800
quartz	−856.46	−910.88	0.35	41.50	2.269	0.1107	−0.5189	0	−1.1283	0.65	750	847	4.95	0.1188
sanidine	−3744.21	−3964.90	2.92	230.00	10.900	0.4488	−1.0075	−1007.3	−3.9731	3.35	574			
stilbite	−10004.33	−10899.10	2.48	710.00	32.870	1.5884	−3.2043	−3071.6	−13.9669	2.38	1000			
stishovite	−816.20	−875.68	0.67	24.50	1.401	0.0681	0.6010	−1978.2	−0.0821	2.50	3160			
tridymite	−853.69	−906.73	0.35	46.10	2.700	0.0979	−0.3350	−636.2	−0.7740	0.50	750			
wairakite	−6220.05	−6666.54	1.21	375.00	19.040	0.8383	−2.1460	−2272.0	−7.2923	2.38	1000			
Oxides														
baddeleyite	−1043.57	−1101.31	1.70	50.40	2.115	0.0907	0	−813.3	−0.4388	3.76	2225			
corundum	−1581.72	−1675.19	0.83	50.90	2.558	0.1395	0.5890	−2460.6	−0.5892	4.19	2520			
geikielite	−1478.98	−1567.42	1.06	74.60	3.086	0.1510	0	−1890.4	−0.6522	4.95	1770			
hematite	−743.73	−825.73	0.70	87.40	3.027	0.1639	0	−2257.2	−0.6576	5.99	1996	955	15.60	0
hercynite	−1843.85	−1959.18	0.93	107.50	4.075	0.2833	−0.5376	609.8	−2.7136	3.95	2120			
ilmenite	−1154.63	−1231.25	0.90	108.90	3.169	0.1389	0.5081	−1288.8	−0.4637	4.95	1770	1900	11.00	0.0200
lime	−602.92	−634.94	0.57	38.10	1.676	0.0524	0.3673	−750.7	−0.0510	6.65	1160			
magnesioferrite	−1329.87	−1440.55	2.14	126.50	4.457	0.2179	0.0355	−3108.0	−0.7459	6.96	1850	665	12.90	0
magnetite	−1012.31	−1115.55	0.98	146.10	4.452	0.2625	−0.7204	−1926.2	−1.6557	6.96	1850	848	35.00	0
manganosite	−362.83	−385.16	0.52	59.70	1.322	0.0598	0.3600	−31.4	−0.2826	6.30	1640			
nickel oxide	−211.27	−239.44	0.38	38.00	1.097	0.0477	0.7824	−392.5	0	6.20	1650	520	5.70	0
periclase	−569.34	−601.65	0.30	26.90	1.125	0.0605	0.0362	−535.8	−0.2992	6.20	1650			
pyrophanite	−1279.93	−1359.14	2.33	104.90	3.288	0.1419	0.3373	−1940.7	−0.4076	4.95	1770			
rutile	−888.92	−944.19	0.83	50.60	1.882	0.0904	0.2900	0	−0.6238	4.43	2225			
spinel	−2175.64	−2300.31	0.93	81.50	3.978	0.2427	−0.6037	−2315.1	−1.6781	4.31	1945			
ulvospinel	−1401.79	−1497.44	1.11	175.00	4.682	−0.1026	14.2520	−9144.5	5.2707	6.90	1850			
Hydroxides														
brucite	−834.31	−924.97	0.33	64.50	2.463	0.1584	−0.4076	−1052.3	−1.1713	13.00	48			
diaspore	−920.73	−999.40	0.42	35.00	1.776	0.1451	0.8709	584.4	−1.7411	7.97	2300			
goethite	−490.86	−561.66	0.37	60.40	2.082	0.1393	0.0147	−212.7	−1.0778	7.97	2300			

Table 5. (*continued*).

End-member	$\Delta_f G$ (kJ)	$\Delta_f H$ (kJ)	σ_H (kJ)	S (J K^{-1})	V (J bar^{-1})	a (kJ K^{-1})	$b(10^5)$ (kJ K^{-2})	c (kJ K)	d (kJ K$^{-1/2}$)	a$^\circ$ (K^{-1})	κ (kbar)	T_c (K)	S_{max} (J K^{-1})	V_{max} (J bar^{-1})
Carbonates														
ankerite	−1819.29	−1971.50	1.48	187.00	6.606	0.3410	−0.1161	0	−3.0548	6.35	900	1273	9.00	0.0100
aragonite	−1128.03	−1207.65	0.52	89.50	3.415	0.1923	−0.3052	1149.7	−2.1183	11.50	650	1240	9.00	0.0400
calcite	−1128.81	−1207.54	0.52	92.50	3.689	0.1409	0.5029	−950.7	−0.8584	4.40	760	1240	10.00	0.0400
dolomite	−2161.51	−2324.56	0.70	156.00	6.434	0.3589	−0.4905	0	−3.4562	6.35	900	1373	13.00	0.0150
magnesite	−1027.74	−1111.59	0.36	65.10	2.803	0.1864	−0.3772	0	−1.8862	6.48	1460			
rhodochrosite	−817.22	−891.06	0.66	98.00	3.107	0.1695	0	0	−1.5343	6.50	800			
siderite	−688.16	−761.50	0.51	95.00	2.938	0.1684	0	0	−1.4836	11.00	1200			
Elements														
diamond	3.13	2.07	0.07	2.30	0.342	0.0243	0.6272	−377.4	−0.2734	1.65	5800			
graphite	0.00	0.00	0.00	5.85	0.530	0.0510	−0.4428	488.6	−0.8055	4.84	390			
iron	0.00	0.00	0.00	27.32	0.709	0.0462	0.5159	723.1	−0.5562	7.46	1680	1042	8.30	0
nickel	0.00	0.00	0.00	29.87	0.659	0.0498	0	585.9	−0.5339	8.86	1870	631	3.00	0
Gas species														
CH4	−50.66	−74.81	0.39	186.26	0	0.1501	0.2062	3427.7	−2.6504	0	0			
CO	−137.13	−110.53	0.19	197.67	0	0.0457	−0.0097	662.7	−0.4147	0	0			
CO2	−394.30	−393.51	0.08	213.70	0	0.0878	−0.2644	706.4	−0.9989	0	0			
H2	0.00	0.00	0.00	130.70	0	0.0233	0.4627	0	0.0763	0	0			
H2O	−228.54	−241.81	0.02	188.80	0	0.0401	0.8656	487.5	−0.2512	0	0			
O2	0.00	0.00	0.00	205.20	0	0.0483	−0.0691	499.2	−0.4207	0	0			
Melt species														
albite liquid	–	−3924.52	1.89	152.00	10.700	0.3585	0	0	0	6.20	320			
anorthite liquid	–	−4281.64	0.92	39.00	10.177	0.4175	0	0	0	7.22	500			
diopside liquid	–	−3209.33	0.86	23.00	7.531	0.3453	0	0	0	9.60	350			
enstatite liquid	–	−3085.65	1.00	1.00	7.059	0.3549	0	0	0	9.60	340			
fayalite liquid	–	−1435.27	0.78	118.00	4.710	0.2397	0	0	0	16.00	600			
Fe-liquid (in KFMASH)	–	−22924.77	9.58	220.00	64.450	2.3750	0	0	0	5.15	230			
forsterite liquid	–	−2162.23	0.79	−26.00	4.374	0.2679	0	0	0	15.40	550			
H_2O liquid	–	−267.43	0.21	75.00	1.164	0.0750	0	0	0	288.00	4			
H_2O liquid (in KFMASH)	–	−220.58	0.65	159.00	0.885	0	0	0	0	375.00	6			
K-feldspar liquid	–	−3971.88	2.93	143.00	11.399	0.3673	0	0	0	8.45	230			
Mg-liquid (in KFMASH)	–	−23108.61	9.56	184.00	64.400	2.3860	0	0	0	5.04	230			
silica liquid	–	−923.09	0.37	11.20	2.640	0.0865	0	0	0	0.10	750			
sillimanite liquid	–	−2505.36	0.87	67.00	6.093	0.2376	0	0	0	5.59	500			

Table 6. Thermodynamic data for aqueous species (see caption for Table 5). The heat capacity is that of the density model of Anderson *et al.* (1991), augmented by the *b* term $C_p^* = C_p^\circ + bT$ (see text). Thermal expansion and compressibility terms are not explicitly needed.

	$\Delta_f H^\circ$ (kJ)	σ_H (kJ)	S (J K^{-1})	V (J bar^{-1})	$b(10^5)$ (kJ K^{-2})	C_p° (kJ K^{-1})
H^+	0	0	0	0	0	0
Cl^-	−167.08	0.11	56.73	1.779	0	−0.1414
OH^-	−230.02	0.11	−10.71	−0.418	0	−0.1372
Na^+	−240.30	0.11	58.40	−0.111	19.13	0.0306
K^+	−252.17	0.11	101.04	0.906	7.27	0.0072
Ca^{2+}	−543.30	1.14	−56.50	−1.806	−6.90	−0.0463
Mg^{2+}	−465.96	1.14	−138.10	−2.155	−4.62	−0.0265
Fe^{2+}	−90.42	3.42	−107.11	−2.220	0	−0.0339
Al^{3+}	−527.23	1.71	−316.30	−4.440	0	−0.1427
CO_3^{2-}	−675.23	0.11	−50.00	−0.502	0	0.2908
$Al(OH)_3^\circ$	−1251.85	1.14	53.60	0	0	0.1015
$Al(OH)_4^-$	−1495.78	1.14	126.90	0	0	0.0965
KOH°	−473.62	1.37	109.62	−0.800	9.45	−0.0293
HCl°	−162.13	0.91	56.73	1.779	9.03	0.0540
KCl°	−400.03	1.48	184.81	4.409	5.43	−0.0380
$NaCl^\circ$	−399.88	1.25	126.09	2.226	19.13	−0.0020
$CaCl_2^\circ$	−877.06	1.37	46.00	3.260	13.69	0.0343
$CaCl^+$	−701.28	1.82	27.36	0.574	−6.90	0.0400
$MgCl_2^\circ$	−796.08	2.39	−22.43	2.920	23.99	0.0186
$MgCl^+$	−632.48	0.91	−81.37	0.126	−4.62	0.1126
$FeCl_2^\circ$	−375.34	3.42	109.88	−2.700	45.03	0.0124
silica(aq)	−887.99	0.74	46.35	1.832	17.75	0.0283

Quartz is now treated with a pressure-dependent Landau tricritical model and so explicit use of α and β quartz, as in HP90, is no longer required.

The calcite–aragonite equilibrium is now fitted over an extended temperature range (80–1100 °C), using the experiments of Johannes & Puhan (1971) and Irving & Wyllie (1975). A Landau model for carbonate group rotational disordering was used for calcite, following Redfern *et al.* (1989); to prevent extreme curvature on the *P–T* boundary, a similar Landau excess had to be added to the free energy of aragonite.

All equilibria involving wollastonite, pseudowollastonite, tilleyite, spurrite and rankinite are well fitted by the data set, with the exception of the cc + q = wo + CO_2 experiments of Greenwood (1967) and Harker & Tuttle (1956). The calculated curve marginally misses the brackets of Zhu *et al.* (1994) for this same reaction by 0.1 kbar.

MgO–SiO_2

New end-members in this subsystem are clinohumite, antigorite and the high-pressure Phase A. Clinohumite data are fitted to the experiments of Duffy & Greenwood (1979) and Phase A to the experiments of Pawley & Wood (1996). The entropy of antigorite was estimated from Holland (1989), the volume was taken from Mellini *et al.* (1987), and the enthalpy was derived from fitting to the experiments of Evans *et al.* (1976). The experiments of Aranovich & Newton (1996) on dehydration of brucite have provided much more stringent constraints on the brucite enthalpy. Data for cummingtonite are now fitted to the experiments of Fonarev & Korolkov (1980), using the Fe–Mg order–disorder model in Holland & Powell (1996b). The experiments of Koziol & Newton (1995, 1997) and those of Johannes & Metz (1968) and Philipp & Girsperger (in Trommsdorff & Connolly, 1990) on magnesite decarbonation are now used, as well as those of Koziol & Newton (1995, 1997) on the reactions 2mag + en = 2fo + 2CO_2 and 2mag + 2q = en + 2CO_2. All are now fitted well.

CaO–MgO–SiO_2

The experiments of Brey *et al.* (1983) on the pressure-sensitive reaction di + 2mag = en + dol are now well fitted, in contrast with HP90, and provide a strong constraint on the enthalpy of dolomite. The experiments of Jenkins *et al.* (1991) for the reactions 2di + ta = tr and 2tr = 3en + 4di + 2q + 2H_2O help to constrain talc and tremolite enthalpies more tightly. Although most reactions in this subsystem are well fitted by the new data set, the experiments of Käse & Metz (1980) on the reaction di + 3 dol = 2fo + 4cc + 2CO_2 are missed (calculated temperatures are 10–17 °C too high), as are the high-pressure brackets of Goldsmith (1980) for the reaction dol = cc + per + CO_2 and the very-high-pressure (above 50 kbar) data of Luth (1995) for the reaction dol + q = di + 2CO_2.

Al_2O_3–SiO_2

New end-members in this subsystem are hydroxy-topaz and kaolinite. Hydroxy-topaz data are derived from the experiments of Wunder *et al.* (1993) on the reaction tpz = ky + H_2O, while kaolinite data are derived using the experimental data of Hemley *et al.* (1980) and McPhail (in Berman, 1988). It was decided to use the experimental data of Holdaway (1971), Bowman (1975), Kerrick & Heninger (1984) and Weill (1966) for the and = sill reaction. Previously in HP90 all experiments on and = sill were left out of the regression, because of the difficulty in deciding which sets of experiments to choose, given that the other equilibria in the analysis favoured a curve midway between the experimental curves of Holdaway (1971) and of Richardson *et al.* (1969). Thermodynamic data for kyanite and andalusite also fit the tightly constraining experiments of Harlov & Newton (1993) on cor + q = ky and the cor + q = and equilibria very successfully. The results of these equilibria can be seen in Table 7(a). Diaspore–corundum experiments of Vidal *et al.* (1994) and Grevel *et al.* (1994) on the reaction 2dsp = cor + H_2O are now used, as are also the brackets of Theye *et al.* (1997) on the reactions 2dsp + 4q = prl and 2dsp + 4coe = prl.

CaO–Al_2O_3–SiO_2

New end-members in this subsystem are laumontite, wairakite, heulandite and stilbite. Enthalpies for these

Table 7a. The experimental data used in setting up the least squares problem for solving for the enthalpies of formation of the phases in LSQDS, and the results of the least squares analysis. The first columns give the experimental data, in the form of the P, T, $x(CO_2)$ and K of the experiments, followed by the corresponding enthalpies of reaction calculated using the entropies, volumes, etc., in Table 5. LSQDS converts the enthalpies of reaction into an enthalpy of reaction bracket given in the first line of the summary. The least squares enthalpy of reaction (cH) is given in the second line of the summary, with its calculated uncertainty. The calc column gives the calculated T or P of the experimental conditions using the least squares results, followed by its uncertainty. The miss column gives the amount that the calculated T or P is outside the experimental bracket (if at all). In the summary information for each reaction, the code on the first line relates to the calculation of the enthalpy of reaction bracket (see Powell & Holland, 1993); the number at the end of the second line (if present) is a factor used in weighting experimental results in the least squares analysis; the comment making up the third line gives an overall appraisal of the relationship between the enthalpy of reaction bracket and the calculated enthalpy of reaction; uH on the fourth line is a measure of the uncertainty on each end of the enthalpy of reaction bracket arising from experimental uncertainties (in P, T, etc.), d/s is a measure of bracket overlap normalized to the uncertainty on bracket ends as discussed in Powell & Holland (1993), and h is the hat matrix diagonal. (a) Example output for the system Al_2O_3–SiO_2. (b) Full output available from one of the JMG Web sites.

66) ky = and (Holdaway, 1971; Newton, 1966a; Richardson *et al*., 1969; Bohlen *et al*., 1991)

ln_K	x(CO2)	P(kbar)		T(C)		H(low)	H(high)	miss	calc	2sd	summary
0	–	2.4		377	409	4.24	4.54		390	12	3 (4.22↔4.42)
0	–	3.6		447	499	3.99	4.47		487	12	cH = 4.36 (sd 0.05)
0	–	4.8		557	590	4.10	4.40		585	12	within bracket
0	–	7.0	5.6	700		3.75	4.79		6.18	0.15	uH = 0.07, d/s = 1.1, h = 0.50
0	–	7.5	5.6	750		3.82	5.23		6.77	0.15	
0	–	7.9	6.5	800		3.96	5.00		7.36	0.15	
0	–	8.5	6.9	800		3.51	4.70		7.36	0.15	
0	–	6.8	6.0	700		3.86	4.49		6.18	0.15	
0	–	7.9	7.2	825		4.18	4.66		7.66	0.15	
0	–	8.2		800		3.73			871	12	

67) ky = sill (Newton, 1966b; Richardson *et al*., 1969; Holdaway, 1971; Bohlen *et al*., 1991)

ln_K	x(CO2)	P(kbar)		T(C)		H(low)	H(high)	miss	calc	2sd	summary
0	–	7.0	5.5	600		6.60	7.43		5.85	0.23	3 (7.27↔7.57)
0	–	8.8	7.0	700		6.81	7.80		8.02	0.23	cH = 7.24 (sd 0.06)
0	–	10.3	9.0	800		7.19	7.90		10.22	0.23	too low but OK
0	–	12.2	11.3	900		7.38	7.86	0.26	12.46	0.23	uH = 0.11, d/s = 0.3, h = 0.24
0	–	15.1	13.9	1000		7.05	7.68		14.74	0.24	
0	–	9.5	7.5	750		7.03	8.12		9.11	0.23	
0	–	9.0	7.2	750		7.30	8.28	0.11	9.11	0.23	
0	–	8.2		685		6.96			708	10	
0	–	7.0			710		7.92		653	10	
0	–	9.2		740		7.07			754	10	
0	–	8.8			785		7.83		736	10	
0	–	10.2		790		7.13			799	10	
0	–	9.8			835		7.88		781	10	
0	–	28.0	26.5	1500		6.80	7.53		27.10	0.26	
0	–	23.5		1300		6.45			1362	10	

68) and = sill (Holdaway, 1971; Bowman, 1975; Heninger, 1984)

ln_K	x(CO2)	P(kbar)		T(C)		H(low)	H(high)	miss	calc	2sd	summary
0	–	1.8		571	663	2.69	2.94		642	28	1 (2.81↔2.89)
0	–	3.6		491	527	2.80	2.90		519	28	cH = 2.88 (sd 0.04)
0	–	3.0		497		2.71			559	28	within bracket
0	–	4.3			506		2.97		475	26	uH = 0.02, d/s = 2.6, h = 0.85
0	–	1.2	2.5	615		2.69	2.94		2.19	0.38	
0	–	0.5		669	806	2.70	3.06		738	30	
0	–	3.0			607		3.01		559	28	
0	–	0.0			805		2.96		776	30	

* and = sill (Richardson *et al*., 1969)

ln_K	x(CO2)	P(kbar)		T(C)		H(low)	H(high)	miss	calc	2sd	summary
0	–	2.0		750	800	3.21	3.35	−122	628	28	** NOT USED **
0	–	3.0		650	750	3.13	3.41	−91	559	28	cH = 2.88 (sd 0.04)
0	–	4.0		650		3.32		−156	494	26	

69) ky = cor + q (Harlov & Newton, 1993)

ln_K	x(CO2)	P(kbar)		T(C)	H(low)	H(high)	miss	calc	2sd	summary
0	–	5.5	4.8	700	6.90	7.24		5.17	0.30	2 (6.88↔7.09)
0	–	8.0	7.5	800	6.84	7.07		7.53	0.31	cH = 7.06 (sd 0.06)
										within bracket
										uH = 0.08, d/s = 1.0, h = 0.33

70) cor + q = and (Harlov & Newton, 1993)

ln_K	x(CO2)	P(kbar)		T(C)	H(low)	H(high)	miss	calc	2sd	summary
0	–	8.0	7.5	700	−2.76	−2.61		7.79	0.19	1 (−2.76↔−2.62)
										cH = −2.70 (sd 0.04) 0.5
										within bracket
										uH = 0.05, d/s = 1.6, h = 0.84

end-members have been derived using the experiments of Cho *et al.* (1987), Liou (1970, 1971a,b), and Thompson (1970). Entropies were estimated using the technique of Holland (1989) to derive an entropy contribution of 29.0 J K^{-1} per mole of zeolitic H_2O.

Data for the clinozoisite–epidote solid solution and for the clinozoisite–orthozoisite transition are improved since HP90. The experiments of Jenkins *et al.* (1983) on the reaction $2cz + ky + q = 4an + H_2O$ together with the experiments of Liou (1973) and Holdaway (1972) on $4cz + q = 5an + gr + H_2O$ and the activity model for epidote described above allow retrieval of an enthalpy of formation for clinozoisite which is consistent with the experiments of Holland (1984) and a preliminary survey of coexisting clino- and orthozoisite assemblages from nature.

Thermodynamic data for meionite, especially its entropy, are now very much better constrained through the experiments of Baker & Newton (1994) on the reactions $3an + cc = me$ and $gr + cc + 2ky + q = me$. Their brackets for the first reaction agree with, but are tighter than, the older data of Goldsmith & Newton (1977). Constraints on lawsonite stability have been augmented by the experiments of Schmidt & Poli (1994) on the reaction $2law + dsp = zo + ky + 4H_2O$, and those of Skrok *et al.* (1994) on the reaction $4law = 2zo + ky + coe + 7H_2O$.

Although the data set agrees with almost all the experimental reactions available in this system, several problem equilibria still remain. Of the two available reactions involving prehnite, the brackets of Chatterjee *et al.* (1984) for $pre = an + wo + H_2O$ and those of Connolly & Kerrick (1985) for $5pre = 2zo + 2gr + 3q + 4H_2O$ are mutually inconsistent. It is not at all clear which of the two competing studies should be chosen, and future experimental work will be required to resolve this discrepancy. The brackets of Hoschek (1974) on the reaction $wo + cc + an = gr + CO_2$, the experiments of Allen & Fawcett (1982) on the reaction $2zo + CO_2 = 3an + cc + H_2O$, and the experiments on the reaction $cc + q + and/ky = an + CO_2$ (Jacobs & Kerrick, 1981) currently cannot be fitted closely with the data set.

$MgO–Al_2O_3–SiO_2$

New end-members in this subsystem are sapphirine, gedrite, sudoite and osumilite. The sapphirine end-members 442-sapphirine and 793-sapphirine have been added to the data set using the experiments of Chatterjee & Schreyer (1972), Hensen (1972), Ackermand *et al.* (1975), Doroshev & Malinovskiy (1974), Seifert (1974) and Newton (pers. comm. 1989). At present the sapphirine data are not consistent with all the experiments in the MASH subsystem, most notably with the quartz-saturated assemblages. It may be that order–disorder behaviour in sapphirine will need accounting for before agreement is complete. Because no data exist for the composition of sapphirine at the end of the experimental runs, an ideal mixing on sites model involving the two sapphirine end-members was used with an iterative approach to generate the equilibrium composition of sapphirine for each experiment. Thus the sapphirine data are to be treated as provisional. Preliminary data for Na-free aluminous gedrite have been added using the experimental data of Schreyer & Seifert (1969), and for sudoite using the data of Vidal *et al.* (1992) and Fransolet & Schreyer (1984).

Al contents of talc from the reversal experiments of Hoschek (1995) were used to refine the enthalpy of the tschermak's talc end-member. Magnesium staurolite data are now more reliable than in HP90 for two reasons. First, the entropy of Mg–staurolite in HP90 was in error and has now been corrected to the value from the entropy estimation model of Holland (1989). Secondly, the enthalpies are now extracted from the better documented high-pressure experiments of Massonne (1995) and Chopin & Sobolev (1995). As already discussed above, the cordierite–H_2O model now incorporates the experimental data of Skippen & Gunter (1996), and uses the measured C_p of Carey (1993) for hydrous cordierite (hcrd) and the calorimetric measurements on cordierite hydration enthalpy from Carey & Navrotsky (1992).

The revised heat capacity model for spinel, taken as an oxide sum with a non-convergent Landau excess added, using the results of Carpenter & Salje (1994a), has made it possible to satisfy the recent palladium solubility measurements of Chamberlin *et al.* (1995) as well as the high-pressure phase equilibria. As a workable approximation, aluminous orthopyroxenes were modelled as ideal solutions of enstatite and Mg–tschermak's pyroxene ($a_{en} = X_{en}$, $a_{mgts} = X_{mgts}$).

Data for the osumilite end-members have been added, following the study of Holland *et al.* (1996). In this study the enthalpies are retrieved entirely from the experimental results of Carrington & Harley (1995), using the mixing model given in Holland *et al.* (1996a).

$CaO–MgO–Al_2O_3–SiO_2$

The hornblende end-member of HP90 has been removed from the data set and replaced with tschermakite. Using the mixing model described earlier, the experimental data on alumina content of amphiboles of Jenkins (1994) on both silica-saturated and -undersaturated assemblages ($tr + di + an + q$, $tr + fo + sp$) as well as the much higher pressure data of Hoschek (1995) on the assemblage ($tr + q + ky + zo$) are simultaneously satisfied (see Fig. 5). Vesuvianite data are derived from the experiments of Hochella *et al.* (1982).

$Na_2O–Al_2O_3–SiO_2$

The only new end-member in this subsystem is analcite, and its enthalpy was retrieved from the experiments of

Manghnani (1970) on the reaction jd + H_2O = anl, and the brackets of Thompson (1971) and Liou (1971c) on the reaction anl + q = abh + H_2O. The entropy of high albite has been raised by adding 2 J mol^{-1} onto the simple tricritical Landau model for albite disordering. An error in the molar volume for nepheline in HP90 led to an unreasonable enthalpy of formation; correction of this error now leads to a derived enthalpy which agrees well with the high-temperature calorimetry of Navrotsky *et al.* (1980).

K_2O–Al_2O_3–SiO_2

All of the experimental results in this subsystem are in good agreement with the thermodynamic data. The potassium feldspars are treated in terms of a simple first order phase transition between microcline and sanidine at 452 °C, a simplification based on the results of the analysis of Carpenter & Salje (1994b).

K_2O–MgO–Al_2O_3–SiO_2

Phlogopite data, consistent with the calorimetry of Circone & Navrotsky (1992), now agree perfectly with the experiments of Peterson & Newton (1990) for 2phl + 6q = 3en + 2san + $2H_2O$, but only marginally with the experiments of Wood (1976) on the same reaction. The agreement with the experiments of Bohlen *et al.* (1983) is less good. Eastonite data are provisional, and are based on the approximate compositions of biotite coexisting with phengite, sanidine and quartz at 5 kbar and 700 °C in the diagrams of Massonne & Schreyer (1987), using the equilibrium 3mu + 2phl = 3east + 2san + 3q + $2H_2O$. The non-ideal mixing model discussed earlier was used.

The celadonite enthalpy was derived from the experiments of Massonne & Schreyer (1989) on the equilibria 2ta + 6mu + 4q/coe = 6 cel + 6ky + $2H_2O$. The resulting data are in reasonable agreement with the experiments of Massonne & Schreyer (1987) and Velde (1965) on the equilibria 3cel = phl + 2san + 3q + $2H_2O$ and of Massonne & Schreyer (1987) on the equilibrium 3mu + 2phl = 3east + 2san + 3q + $2H_2O$. However, the calculated curve for the talc + muscovite breakdown curve ta + mu = phl + ky + 3q + H_2O does not agree well with the experiments of Massonne & Schreyer (1989), signalling that thermodynamic modelling of phengites and aluminous biotites requires further work.

K_2O–Na_2O–CaO–MgO–Al_2O_3–SiO_2

Pargasite enthalpy is now fitted to the experimental data of Lykins & Jenkins (1993) for the reaction 2parg + 5en = 2di + 8fo + 2an + 2abh + $2H_2O$. The composition of the amphiboles were shown by Lykins & Jenkins (1993) to be close to pargasite, in contrast to the experiments of Sharma (1995) which involved tremolitic amphiboles with a small pargasite component. Therefore it would be unwise to extract thermodynamic data for pargasite from the experiments of Sharma (1995), especially as there probably exists a large miscibility gap between the tremolitic and pargasitic ends of the solid solution series.

FeO–SiO_2

The new end-member in this subsystem is goethite, and its enthalpy has been derived from the high-pressure experiments of Voigt & Will (1981) on the reaction 2gth = hem + H_2O.

The data for fayalite, quartz, magnetite, hematite and iron are now in excellent agreement with the experiments of Bohlen *et al.* (1980), Chou (1978), Myers & Eugster (1983), Hewitt (1978), and especially O'Neill (1987, 1988). Siderite enthalpy is now fitted to the experiments of Koziol & Newton (1993) on the reaction sid + hem = mt + CO_2.

Deerite data are fitted to the experiments of Lattard & LeBreton (1994) for the reactions 2 deer = 9fs + 6mt + 6q + $10H_2O$ and deer + Ni = 6fs + 2mt + NiO + $5H_2O$. Grunerite data are derived from the experiments of Lattard & Evans (1992) on the reactions 2grun = 7fs + 2q + $2H_2O$ and 2grun = 7fa + 9q + $2H_2O$.

FeO–Al_2O_3–SiO_2

The almandine enthalpy is based largely on the reaction alm + 3hem = 3mt + ky + 2q determined experimentally by Harlov & Newton (1992). The calculated slope fitted to the iron cordierite breakdown reaction 2alm + 4sill + 5q = 3fcrd in HP90 had a positive slope relative to the earlier experimental brackets on this reaction. However, the more recent experiments of Mukhopadhyay & Holdaway (1994) have confirmed the positive slope for this breakdown reaction. These data for Fe-cordierite are in excellent agreement with the Fe–Mg exchange equilibrium experiments of Perchuk & Lavrent'eva (1983) for garnet–cordierite, as shown below.

A model for staurolite involving variable H_2O contents (as suggested by Holdaway *et al.*, 1995) was found to be successful at fitting most of the equilibria involving Fe- and Mg-rich staurolites. However, this model has not been included here because (a) the simpler model of HP90 gave almost indistinguishable *P–T* locations for all equilibria, and (b) the activity models used involve assumptions about site distributions for Fe, Mg, Al, Si and H in natural and synthetic staurolites which are probably not well enough understood (Hawthorne *et al.*, 1993) to make robust activity estimates. Most of the experimental equilibria, other than those of Richardson (1968), involving garnet, staurolite and chloritoid are quite well fitted by the data. The recent high-pressure equilibria on chloritoid stability from Vidal *et al.* (1994) are very well fitted.

K_2O–Na_2O–FeO–Al_2O_3–SiO_2

Riebeckite thermodynamic data are now fitted to experiments of Ernst (1962) for the reaction rieb + 3hem = 2acm + 3mt + 4q + H_2O. This equilibrium relies on the availability of data for acmite, which were retrieved on the basis of the reaction 2acm + pa + 2q = 3ab + hem + H_2O. No experiments are available for this reaction, but it has occurred in the Eastern Alps at around 9 kbar and 450 °C (Holland & Ray, 1985) in an assemblage with pure albite, hematite, paragonite and a sodic pyroxene of composition $jadeite_{44}acmite_{56}$. Thus data for both acmite and riebeckite must be regarded as provisional.

Data for ferroglaucophane are now fitted to the experiments of Hoffmann (1972) on the reaction 2fgl = 4abh + 3fa + q + 2H_2O. These data are in agreement with the Fe–Mg exchange equilibria seen in natural assemblages (see below).

Data for annite, derived from the exchange reaction of Ferry & Spear (1978), also fit the experiments of Holdaway & Lee (1977) for the reaction 2ann + 6sill + 9q = 2san + 3fcrd + 2H_2O.

CaO–FeO–Al_2O_3–SiO_2

This subsystem includes the problematic relations involving andradite, epidote and hedenbergite. It has not been possible to derive data which will satisfy all the experiments, probably because of the unknown extent of ferric and ferrous iron incorporation into wollastonite and ferric iron into hedenbergite in the experiments at high temperatures. However, the andradite data are consistent with the experiments of Huckenholz & Yoder (1971) for the reaction andr = 3pswo + hem, and of Gustafson (1974) and Moecher & Chou (1990) for the reaction 6andr = 4mt + 18wo + O_2, as well as the data of Liou (1973) and Holdaway (1972) on coexisting epidote and garnet in their epidote breakdown experiments. Reactions involving andradite with hedenbergite did not yield consistent data when compared with the exchange equilibria involving clino- and orthopyroxenes (see below).

Ferroactinolite was derived from the experiments of Ernst (1966) on the reaction 2fact = 3fa + 5q + 4hed + 2H_2O. These data are also nicely consistent with Fe–Mg exchange equilibrium seen in natural assemblages (see below).

Equilibria for phases containing Ni, Ti or Zr

New phases in this subsystem are nickel, nickel oxide (bunsenite), zircon, baddeleyite, geikielite and pyrophanite. For both nickel and nickel oxide, a Landau excess heat capacity was used to model their lambda anomalies. The experimental data of O'Neill (1987) was used to derive the enthalpy of formation of nickel oxide. Data for zircon were added using the reaction zrc = bdy + q from Robie *et al.* (1978). The geikielite enthalpy was derived from the experiments of Haselton *et al.* (1978) on the reaction mag + ru = geik + CO_2. Pyrophanite data were retrieved from the experimental exchange data of Pownceby *et al.* (1987) on the equilibrium spss + 3ilm = alm + 3pnt.

Ilmenite and ulvospinel data have been further refined through inclusion of the experiments of O'Neill *et al.* (1988) for the reactions 2ilm = 2iron + 2ru + O_2 and 2usp = 2ilm + 2iron + O_2 in the fitting process. The entropy of ulvospinel was changed to 175 J K^{-1} on the basis of arguments in O'Neill *et al.* (1988). The data for sphene was also fitted to the experiments of Manning & Bohlen (1991) for the reaction sph + ky = an + ru.

Exchange equilibria

Exchange equilibria can be fruitful sources of thermodynamic data for end-members which only occur as solid solutions. They are of most practical use when the two solid solutions are relatively simple (e.g. just Fe–Mg mixing in each) and where the mixing properties of at least one is well known. In more complex solutions, the uncertainties may be too large to make these equilibria useful for extracting thermodynamic data. Consider the exchange of Fe and Mg between phases *A* and *B*, each being a simple regular solution, expressed as a one-site phase:

$$\mathrm{Fe}(A) + \mathrm{Mg}(B) = \mathrm{Mg}(A) + \mathrm{Fe}(B)$$

$$K_\mathrm{D} = \frac{X^B_\mathrm{Fe} X^\mathrm{A}_\mathrm{Mg}}{X^\mathrm{B}_\mathrm{Mg} X^\mathrm{A}_\mathrm{Fe}}$$

$$\mathrm{R}T\ln K = \mathrm{R}T\ln K_\mathrm{D} + W_{A(2}X^A_\mathrm{Fe} - 1) - W_B(2X^B_\mathrm{Fe} - 1).$$

If the mixing properties of one phase, say *A*, are known then $\mathrm{R}T\ln K_\mathrm{D}$ becomes a linear function of $2X^B_\mathrm{Fe} - 1$, and a plot will yield both the free energy of reaction ($-\mathrm{R}T\ln K$) and the magnitude of W_B. If the composition of phase *B* is very close to $X^B_\mathrm{Fe} = 0.5$ the last term in the expression above vanishes. These considerations have been used to extract enthalpies (and a consistent set of *W* terms) from Fe–Mg exchange reactions. If one of the phases is a ternary or higher order solid solution, further terms come into play and care is required. For example if phase *B* is a garnet containing variable quantities of Ca, then $\mathrm{R}T\ln K_\mathrm{D}$ is a strong function of the Ca content, and this, unless adequately accounted for, can lead to serious uncertainties.

Phases whose enthalpies rely on Fe–Mg exchange equilibria are ankerite, annite, Fe–celadonite, hedenbergite, magnesioferrite, Fe–anthophyllite, daphnite, Fe–sapphirine, Fe–carpholite, Fe–sudoite and Fe–talc. Experimental partition data of Dalton & Wood (1993) at 1000 °C on olivine–carbonate experiments were used to derive data for ankerite and to confirm the data for siderite. Taking a value for $W_\mathrm{ol} = 4.2$ kJ leads to $W_\mathrm{mag} = 4.0$ kJ and $W_\mathrm{dol} = 3.0$ kJ (all values on a one-site basis).

These values are also consistent with the lower-temperature partitioning data on dolomite–magnesite exchange (Rosenberg, 1967) and the natural data for dolomite–magnesite of Anovitz & Essene (1987).

The experimental data of Ferry & Spear (1978) on the reaction py + ann = alm + phl were used together with $W_{gt} = 0.8$ kJ and $W_{bi} = 3.0$ kJ. The experiments of Perchuk & Lavrent'eva (1983) are not consistent with this analysis, probably because they involved much more aluminous biotites, and were not used. For hedenbergite, two sets of equilibria were used, those of Lindsley (1983) on 2hed + en = fs + 2di and those of Perkins & Vielzeuf (1992) on 2hed + fo = fa + 2di and are consistent with $W_{cpx} = 2.5$ and $W_{opx} = 0.5$. For magnesioferrite, the experiments of Jamieson & Roeder (1984) on the equilibrium fa + 2mft = 2mt + fo were used, and the value for K was taken directly from the analysis of Nell & Wood (1989). For Fe-anthophyllite, the partitioning data were taken from natural assemblages at low-temperature granulite grade (5 kbar, 725 °C) for the equilibrium 7en + 2fanth = 2anth + 7fs.

For daphnite, the Fe–Mg partitioning between garnet and chlorite and between chlorite and biotite used in HP90 are consistent with the analysis of a larger suite of samples by Dickenson & Hewitt (1986). Therefore the daphnite enthalpy has been derived from partitioning using the expression of Dickenson & Hewitt (in Laird, 1989) for the reaction 5alm + 3clin = 5py + 3daph, and from the equilibrium 5phl + 3daph = 5ann + 3clin (Laird, 1989). As a mutual check on such equilibria, the natural chlorite–actinolite partitioning (Laird, 1982) for the equilibrium clin + fact = tr + daph was also fitted successfully. This last reaction makes a link back to hedenbergite via the experiments of Ernst (1966) on the reaction 2fact = 3fa + 5q + 4hed + $2H_2O$ discussed above, and shows that the exchange data in the laboratory at high temperatures, the end-member experiments and the low-temperature natural exchange data are all mutually compatible.

Data for Fe–sapphirine were taken from the cordierite–sapphirine partitioning in Waters (1986) for the reaction 4spr7 + 7fcrd = 4fspr + 7crd. The data for Fe–osumilite were taken from the study of Holland *et al.* (1996a) using the partitioning of osumilite with orthopyroxene and with cordierite. The entropy of Fe–osumilite has been corrected to 762 J mol^{-1} by incorporation of the magnetic contribution erroneously omitted in Holland *et al.* (1996a). For Fe-talc the natural partitioning in eclogites from Chinner & Dixon (1974), Chopin & Monie (1984) and Miller (1986) for talc–chloritoid pairs was used. Data for ferrocarpholite were derived from natural partitioning between chloritoid and carpholite using analyses from Seidel & Okrusch (1977) and Theye *et al.* (1992). Finally, the enthalpy for Fe–sudoite is taken from the sudoite–chlorite partitioning measured by Theye *et al.* (1992).

Experimental and natural partitioning data have also been used to check for consistency, rather than in deriving enthalpies, in several other equilibria. Good agreement of the data set is found with the garnet–olivine data of O'Neill & Wood (1979) and Hackler & Wood (1989), the olivine–orthopyroxene experiments of von Seckendorff & O'Neill (1993), the garnet–orthopyroxene experiments of Lee & Ganguly (1988), the garnet–cordierite experiments of Perchuk & Lavrent'eva (1983) and the biotite–orthopyroxene experiments of Fonarev & Konilov (1986). The olivine–spinel exchange experiments of Engi (1983) and Jamieson & Roeder (1984) are not reproduced well with the current data set, the problem possibly stemming from the variable disordering state in the spinels.

Mn minerals

Mn-bearing phases were introduced into the data set of HP90, but were limited to few usable end-members through lack of suitable experiments linking garnet to other common phases. The recent experimental study of Wood *et al.* (1994) on exchange equilibria between olivine and oxides, fo + 2mang = teph + 2per, and between olivine and garnets, 2spss + 3fo = 2py + 3teph, has allowed the incorporation of a much more reliable set of data for Mn phases. The enthalpy for spessartine was retrieved from the experiments of Wood *et al.* (1994), using their derived mixing properties for both olivine and garnet. Their study of the exchange of Mg and Mn between olivine and oxides provides a powerful check on the quality of mutual agreement between calorimetric and phase equilibrium data. With the enthalpy of spessartine known, the enthalpies of several other Mn-bearing end-members were extracted from measured partitioning in natural assemblages. The results of Mahar *et al.* (1997) were incorporated into this data set, using the methods outlined in that paper. As stated above, the data for Mn–biotite, Mn–chlorite, Mn–staurolite, Mn–cordierite and Mn–chloritoid are to be taken as those of fictive end-members which mix ideally with the real Fe and Mg end-members in the dilute composition ranges found in typical metamorphosed metapelitic rocks. The data for the other Mn end-members, however, refer to the accessible real phases (e.g. manganosite, spessartine, pyrophanite, rhodonite, pyroxmangite, rhodochrosite and tephroite).

Melt phases

Melt phases have been discussed above, and here it is merely noted that the phase equilibria used (melting curves of end-member silicates) are all well reproduced by the data set. The data for melts of sillimanite composition are based on an approximate melting temperature (Holland & Carpenter, 1986), and are provisional. Because the molar proportion of sillimanite liquid in any practical calculation for melting of common mineral assemblages is likely to be very small, the uncertainty will probably not contribute much

error. More serious is the crude assumption that the heat capacities of the melt components are constant, and this could lead to problems when applying such melt models at the low temperatures involved in wet silica-saturated systems.

Aqueous species

Aqueous species and the modified density model were discussed above. A preliminary list of aqueous species includes H^+, Na^+, K^+, Ca^{++}, Mg^{++}, Fe^{++}, Al^{3+}, CO_3^{2-}, OH^-, Cl^-, HCl°, $NaCl^\circ$, KCl°, $CaCl_2^\circ$, $MgCl_2^\circ$, $FeCl_2^\circ$, $CaCl^+$, $MgCl^+$, KOH°, $Al(OH)_3^\circ$, $Al(OH)_4^-$. Thermodynamic data for the simple ionic species are taken from the tabulations of Shock & Helgeson (1988), but the properties of the complexes have been derived by fitting the high-pressure and high-temperature dissociation data for HCl° to the data of Ruaya & Seward (1987) and Sverjensky *et al.* (1991), for $NaCl^\circ$ to the data of Quist & Marshall (1968), for KCl° to the data in Oelkers & Helgeson (1988), for $CaCl^+$ and $MgCl^+$ to the data of Frantz & Marshall (1982, 1984) at high pressures and to the low-pressure data in Ruaya (1988). The data for $CaCl_2^\circ$ were derived from the data of Williams-Jones & Seward (1989) at low temperatures; on the basis of the results of Ruaya (1988), $MgCl_2^\circ$ is assumed to behave identically at low temperatures to $CaCl_2^\circ$. At temperatures above 600 °C, where the neutral $CaCl_2^\circ$ and $MgCl_2^\circ$ complexes dominate, the experiments of Frantz & Popp (1979) and Popp & Frantz (1979) were used. Molar volumes for the Mg and Ca chloride complexes were taken from Sverjensky *et al.* (1997). The data for $FeCl_2^\circ$ were derived from the dissociation experiments of Fein *et al.* (1992). The tabulations of Oelkers & Helgeson (1988) were also used in constraining the enthalpies and entropies of KCl° and $NaCl^\circ$. The data for KOH° are taken from Sverjensky *et al.* (1991), and those for $Al(OH)_3^\circ$ and $Al(OH)_4^-$ are from Castet *et al.* (1993). The data for the CO_3^{2-} ion are in excellent agreement with the calcite and aragonite solubility measurements of Plummer & Busenberg (1982) over the range 20–90 °C (Fig. 6).

Thermodynamic data for aqueous silica were derived, using the modified density model, to the quartz solubility measurements of Anderson & Burnham (1965), Walther & Orville (1983), Walther & Helgeson (1977), Manning (1994) and the recent low-temperature study of Rimstidt (1997) for the equilibrium q = aqSi. The model has been fitted to the experiments from 25 to 900 °C and 0.001 to 20 kbar, with an average absolute deviation of 0.02 in logarithm of the silica molality.

PETROLOGICAL EXAMPLES INVOLVING CALCULATED PHASE EQUILIBRIA

The calculations presented in this section are to show that the new Holland & Powell data set, used with the software THERMOCALC (Powell & Holland, 1988; Powell *et al.*, 1998), allows increasingly sophisticated phase equilibrium calculations, so that natural systems can be more closely modelled. Look in the JMG web site for the THERMOCALC data files to run these and other phase equilibrium calculations, and look in one of the web sites, e.g. http://www.geol.umd.edu/, for the current version of THERMOCALC to run them. As these petrological examples are to illustrate types of calculations, the assumptions involved, particularly as regards *a–X* relationships used, although plausible, are presented with little discussion.

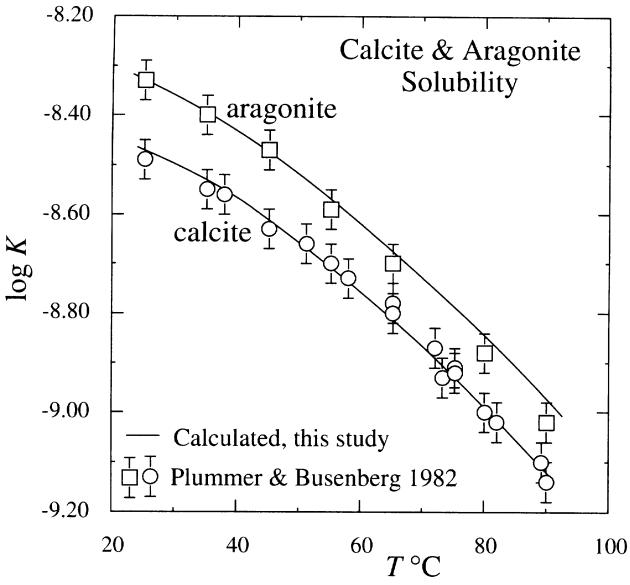

Fig. 6. Calculated curves and experimentally determined values for the equilibrium constant for the reaction $CaCO_3 = Ca^{++} + CO_3^{2-}$. The open symbols are the experimental values from Plummer & Busenberg (1982), with uncertainty brackets estimated from the spread in their data.

A first example, involving melting, is a further application of the simple model of Holland *et al.* (1996a) to examine the consequences of varying the absolute amounts of water on the melting relations of a pelitic bulk composition in the KFMASH system. A T–X_{H_2O} pseudosection for $P = 6$ kbar was calculated for a pelitic rock of bulk composition varying from $Al_2O_3 = 46.25$, $MgO = 16.83$, $FeO = 25.24$, $K_2O = 11.68$, $H_2O = 0.0$ ($X_w = 0$) to $Al_2O_3 = 31.62$, $MgO = 11.50$, $FeO = 17.26$, $K_2O = 7.99$, $H_2O = 31.62$ ($X_w = 1$). This series represents addition of H_2O to a fixed anhydrous pelite composition lying just above the garnet–cordierite tie line on an AFM projection (from ksp + q) and with $Fe/Fe + Mg = 0.6$. The lines and points on such T–X pseudosections can now be calculated directly in THERMOCALC (Powell *et al.*, 1998). The beginning of melting for low water content compositions involves the univariant reaction

$$50bi + 71sill + 308q = 10g + 42cd + 18ksp + 84liq$$

which is expressed in Fig. 7 as a horizontal line at

803 °C (with the reaction coefficients being those calculated at 6 kbar). This is the biotite dehydration–melting reaction commonly invoked for an important melting step in pelites, as well as for the beginning of the granulite facies. At larger water contents, melting can occur at temperatures lower than this univariant line, via quadrivariant, trivariant and divariant assemblages. Although melting in pelitic systems is commonly envisaged in terms of two alternative scenarios, water-saturated melting on the one hand and fluid-absent dehydration melting on the other, variations in water content of the protolith (through previous metamorphic cycles, for example) can lead to a large variety of assemblages in the melting process. It is clear from this diagram that the melting relations in rock–water systems (even for fixed composition of the silicate part) are complex, with many different assemblages accessible over small ranges in temperature or water content. In an experimental context, where the absolute water content may be difficult to control, this feature could lead to possible confusion in interpreting the assemblages seen in run products. In practical applications to melting of pelitic assemblages in nature, typical bulk water contents will lie very close to the biotite + sillimanite + K-feldspar + quartz field (X_w = 0.48) in Fig. 7 because the mineral assemblage is likely to be one involving biotite + sillimanite + K-feldspar + quartz and a tiny amount of melt, at the lowest temperatures of this figure, as a consequence of muscovite dehydration melting at lower temperatures. Such rocks will begin to produce more melt (at 6 kbar in KFMASH) at 790 °C to produce garnet + K-feldspar as products, and then to melt more extensively at 803 °C by losing biotite and producing cordierite.

A second example is the calculation of the basalt–granulite–eclogite transitions in a model NCFMAS silica-saturated aluminous basalt. The example involves only anhydrous relations – the bulk composition will develop hydrous silicates such as amphibole, clinozoisite and chlorite at low temperatures and would melt at high temperatures. The bulk composition used corresponds to an aluminous calcalkali andesitic basalt (in wt%: SiO_2 = 54.5, Al_2O_3 = 19.2, CaO = 8.4, MgO = 6.0, FeO = 8.2, Na_2O = 3.7) with less than 0.5% normative quartz. The phase relations are relatively simple, with alternating quadrivariant and trivariant assemblages as a function of pressure at high temperatures (Fig. 8). The divariant loop closing at 775 °C is due to the miscibility gap involving two coexisting clinopyroxenes, one an ordered omphacitic pyroxene and the other a disordered diopsidic clinopyroxene. The basaltic clinopyroxene + orthopyroxene + plagioclase assemblage gains garnet, and then loses orthopyroxene with rising pressure, before gaining kyanite and then finally losing plagioclase as it enters the eclogite field at highest pressures (Fig. 8). The modal changes as a function of pressure at 800 °C are illustrated in Fig. 9(a), where the major changes are shown by the

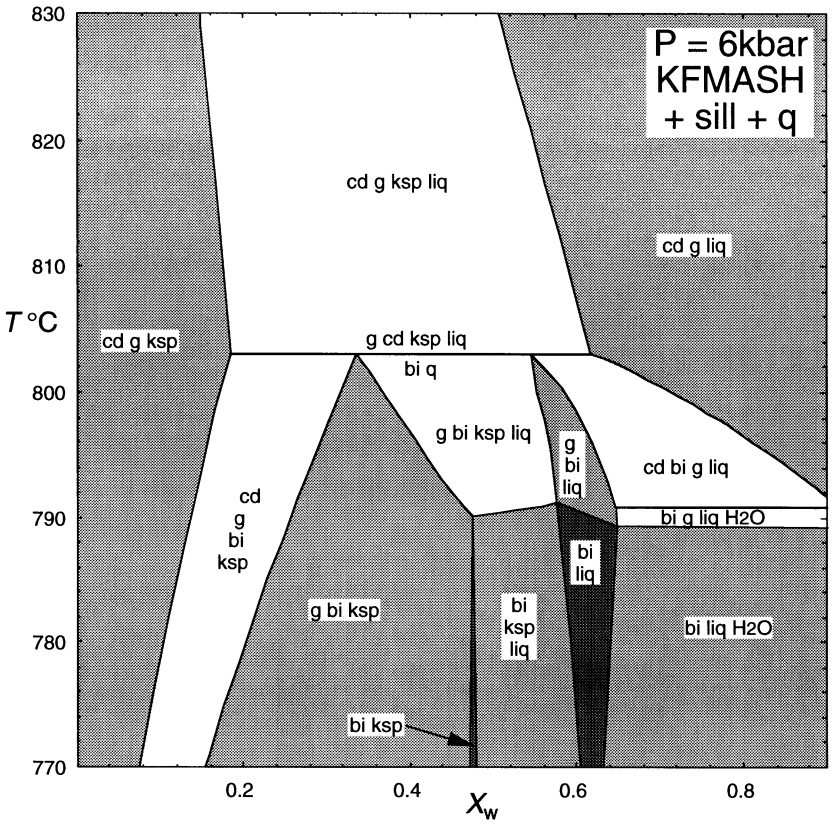

Fig. 7. Partial melting relations of a pelitic composition in KFMASH as a function of H_2O content. The bulk composition varies from Al_2O_3 = 46.25, MgO = 16.83, FeO = 25.24, K_2O = 11.68, H_2O = 0.0 (X_w = 0) to Al_2O_3 = 31.62, MgO = 11.50, FeO = 17.26, K_2O = 7.99, H_2O = 31.62 (X_w = 1). The Fe/Fe + Mg is fixed to be 0.6. At the biotite dehydration melting univariant (803 °C) the Fe/Fe + Mg compositions of the phases are cd 0.40, g 0.79, bi 0.52 and liq 0.87. Divariant fields are white, trivariants are lightly shaded and quadrivariants are in a darker shading.

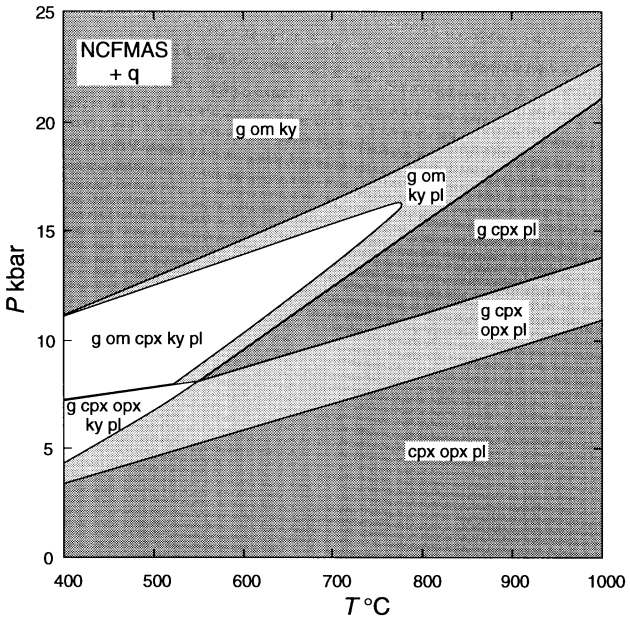

Fig. 8. A P–T pseudosection for an aluminous andesitic basalt bulk composition in NCFMAS given by (in wt%) $SiO_2 = 54.5$, $Al_2O_3 = 19.2$, $CaO = 8.4$, $MgO = 6.0$, $FeO = 8.2$, $Na_2O = 3.7$. Divariant fields are in white, trivariant fields in light grey, quadrivariant fields in dark grey. Below 775 °C, two pyroxenes may coexist, an ordered omphacite and a disordered diopsidic clinopyroxene. Thermodynamics of mixing in omphacite follow Holland & Powell (1996b). Under wet conditions, various hydrous assemblages involving amphibole, clinozoisite and chlorite would become stable at lower temperatures and melting would occur at higher temperatures.

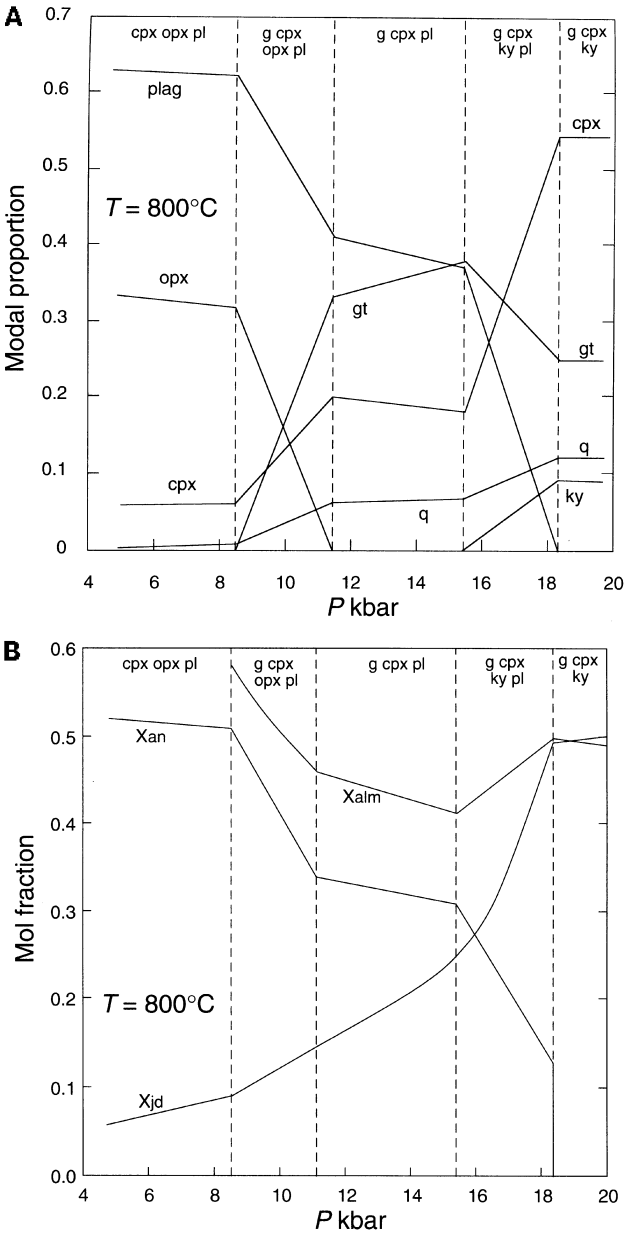

Fig. 9. Compositions and modal variation as a function of pressure at 800 °C for the andesitic basalt of Fig. 8. (a) Modal proportions of garnet, orthopyroxene, clinopyroxene, kyanite, plagioclase and quartz. (b) Compositions of pyroxene (X_{jd}), garnet (X_{alm}) and plagioclase (X_{an}).

increases in clinopyroxene and garnet and the decrease in plagioclase abundances, with dramatic increase in garnet above 8.4 kbar. More dramatic changes in mode take place in the trivariant fields with only minor changes occurring across the quadrivariant fields, as might be expected. Once plagioclase is lost, the kyanite eclogite modes change only slowly, being controlled almost entirely by bulk composition. The compositions of the garnet, pyroxene and plagioclase at 800 °C are shown in Fig. 9(b) where the pyroxene becomes increasingly rich in jadeite component with pressure until the plagioclase-out boundary at 18.3 kbar. The anorthite content in plagioclase decreases from 0.52 in a stepwise fashion until it reaches 0.13 at the eclogite boundary where plagioclase reacts out. The garnet contains between 15 and 18% grossular over the whole pressure range illustrated, and its almandine content shows a steady decrease until the kyanite granulite field where it starts to increase again before decreasing again slowly in the eclogite field.

The mixing properties used for the solid solutions were as follows: garnet was modelled as a non-ideal regular solution with all interaction energies set to zero except for $W_{CaMg} = 11$ kJ per mixing atom. Orthopyroxene was modelled as an ideal one-site solid solution of enstatite, magnesium tschermakite and ferrosilite with a fictive orthodiopside end-member made by incrementing the enthalpy of diopside by 30 kJ to keep the calcium content to the low values of the two-pyroxene solvus. Clinopyroxene was modelled using the symmetric formalism for order–disorder in omphacitic pyroxenes from Holland & Powell (1996b) together with the assumption that the jadeite–hedenbergite system behaves identically to the jadeite–diopside system; the small amount of enstatite and calcium tschermak components below 800 °C are ignored here. Plagioclase was modelled using the simple DQF model for $C\bar{1}$ from Holland & Powell

(1992), in which albite mixes with a fictive anorthite end-member whose Gibbs energy is incremented by 6.01–0.0035TkJ.

These calculations are important because they provide reliable constraints on the slopes of these granulite to eclogite transition boundaries, and they make it clear that quartz–kyanite eclogites will not form in continental crust of normal thickness. Indeed, the minimum pressure required to stabilize kyanite eclogite at 600 °C (as in many tectonic environments such as the Alps) is more than 14 or 15 kbar.

ACKNOWLEDGEMENTS

We thank E. Essene and J. Cheney for their very helpful and much appreciated comments and suggestions for improvement of the manuscript. B. Hemingway is thanked for valuable suggestions concerning the enthalpies of formation of sodium and potassium silicates. We thank A. Koziol for her kind provision of experimental data on decarbonation equilibria on magnesite and siderite.

REFERENCES

Ackermand, D., Seifert, F. & Schreyer, W., 1975. Instability of sapphirine at high pressures. *Contributions to Mineralogy and Petrology*, **50,** 79–92.

Allen, J. M. & Fawcett, J. J., 1982. Zoisite-anorthite-calcite stability relations in H_2O-CO_2 fluids at 5000 bars: An experimental and SEM study. *Journal of Petrology*, **23,** 215–239.

Anderson, G. M. & Burnham, C. W., 1965. The solubility of quartz in supercritical water. *American Journal of Science*, **263,** 494–511.

Anderson, G. M., Castet, S., Schott, J. & Mesmer, R. E., 1991. The density model for estimation of thermodynamic parameters of reactions at high temperatures and pressures. *Geochimica et Cosmochimica Acta*, **55,** 1769–1779.

Anderson, P. A. M. & Kleppa, O. J., 1969. The thermochemistry of the kyanite-sillimanite equilibrium. *American Journal of Science*, **267,** 285–290.

Anderson, P. A. M., Newton, R. C. & Kleppa, O. J., 1977. The enthalpy change of the andalusite-sillimanite reaction and the Al_2SiO_5 diagram. *American Journal of Science*, **277,** 585–593.

Angel, R. J., Hazen, R. M., McCormick, T. C., Prewitt, C .T. & Smyth, J. R., 1988. Comparative compressibility of end-member feldspars. *Physics and Chemistry of Minerals*, **15,** 313–318.

Anovitz, L. M. & Essene, E. J., 1987. Phase equilibria in the system $CaCO_3$-$MgCO_3$-$FeCO_3$. *Journal of Petrology*, **28,** 389–414.

Aranovich, L. Y. & Newton, R. C., 1996. H_2O activity in concentrated NaCl solutions at high pressures and temperatures measured by the brucite-periclase equilibrium. *Contributions to Mineralogy and Petrology*, **125,** 200–212.

Baker, J., 1995. Thermal expansion of scapolite. *American Mineralogist*, **79,** 878–884.

Baker, J. & Holland, T. J. B., 1996. Experimental reversals of chlorite compositions in divariant MgO-Al_2O_3-SiO_2-H_2O assemblages: implications for order-disorder in chlorites. *American Mineralogist*, **81,** 676–684.

Baker, J. & Newton, R. C., 1994. Standard thermodynamic properties of meionite, $Ca_4Al_6Si_6O_{24}CO_3$, from experimental phase equilibria. *American Mineralogist*, **79,** 478–484.

Bass, J. D., 1986. Elasticity of uvarovite and andradite garnets. *Journal of Geophysical Research*, **91,** 7505–7516.

Bass, J. D., 1989. Elasticity of grossular and spessartite garnets by Brilloiun spectroscopy. *Journal of Geophysical Research*, **94,** 7621–7628.

Berman, R. G., 1988. Internally-consistent thermodynamic data for minerals in the system Na_2O-K_2O-CaO-MgO-FeO-Fe_2O_3-Al_2O_3-SiO_2-TiO_2-H_2O-CO_2. *Journal of Petrology*, **29,** 445–522.

Berman, R. G. & Brown, T. H., 1987. Development of models for multicomponent melts: analysis of synthetic systems. In: *Reviews in Mineralogy* (eds Carmichael, I. S. E & Eugster, H. P.), **17,** 405–442.

Birch, F., 1966. Compressibility; elastic constants. In: Handbook of Physical Constants (ed. Clark, S. P.): *Geological Society of America Memoir*, **97,** 97–173.

Bird, D. K. & Helgeson, H. C., 1980. Chemical interaction of aqueous solutions with epidote-feldspar mineral assemblages in geologic systems. 1. Thermodynamic analysis of phase relations in the system CaO-FeO-Fe_2O_3-Al_2O_3-SiO_2-H_2O-CO_2. *American Journal of Science*, **280,** 907–941.

Bohlen, S. R. & Boettcher, A. L., 1982. The quartz-coesite transformation: A precise determination and the effects of other components. *Journal of Geophysical Research*, **87,** 7073–7078.

Bohlen, S. R., Essene, E. J. & Boettcher, A. L., 1980. Reinvestigation and application of olivine-quartz-orthopyroxene barometry. *Earth and Planetary Science Letters*, **47,** 1–10.

Bohlen, S. R., Boettcher, A. L., Wall, V. J. & Clemens, J. D., 1983. Stability of phlogopite-quartz and sanidine-quartz: A model for melting in the lower crust. *Contributions to Mineralogy and Petrology*, **83,** 270–277.

Bose, K. & Ganguly, J., 1995. Quartz-coesite transition revisited: reversed experimental determination at 500–1200 °C and retrieved thermochemical properties. *American Mineralogist*, **80,** 231–238.

Bottinga, Y., 1991. Thermodynamic properties of silicate liquids at high pressure and their bearing on igneous petrology, In: *Physical Chemistry of Magmas* (eds Perchuk, L. & Kushiro, I.): *Advances in Physical Geochemistry*, **9,** 213–232.

Bowen, N. L., 1915. Crystallisation of haplobasaltic, haplodioritic, and related magmas. *American Journal of Science*, **40,** 161–185.

Bowman, A. F., 1975. An investigation of Al_2SiO_5 phase equilibrium utilizing the scanning electron microscope. *MS thesis, University of Oregon, Eugene, Oregon, USA*.

Brace, W. F., Scholz, C. H. & La Mori, P. N., 1969. Isothermal compressibility of kyanite, andalusite and sillimanite from synthetic aggregates. *Journal of Geophysical Research*, **74,** 2089–2098.

Brey, G., Brice, W. R., Ellis, D. J., Green, D. H., Harris, K. L. & Ryabchikov, I. D., 1983. Pyroxene-carbonate reactions in the upper mantle. *Earth and Planetary Science Letters*, **62,** 63–74.

Brousse, C., Newton, R. C. & Kleppa, O. J., 1984. Enthalpy of formation of forsterite, enstatite, akermanite, monticellite and merwinite at 1073K determined by alkali borate solution calorimetry. *Geochimica et Cosmochimica Acta*, **48,** 1081–1088.

Burnham, C. W. & Davis, N. F., 1971. The role of H_2O in silicate melts: I. P–V–T relations in the system $NaAlSi_3O_8$–H_2O to 10 kilobars and 1000 °C. *American Journal of Science*, **270,** 54–79.

Burnham, C. W. & Davis, N. F., 1974. The role of H_2O in silicate melts: II. Thermodynamic and phase relations in the system $NaAlSi_3O_8$–H_2O to 10 kilobars, 700 °C to 1000 °C. *American Journal of Science*, **274,** 902–940.

Carey, J. W., 1993. The heat capacity of hydrous cordierite above 295 K. *Physics and Chemistry of Minerals*, **19,** 578–583.

Carey, J. W. & Navrotsky, A., 1992. The molar enthalpy of dehydration of cordierite. *American Mineralogist*, **77,** 930–936.

Carman, J. H., 1974. Synthetic sodium phlogopite and its two hydrates: Stabilities, properties and mineralogic implications. *American Mineralogist*, **59,** 261–273.

Carpenter, M. A., 1992. Equilibrium Thermodynamics of Al/Si

ordering in anorthite. *Physics and Chemistry of Minerals*, **19,** 1–24.
Carpenter, M. A. & Salje, E. K. H., 1994a. Thermodynamics of non-convergent cation ordering in minerals, II: spinels and the orthopyroxene solid solution. *American Mineralogist*, **79,** 1068–1083.
Carpenter, M. A. & Salje, E. K. H., 1994b. Thermodynamics of non-convergent cation ordering in minerals, III: order parameter coupling in K-feldspar. *American Mineralogist*, **79,** 1084–1098.
Carrington, D. P. & Harley, S. L., 1995. Partial melting and phase relations in high-grade metapelites: an experimental petrogenetic grid in KFMASH system. *Contributions to Mineralogy and Petrology*, **120,** 270–291.
Castet, S., Dandurand, J. L., Schott, J. & Gout, R., 1993. Boehmite solubility and aqueous aluminium speciation in hydrothermal solutions (90–350 °C): experimental data and modelling. *Geochimica et Cosmochimica Acta*, **57,** 4869–4884.
Catti, M., Ferraris, G., Hull, S. & Pavese, A., 1995. Static compression and disorder in brucite, $Mg(OH)_2$, to 11 GPa: a powder neutron diffraction study. *Physics and Chemistry of Minerals*, **22,** 200–206.
Chai, L. & Navrotsky, A., 1993. Thermochemistry of carbonate-pyroxene equilibria. *Contributions to Mineralogy and Petrology*, **114,** 139–147.
Chamberlin, L., Beckett, J. R. & Stolper, E., 1995. Palladium oxide equilibration and the thermodynamic properties of $MgAl_2O_4$ spinel. *American Mineralogist*, **80,** 285–296.
Charlu, T. V., Newton, R. C. & Kleppa, O. J., 1975. Enthalpies of formation at 970 K of compounds in the system MgO-Al_2O_3-SiO_2 from high temperature solution calorimetry. *Geochimica et Cosmochimica Acta*, **39,** 487–497.
Charlu, T. V., Newton, R. C. & Kleppa, O. J., 1978. Enthalpy of formation of some lime silicates by high temperature solution calorimetry, with discussion of high pressure phase equilibria. *Geochimica et Cosmochimica Acta*, **42,** 367–375.
Chatillon-Colinet, C., Kleppa, O. J., Newton, R. C. & Perkins, D. III., 1983. Enthalpy of formation of $Fe_3Al_2Si_3O_{12}$ (almandine) by high temperature alkali borate solution calorimetry. *Geochimica et Cosmochimica Acta*, **47,** 439–444.
Chatterjee, N. D., 1976. Margarite stability and compatibility relations in the system CaO-Al_2O_3-SiO_2-H_2O as a pressure-temperature indicator. *American Mineralogist*, **61,** 699–709.
Chatterjee, N. D. & Schreyer, W., 1972. The reaction enstatite + sillimanite = sapphirine + quartz in the system MgO-Al_2O_3-SiO_2. *Contributions to Mineralogy and Petrology*, **36,** 49–62.
Chatterjee, N. D., Johannes, W. & Leistner, H., 1984. The system CaO-Al_2O_3-SiO_2-H_2O: New phase equilibria data, some calculated phase relations, and their petrological applications. *Contributions to Mineralogy and Petrology*, **88,** 1–13.
Chinner, G. A. & Dixon, J. E., 1974. Some high pressure parageneses of the Allalin Gabbro, Valais, Switzerland. *Journal of Petrology*, **14,** 185–202.
Cho, M., Maruyama, S. & Liou, J. G., 1987. An experimental investigation of heulandite-laumontite equilibrium at 1000 and 2000 bar P_{fluid}. *Contributions to Mineralogy and Petrology*, **97,** 43–50.
Chopin, C. & Monie, P., 1984. A unique magnesiochloritoid-bearing, high pressure assemblage from the Monte Rosa: a petrologic and ^{40}Ar-^{39}Ar study. *Contributions to Mineralogy and Petrology*, **87,** 388–398.
Chopin, C. & Schreyer, W., 1983. Magnesiocarpholite and magnesiochloritoid: Two index minerals of pelitic blueschists and their preliminary phase relations in the model system MgO-Al_2O_3-SiO_2-H_2O. *American Journal of Science*, **283A,** 72–96.
Chopin, C. & Sobolev, N. V., 1995. Principal mineralogical indicators of UHP in crustal rocks. In: *Ultrahigh Pressure Metamorphism* (eds Coleman, R. G. & Wang, X.), pp. 96–131. Cambridge University Press.
Chou, I. M., 1978. Calibration of oxygen buffers at elevated P and T using the hydrogen fugacity sensor. *American Mineralogist*, **63,** 690–703.
Christy, A. G., Phillips, B. L., Güttler, B. K. & Kirkpatrick, R. J., 1992. A ^{27}Al and ^{29}Si MAS NMR and infrared spectroscopic study of Al-Si ordering in natural and synthetic sapphirine. *American Mineralogist*, **77,** 8–18.
Circone, S. & Navrotsky, A., 1992. Substitution of Al in phlogopite: High temperature solution calorimetry, heat capacities, and thermodynamic properties of the phlogopite-eastonite join. *American Mineralogist*, **77,** 1191–1205.
Clark, S. P., 1966. High pressure phase equilibria. In: *Handbook of Physical Constants* (ed. Clark, S. P.): *Geological Society of America Memoir*, **97,** 345–370.
Comodi, P., Mellini, M., Ungaretti, L. & Zanazzi, P. F., 1991a. Compressibility and high pressure structure refinement of tremolite, pargasite, and glaucophane. *European Journal of Mineralogy*, **3,** 485–499.
Comodi, P., Mellini, M. & Zanazzi, P. F., 1991b. Magnesiochloritoid: compressibility and high pressure structure refinement. *Physics and Chemistry of Minerals*, **18,** 483–490.
Comodi, P. & Zanazzi, P. F., 1994. High pressure structural study of muscovite. IMA 16th General Meeting, Pisa, abstracts, 79–80.
Comodi, P. & Zanazzi, P. F., 1996. Effects of temperature and pressure on the structure of lawsonite. *American Mineralogist*, **81,** 833–841.
Comodi, P. & Zanazzi, P. F., 1997. The pressure behaviour of clinozoisite and zoisite: an X-ray diffraction study. *American Mineralogist*, **82,** 61–68.
Connolly, J. A. D. & Kerrick, D. M., 1985. Experimental and thermodynamic analysis of prehnite. *EOS*, **66,** 388.
Dalton, J. A. & Wood, B. J., 1993. The partitioning of Fe and Mg between olivine and carbonate and the stability of carbonate under mantle conditions. *Contributions to Mineralogy and Petrology*, **114,** 501–509.
Dalton, J. A. & Wood, B. J., 1995. The stability of carbonate under upper mantle conditions as a function of temperature and oxygen fugacity. *European Journal of Mineralogy*, **7,** 883–891.
Davidson, P. M., Symmes, G. H., Cohen, B. A., Reeder, R. J. & Lindsley, D. H., 1993. Synthesis of the new compound $CaFe(CO_3)_2$ and experimental constraints on the $(Ca,Fe)CO_3$ join. *Geochimica et Cosmochimica Acta*, **57,** 5105–5109.
Davies, P. K. & Navrotsky, A., 1983. Quantitative correlations of deviations from ideality in binary and pseudo-binary solid solutions. *Journal of Solid State Chemistry*, **46,** 1–22.
Dickenson, M. P. & Hewitt, D., 1986. A garnet-chlorite geothermometer. *Geological Society of America Abstracts with Programs*, **18,** 584.
Dollase, W., 1973. Mössbauer spectra and iron distribution in the epidote-group minerals. *Zeitschrift für Kristallographie*, **138,** 41–63.
Dorogokupets, P. I., 1995. Equation of state for lambda transition in quartz. *Journal of Geophysical Research*, **100,** 8489–8499.
Doroshev, A. M. & Malinovskiy, I. Y., 1974. Upper pressure limit of stability of sapphirine. *Doklady Akad Nauk SSSR*, **219,** 136–138.
Downs, R. T., Zha, C-S., Duffy, T. S. & Finger, L. W., 1996. The equation of state of forsterite to 17.2 GPa and effects of pressure media. *American Mineralogist*, **81,** 51–55.
Duffy, C. J. & Greenwood, H. J., 1979. Phase equilibria in the system MgO-MgF_2-SiO_2-H_2O. *American Mineralogist*, **64,** 1156–1174.
Engi, M., 1983. Equilibria involving Al-Cr spinel: Mg-Fe exchange with olivine. Experiments, thermodynamic analysis, and consequences for geothermometry. *American Journal of Science*, **283A,** 29–71.
Ernst, W. G., 1962. Synthesis, stability relations, and occurrence of riebeckite and riebeckite-arfvedsonite solid solutions. *Journal of Geology*, **70,** 689–736.
Ernst, W. G., 1966. Synthesis and stability relations of ferrotremolite. *American Journal of Science*, **264,** 37–65.
Evans, B. W. & Ghiorso, M. S., 1995. Thermodynamics and

petrology of cummingtonite. *American Mineralogist*, **80,** 649–663.

Evans, B. W., Johannes, W., Oterdoom, W. H. & Trommsdorff, V., 1976. Stability of chrysotile and antigorite in the serpentine multisystem. *Schweizerische Mineralogische Petrologische Mitteilungen*, **56,** 79–93.

Fein, J. B., Hemley, J. J., d'Angelo, W. M., Komninou, A. & Sverjensky, D. A., 1992. Experimental study of iron-chloride complexing in hydrothermal fluids. *Geochimica et Cosmochimica Acta*, **56,** 3179–3190.

Ferry, J. M. & Spear, F. S., 1978. Experimental calibration of the partitioning of Fe and Mg between biotite and garnet. *Contributions to Mineralogy and Petrology*, **66,** 113–117.

Finger, L. W. & Hazen, R. M., 1978. Crystal structure and compression of ruby to 46 kbars. *Journal of Applied Physics*, **49,** 5823–5826.

Finger, L. W. & Hazen, R. M., 1980. Crystal structure and isothermal compression of Fe_2O_3, Cr_2O_3, and V_2O_3 to 50 kbars. *Journal of Applied Physics*, **51,** 5362–5367.

Finger, L. W., Hazen, R. M. & Hofmeister, A., 1986. High pressure crystal chemistry of spinel ($MgAl_2O_4$) and magnetite (Fe_3O_4): comparisons with other silicate spinels. *Physics and Chemistry of Minerals*, **13,** 215–220.

Finger, L. W. & Ohashi, Y., 1976. The thermal expansion of diopside to 800 °C and a refinement of the crystal structure at 700 °C. *American Mineralogist*, **61,** 303–310.

Fonarev, V. I. & Konilov, A. N., 1986. Experimental study of Fe–Mg distribution between biotite and orthopyroxene. *Contributions to Mineralogy and Petrology*, **93,** 227–235.

Fonarev, V. I. & Korolkov, G. J., 1980. The assemblage orthopyroxene + cummingtonite + quartz. The low-temperature stability limit. *Contributions to Mineralogy and Petrology*, **73,** 413–420.

Fransolet, A. M. & Schreyer, W., 1984. Sudoite, di/trioctahedral chlorite: a stable low-temperature phase in the system MgO-Al_2O_3-H_2O. *Contributions to Mineralogy and Petrology*, **86,** 409–417.

Frantz, J. D. & Marshall, W. D., 1982. Electrical conductances and ionization constants of salts, acids and bases in aqueous solutions at temperatures to 600 °C and pressures to 4000 bars. *American Journal of Science*, **284,** 611–667.

Frantz, J. D. & Marshall, W. D., 1984. Electrical conductances and ionization constants of calcium chloride and magnesium chloride in supercritical aqueous fluids: 1. Hydrochloric acid from 100 °C to 700 °C and at pressures up to 4000 bars. *American Journal of Science*, **284,** 611–667.

Frantz, J. D. & Popp, R. K., 1979. Mineral-solution equilibria – 1. An experimental study of complexing and thermodynamic properties of aqueous $MgCl_2$ in the system MgO-SiO_2-H_2O-HCl. *Geochimica et Cosmochimica Acta*, **43,** 1223–1239.

Gasparik, T. & Newton, R. C., 1984. The reversed alumina contents of orthopyroxene in equilibrium with spinel and forsterite in the system MgO-Al_2O_3-SiO_2. *Contributions to Mineralogy and Petrology*, **85,** 186–196.

Ghiorso, M. S. & Sack, R. O., 1995. Chemical mass transfer in magmatic processes IV. A revised and internally consistent thermodynamic model for the interpretation and extrapolation of liquid-solid equilibria in magmatic systems at elevated temperatures and pressures. *Contributions to Mineralogy and Petrology*, **119,** 197–212.

Goldsmith, J. R., 1980. Thermal stability of dolomite at high temperatures and pressures. *Journal of Geophysical Research*, **85,** 6949–6954.

Goldsmith, J. R. & Jenkins, D. M., 1985. The hydrothermal melting of low and high albite. *American Mineralogist*, **70,** 924–933.

Goldsmith, J. R. & Newton, R. C., 1977. Scapolite-plagioclase stability relations at high pressures and temperatures in the system $NaAlSi_3O_8$-$CaAl_2Si_2O_8$-$CaCO_3$-$CaSO_4$. *American Mineralogist*, **62,** 1063–1081.

Gottschalk, M., 1997. Internally consistent thermodynamic data for rock forming minerals. *European Journal of Mineralogy*, **9,** 175–223.

Greenwood, H. J., 1967. Wollastonite: Stability in H_2O-CO_2 mixtures and occurrence in a contact-metamorphic aureole near Salmo, British Columbia, Canada. *American Mineralogist*, **52,** 1669–1680.

Grevel, K.-D., Fockenberg, T., Wunder, B. & Burchard, M., 1994. Experimental determination of the equilibrium curve 2 diaspore = corundum + H_2O to high pressures and modified thermodynamic data for diaspore. *Terra Nova Abstract Supplement*, 20.

Grundy, H. D. & Brown, W. L., 1974. A high temperature X-ray study of low and high plagioclase feldspars. In: *The Feldspars* (eds MacKenzie, W. S. & Zussman, J.), pp. 162–173. Proceedings of a NATO Advanced Study Institute. University of Manchester Press.

Guggenheim, S., Chang, Y. H. & Koster Van Groos, A. F., 1987. Muscovite dehydroxylation: high-temperature studies. *American Mineralogist*, **72,** 537–550.

Gustafson, W., 1974. The stability of andradite, hedenbergite, and related minerals in the system Ca-Fe-Si-O-H. *Journal of Petrology*, **15,** 455–496.

Hackler, R. T. & Wood, B. J., 1989. Experimental determination of Fe and Mg exchange between garnet and olivine and estimation of Fe-Mg mixing properties in garnet. *American Mineralogist*, **74,** 994–999.

Harker, R. I., 1959. The synthesis and stability of tilleyite, $Ca_5Si_2O_7(CO_3)_2$. *American Journal of Science*, **257,** 656–667.

Harker, R. I. & Tuttle, O. F., 1956. Experimental data on the PCO_2-T curve for the reaction: calcite + quartz = wollastonite + carbon dioxide. *American Journal of Science*, **254,** 239–256.

Harlov, D. E. & Newton, R. C., 1992. Experimental determination of the reaction 2 magnetite + 2 kyanite + 4 quartz = 2 almandine + O_2 at high pressure on the magnetite-hematite buffer. *American Mineralogist*, **77,** 558–564.

Harlov, D. E. & Newton, R. C., 1993. Reversal of the metastable kyanite + corundum + quartz and andalusite + corundum + quartz equilibria and the enthalpy of formation of kyanite and andalusite. *American Mineralogist*, **78,** 594–600.

Harrison, R. J., 1997. Magnetic properties of the magnetite-spinel solid solution. *PhD thesis, University of Cambridge*.

Haselton, H. T. & Cygan, G. L., 1988. Stability of muscovite in HCl-KCl solutions: tetrahedral site disorder. *EOS*, **69,** 529.

Haselton, H. T., Sharp, W. R. & Newton, R. C., 1978. CO_2 fugacity at high temperatures and pressures from experimental decarbonation reactions. *Geophysical Research Letters*, **5,** 753–756.

Haselton, H. T., Hemingway, B. S. & Robie, R. A., 1984. Low temperature heat capacities of $CaAl_2SiO_6$ glass and pyroxene and thermal expansion of $CaAl_2SiO_6$ pyroxene. *American Mineralogist*, **69,** 481–489.

Haselton, H. T., Robie, R. A. & Hemingway, B. S., 1987. Heat capacities of synthetic hedenbergite, ferrobustamite and $CaFeSi_2O_6$ glass. *Geochimica et Cosmochimica Acta*, **51,** 2211–2217.

Hawthorne, F. C., Ungaretti, L., Oberti, R., Caucia, F. & Callegari, A., 1993. The crystal chemistry of staurolite: I. Crystal structure and site occupancies. *Canadian Mineralogist*, **31,** 551–582.

Hazen, R. M., 1976. Effects of temperature and pressure on the crystal structure of forsterite. *American Mineralogist*, **61,** 1280–1293.

Hazen, R. M., Downs, R. T., Conrad, P. G., Finger, L. W. & Gasparik, T., 1994. Comparative compressibilities of majorite-type garnets. *Physics and Chemistry of Minerals*, **21,** 344–349.

Hazen, R. M. & Finger, L. W., 1978. The crystal structures and compressibilities of layer minerals at high pressure. II. Phlogopite and chlorite. *American Mineralogist*, **63,** 293–296.

Hazen, R. M. & Finger, L. W., 1981. Bulk moduli and high-pressure crystal structures of rutile-type compounds. *Journal of Physics and Chemistry of Solids*, **42,** 143–151.

Hazen, R. M. & Finger, L. W., 1989. The crystal chemistry of andradite and pyrope: revised procedures for high-pressure diffraction experiments. *American Mineralogist*, **74,** 352–359.

Hazen, R. M. & Sharp, Z. D., 1988. Compressibility of sodalite and scapolite. *American Mineralogist*, **73,** 1120–1122.

Helgeson, H. C., Delany, J. M., Nesbitt, H. W. & Bird, D. K., 1978. Summary and critique of the thermodynamic properties of rock-forming minerals. *American Journal of Science*, **278A,** 229.

Hemingway, B. S. & Robie, R. A., 1984. Heat capacity and thermodynamic functions for gehlenite and staurolite: With comments on the Schottky anomaly in the heat capacity of staurolite. *American Mineralogist*, **69,** 307–318.

Hemingway, B. S., Evans, H. T., Nord, G. L., Haselton, H. T., Robie, R. A. & McGee, J. J., 1986. Akermanite: Phase transitions in heat capacity and thermal expansion, and revised thermodynamic data. *Canadian Mineralogist*, **24,** 425–434.

Hemley, J. J., Marinenko, J. W. & Luce, R. W., 1980. Equilibria in the system Al_2O_3-SiO_2-H_2O and some general implications for alteration/mineralisation processes. *Economic Geology*, **75,** 210–228.

Henderson, C. M. B. & Taylor, D., 1988. The structural behaviour of the nepheline family: (3) Thermal expansion of kalsilite. *Mineralogical Magazine*, **52,** 708–710.

Hensen, B. J., 1972. Phase relations involving pyrope, enstatite$_{ss}$, and sapphirine$_{ss}$ in the system MgO-Al_2O_3-SiO_2. *Carnegie Institution of Washington Yearbook*, **71,** 421–427.

Hewitt, D. A., 1975. Stability of the assemblage phlogopite-calcite-quartz. *American Mineralogist*, **60,** 391–397.

Hewitt, D. A., 1978. A redetermination of the fayalite-magnetite-quartz equilibrium between 650 °C and 850 °C. *American Journal of Science*, **278,** 715–724.

Hewitt, D. A. & Wones, D. R., 1975. Physical properties of some synthetic Fe-Mg-Al trioctahedral biotites. *American Mineralogist*, **60,** 854–862.

Higgins, J. B. & Ribbe, P. H., 1979. Sapphirine II: A neutron and X-ray diffraction study of Mg-Al and Al-Si ordering in monoclinic sapphirine. *Contributions to Mineralogy and Petrology*, **68,** 357–368.

Hochella, M. F., Liou, J. G., Keskinen, M. J. & Kim, H. S., 1982. Synthesis and stability relations of magnesian idocrase. *Economic Geology*, **77,** 798–808.

Hoffmann, C., 1972. Natural and synthetic ferroglaucophane. *Contributions to Mineralogy and Petrology*, **34,** 135–149.

Holdaway, M. J., 1971. Stability of andalusite and the aluminum silicate phase diagram. *American Journal of Science*, **271,** 97–131.

Holdaway, M. J., 1972. Thermal stability of Al-Fe epidote as a function of f_{O2} and Fe content. *Contributions to Mineralogy and Petrology*, **37,** 307–340.

Holdaway, M. J. & Lee, S. M., 1977. Fe-Mg cordierite stability in high-grade pelitic rocks based on experimental, theoretical and natural observations. *Contributions to Mineralogy and Petrology*, **63,** 175–198.

Holdaway, M. J., Mukhopadhyay, B. & Dutrow, B. L., 1995. Thermodynamic properties of stoichiometric staurolite $H_2Fe_4Al_{18}Si_8O_{48}$ and $H_6Fe_2Al_{18}Si_8O_{48}$. *American Mineralogist*, **80,** 520–533.

Holland, T. J. B., 1979. Experimental determination of the reaction paragonite = jadeite + kyanite + quartz + water, and internally consistent thermodynamic data for part of the system Na_2O-Al_2O_3-SiO_2-H_2O, with applications to eclogites and blueschists. *Contributions to Mineralogy and Petrology*, **68,** 293–301.

Holland, T. J. B., 1984. Stability relations of ortho- and clinozoisite. *Natural Environment Research Council Progress Report for Research*, **6,** 185–186.

Holland, T. J. B., 1988. Preliminary phase relations involving glaucophane and applications to high pressure petrology: new heat capacity and thermodynamic data. *Contributions to Mineralogy and Petrology*, **99,** 134–142.

Holland, T. J. B., 1989. The dependence of entropy on volume for silicate and oxide minerals: a review and a predictive model. *American Mineralogist*, **74,** 5–13.

Holland, T. J. B. & Carpenter, M. A., 1986. Aluminium/silicon disordering and melting in sillimanite at high pressures. *Nature*, **320,** 151–153.

Holland, T. J. B. & Powell, R., 1985. An internally consistent thermodynamic dataset with uncertainties and correlations: 2. Data and results. *Journal of Metamorphic Geology*, **3,** 343–370.

Holland, T. J. B. & Powell, R., 1990. An internally-consistent thermodynamic dataset with uncertainties and correlations: the system Na_2O-K_2O-CaO-MgO-MnO-FeO-Fe_2O_3-Al_2O_3-SiO_2-TiO_2-C-H_2-O_2. *Journal of Metamorphic Geology*, **8,** 89–124.

Holland, T. J. B. & Powell, R., 1991. A Compensated-Redlich-Kwong (CORK) equation for volumes and fugacities of CO_2 and H_2O in the range 1 bar to 50 kbar and 100–1600 °C. *Contributions to Mineralogy and Petrology*, **109,** 265–273.

Holland, T. J. B. & Powell, R., 1992. Plagioclase feldspars: activity-composition relations based upon Darken's Quadratic Formalism and Landau theory. *American Mineralogist*, **77,** 53–61.

Holland, T. J. B. & Powell, R., 1996a. Thermodynamics of order-disorder in Minerals 1: symmetric formalism applied to minerals of fixed composition. *American Mineralogist*, **81,** 1413–1424.

Holland, T. J. B. & Powell, R., 1996b. Thermodynamics of order-disorder in Minerals 2: symmetric formalism applied to solid solutions. *American Mineralogist*, **81,** 1425–1437.

Holland, T. J. B. & Ray, N. J., 1985. Glaucophane and pyroxene breakdown reactions in the Pennine units of the eastern Alps. *Journal of Metamorphic Geology*, **3,** 417–438.

Holland, T. J. B., Babu, E. V. S. S. K. & Waters, D. J., 1996a. Phase relations of osumilite and dehydration melting in pelitic rocks: a simple thermodynamic model for the KFMASH system. *Contributions to Mineralogy and Petrology*, **124,** 383–394.

Holland, T. J. B., Baker, J. M. & Powell, R., 1998. Mixing properties and activity–composition relationships of chlorites in the system MgO-FeO-Al_2O_3-SiO_2-H_2O. *European Journal of Mineralogy* (in press).

Holland, T. J. B., Redfern S. A. T. & Pawley A. R., 1996b. Volume behaviour of hydrous minerals at high pressure and temperature: 2. Compressibilities of lawsonite, zoisite, clinozoisite and epidote. *American Mineralogist*, **81,** 341–348.

Holm, J. L. & Kleppa, O. J., 1966. The thermodynamic properties of the aluminum silicates. *American Mineralogist*, **51,** 1608–1622.

Hoschek, G., 1974. Gehlenite stability in the system CaO-Al_2O_3-SiO_2-H_2O-CO_2. *Contributions to Mineralogy and Petrology*, **47,** 245–254.

Hoschek, G., 1995. Stability relations and Al content of tremolite and talc in CMASH assemblages with kyanite + zoisite + quartz + H_2O. *European Journal of Mineralogy*, **7,** 353–362.

Hsu, L. C., 1968. Selected phase relationships in the system Al-Mn-Fe-Si-O; a model for garnet equilibria. *Journal of Petrology*, **9,** 40–83.

Huckenholz, H. G. & Yoder, H. S., 1971. Andradite stability relations in the $CaSiO_3$-Fe_2O_3 join up to 30 kb. *Neues Jahrbuch für Mineralogie Abhandlungen*, **114,** 246–280.

Irving, A. J. & Wyllie, P. J., 1975. Subsolidus and melting relationships for calcite, magnesite, and the join $CaCO_3$-$MgCO_3$ to 36 kb. *Geochimica et Cosmochimica Acta*, **39,** 35–53.

Isaak, D. G., Graham, E. K., Bass, J. D. & Wang, H., 1993. The elastic properties of single-crystal fayalite as determined by dynamical measurement techniques. *Pure and Applied Geophysics*, **141,** 393–414.

Ito, H., Kawada, K. & Akimoto, S., 1974. Thermal expansion of stishovite. *Physics of the Earth and Planetary Interiors*, **8,** 277–281.

Ivaldi, G., Catti, M. & Ferraris, G., 1988. Crystal structure at 25 and 700° of magnesiochloritoid from a high pressure assemblage (Monte Rosa). *American Mineralogist*, **73,** 358–364.

Jackson, I., 1976. Melting of the silica isotypes SiO_2, BeF_2 and GeO_2 at elevated pressures. *Physics of the Earth and Planetary Interiors*, **13,** 218–231.

Jacobs, G. K. & Kerrick, D. M., 1981. Devolatilisation equilibria in H_2O-CO_2 and H_2O-CO_2-NaCl fluids: an experimental and thermodynamic evaluation at elevated pressures and temperatures. *American Mineralogist*, **66,** 1135–1153.

Jamieson, H. E. & Roeder, P. L., 1984. The distribution of Mg and Fe^{2+} between olivine and spinel at 1300 °C. *American Mineralogist*, **69,** 283–291.

Jenkins, D. M., 1984. Upper pressure stability of synthetic margarite + quartz. *Contributions to Mineralogy and Petrology*, **88,** 332–339.

Jenkins, D. M., 1994. Experimental reversals of the aluminum content of tremolitic amphiboles in the system H_2O-CaO-MgO-Al_2O_3-SiO_2. *American Journal of Science*, **294,** 593–620.

Jenkins, D. M., Newton, R. C. & Goldsmith, J. G., 1983. Fe-free clinozoisite stability relative to zoisite. *Nature*, **304,** 622–623.

Jenkins, D. M., Holland, T. J. B. & Clare, A. K., 1991. Experimental Determination of the Pressure-Temperature Stability Field and Thermochemical Properties of Synthetic Tremolite. *American Mineralogist*, **76,** 458–469.

Johannes, W. & Metz, P., 1968. Experimentelle Bestimmung von Gleichgewichtsbeziehungen im System MgO-CO_2-H_2O. *Neues Jahrbuch für Mineralogie Monatshefte*, **112,** 15–26.

Johannes, W. & Puhan, D., 1971. The calcite-aragonite transition re-investigated. *Contributions to Mineralogy and Petrology*, **31,** 28–38.

Kandelin, J. & Weidner, D. J., 1988. Elastic properties of hedenbergite. *Journal of Geophysical Research*, **93,** 1063–1072.

Karpinskaya, T. B. & Ostrovsky, N. A., 1982. Compressibility of brucite and the reaction of its formation from oxides as related to the possible existence of hydrothermal fluids in the mantle. *International Geology Review*, **24,** 1071–1073.

Käse, H.-R. & Metz, P. 1980. Experimental investigation of the metamorphism of siliceous dolomites. *Contributions to Mineralogy and Petrology*, **73,** 151–159.

Kerrick, D. M. & Heninger, S. G., 1984. The andalusite-sillimanite equilibrium revisited. *Geological Society of America Abstracts with Programs*, **16,** 558.

Khodakovsky, I. L., Westrum, E. F. & Hemingway, B. S., 1990. CODATA, *International Geothermodynamic Tables. Guidelines and a set of prototype tables.*

King, E. G., Barany, R., Weller, W. W. & Pankratz, L. B., 1967. Thermodynamic properties of forsterite and serpentine. *United States Bureau of Mines Report of Investigations*, **6962,** 4320–4321.

Kiseleva, I. A., Ogorodova, L. P., Sidorov, Y. I. & Khodakovsky, I. L., 1990. Thermodynamic properties of alkali feldspars. *Geokhimiya*, **3,** 406–409.

Koziol, A. M. & Newton, R. C., 1993. On the stability of siderite. *EOS*, **74,** 166.

Koziol, A. M. & Newton, R. C., 1995. Experimental determination of the reactions magnesite + quartz = enstatite + CO_2 and magnesite = periclase + CO_2, and enthalpies of formation of enstatite and magnesite. *American Mineralogist*, **80,** 1252–1262.

Koziol, A. M. & Newton, R. C., 1997. Experimental determination of the reaction: magnesite + enstatite = forsterite + CO_2 in the range 6–25 kbar and 700–1100 °C and the enthalpy of formation of forsterite. *American Mineralogist*, (in press).

Kress, V. C. & Carmichael, I. S. E., 1991. The compressibility of silicate liquids containing Fe_2O_3 and the effect of composition, temperature, oxygen fugacity and pressure on their redox states. *Contributions to Mineralogy and Petrology*, **108,** 82–92.

Krupka, K. M., Robie, R. A., Hemingway, B. S., Kerrick, D. M. & Ito, J., 1985a. Low-temperature heat capacities and derived thermodynamic properties of anthophyllite, diopside, enstatite, bronzite and wollastonite. *American Mineralogist*, **70,** 249–260.

Krupka, K. M., Robie, R. A., Hemingway, B. S. & Kerrick, D. M., 1985b. High-temperature heat capacities and derived thermodynamic properties of anthophyllite, diopside, dolomite, enstatite, bronzite, talc, tremolite and wollastonite. *American Mineralogist*, **70,** 261–271.

Lager, G. A. & Meagher, E. P., 1978. High-temperature study of six olivines. *American Mineralogist*, **63,** 365–377.

Laird, J., 1982. Amphiboles in metamorphosed basaltic rocks. In: Amphiboles, *MSA Reviews in Mineralogy*, **9B,** 113–158.

Laird, J., 1989. Chlorites: Metamorphic petrology. In: Hydrous phyllosilicates (exclusive of micas), *MSA Reviews in Mineralogy*, **19,** 405–453.

Lange, R. A. & Carmichael, I. S. E., 1987. Densities of Na_2O-K_2O-CaO-MgO-FeO-Fe_2O_3-Al_2O_3-TiO_2-SiO_2 liquids: New measurements and derived partial molar properties. *Geochimica et Cosmochimica Acta*, **51,** 2931–2946.

Lange, R. A. & Carmichael, I. S. E., 1990. Thermodynamic properties of silicate liquids with emphasis on density, thermal expansion and compressibility. In: Modern methods of igneous petrology: understanding magmatic processes (eds Nicholls, J. & Russel, J. K.): *MSA Reviews in Mineralogy*, **24,** 25–59.

Lange, R. A., Carmichael, I. S. E. & Stebbins, J. F., 1986. Phase transitions in leucite $KAlSi_2O_6$, orthorhombic $KAlSiO_4$, and their iron analogues ($KFeSi_2O_6$, $KFeSiO_4$). *American Mineralogist*, **71,** 937–945.

Lattard, D. & Evans, B. W., 1992. New experiments on the stability of grunerite. *European Journal of Mineralogy*, **4,** 219–238.

Lattard, D. & LeBreton, N., 1994. The P-T-f_{O2} stability of endmember deerite, $Fe^{2+}_{12}Fe^{3+}_{6}Si_{12}O_{40}(OH)_{10}$. *Contributions to Mineralogy and Petrology*, **115,** 474–487.

Lee, H. Y. & Ganguly, J., 1988. Equilibrium compositions of coexisting garnet and orthopyroxene: experimental determinations in the system FeO-MgO-Al_2O_3-SiO_2, and applications. *Journal of Petrology*, **29,** 93–113.

Levien, L. & Prewitt, C. T., 1981. High pressure crystal structure and compressibility of coesite. *American Mineralogist*, **66,** 324–333.

Lindsley, D. H., 1983. Pyroxene thermometry. *American Mineralogist*, **68,** 477–493.

Liou, J. G., 1970. Synthesis and stability relations of wairakite $CaAl_2Si_4O_{12}.2H_2O$. *Contributions to Mineralogy and Petrology*, **27,** 259–282.

Liou, J. G., 1971a. P-T stabilities of laumontite, wairakite, lawsonite, and related minerals in the system $CaAl_2Si_2O_8$-SiO_2-H_2O. *Journal of Petrology*, **12,** 379–411.

Liou, J. G., 1971b. Stilbite-laumontite equilibrium. *Contributions to Mineralogy and Petrology*, **31,** 171–177.

Liou, J. G., 1971c. Analcime equilibria. *Lithos*, **4,** 389–402.

Liou, J. G., 1973. Synthesis and stability relations of epidote, $Ca_2Al_2FeSi_3O_{12}(OH)$. *Journal of Petrology*, **14,** 381–413.

Liu, J., Zheng, J., Navrotsky, A. & Liebermann, R. C., 1996. Calorimetric study of the coesite-stishovite transformation and calculation of the phase boundary. *Physics and Chemistry of Minerals*, **23,** 11–16.

Luce, R. W., Cygan, G. L., Hemley, J. J. & D'Angelo, W. M., 1985. Some mineral stability relations in the system CaO-MgO-SiO_2-H_2O-HCl. *Geochimica et Cosmochimica Acta*, **49,** 525–538.

Luth, R. W., 1995. Experimental determination of the reaction dolomite + 2 coesite = diopside + 2 CO_2 to 6 GPa. *Contributions to Mineralogy and Petrology*, **122,** 152–158.

Lykins, R. W. & Jenkins, D. M., 1993. Experimental determination of pargasite stability relations in the presence of orthopyroxene. *Contributions to Mineralogy and Petrology*, **112,** 405–413.

Mahar, E. M., Baker, J. M., Powell, R. Holland, T. J. B. & Howell, N., 1997. The effect of Mn on mineral stability in metapelites. *Journal of Metamorphic Geology*, **15,** 223–238.

Manghnani, M. H., 1970. Analcite-jadeite phase boundary. *Physics of the Earth and Planetary Interiors*, **3,** 456–461.

Manning, C. E., 1994. The solubility of quartz in H_2O in the lower crust and upper mantle. *Geochimica et Cosmochimica Acta*, **58,** 4831–4839.

Manning, C. E. & Bohlen, S. R., 1991. The reaction titanite + kyanite = anorthite + rutile and titanite-rutile barometry in eclogites. *Contributions to Mineralogy and Petrology*, **109,** 1–9.

Markgraf, S. A. & Reeder, R. J., 1985. High-temperature refinements of calcite and magnesite. *American Mineralogist*, **70,** 590–600.

Martens, R., Rosenhauer, M. & Gehlen, V. K., 1982. Compressibilities of carbonates. In: *Researches in Geoscience* (ed. Schreyer, W.), pp. 215–222. Schweizerbart'sche Verlagsbuchhandlung, Stuttgart.

Martinez, I., Zhang, J. & Reeder, R. J., 1996. In-situ X-ray diffraction at high pressure and high temperature of aragonite and dolomite. Evidence for dolomite breakdown to aragonite and magnesite. *American Mineralogist*, **81,** 611–624.

Massonne, H-J., 1995. Experimental and petrogenetic study of UHPM. In: *Ultrahigh Pressure Metamorphism* (eds Coleman, R. G. & Wang, X.), pp. 33–95. Cambridge University Press.

Massonne, H-J. & Schreyer, W., 1987. Phengite geobarometry based on the limiting assemblage with K-feldspar, phlogopite, and quartz. *Contributions to Mineralogy and Petrology*, **96,** 212–224.

Massonne, H-J. & Schreyer, W., 1989. Stability field of the high pressure assemblage talc + phengite and two new phengite barometers. *European Journal of Mineralogy*, **1,** 391–410.

McCormick, T. C., Hazen, R. M. & Angel, R. J., 1989. Compressibility of omphacite to 60 Kbar: role of vacancies. *American Mineralogist*, **74,** 1287–1292.

Mellini, M., Trommsdorff, V. & Compagnoni, R., 1987. Antigorite polysomatism: behaviour during progressive metamorphism. *Contributions to Mineralogy and Petrology*, **97,** 147–155.

Miller, Ch., 1986. Alpine high-pressure metamorphism in the Eastern Alps. *Schweitzerische Mineralogische und Petrologische Mitteilungen*, **66,** 139–144.

Mirwald, P. W., 1981. Thermal expansion of anhydrous Mg-cordierite between 25 and 950 °C. *Physics and Chemistry of Minerals*, **7,** 268–270.

Mirwald, P. W., Malinowski, M. & Schulz, H., 1984. Isothermal compression of low cordierite to 30 kbar (25 °C). *Physics and Chemistry of Minerals*, **11,** 140–148.

Mirwald, P. W., Maresch, W. V. & Schreyer, W., 1979. Der Wassergehalt von Mg Cordierit zwischen 500 und 800 °C sowie 0, 5, und 11 kbar. *Fortschritte der Mineralogie*, **57,** 462–472.

Moecher, D. P. & Chou, I. M., 1990. Experimental investigation of andradite and hedenbergite equilibria employing the hydrogen sensor technique, with revised estimates of $\Delta_f G$ for andradite and hedenbergite. *American Mineralogist*, **75,** 1327–1341.

Moore, P. B., 1969. The crystal structure of sapphirine. *American Mineralogist*, **54,** 31–49.

Moore, P. B. & Araki, T., 1972. Atomic arrangement of merwinite, $Ca_3Mg[SiO_4]_2$, an unusual dense-packed structure of geophysical interest. *American Mineralogist*, **57,** 1355–1374.

Mukhopadhyay, B. & Holdaway, M. J., 1994. Cordierite-garnet-sillimanite-quartz equilibrium: New experimental calibration in the system FeO-Al_2O_3-SiO_2-H_2O and certain P–T–X_{H_2O} relations. *Contributions to Mineralogy and Petrology*, **116,** 462–472.

Myers, J. & Eugster, H. P., 1983. The system Fe-Si-O: Oxygen buffer calibration to 1500K. *Contributions to Mineralogy and Petrology*, **82,** 75–90.

Navrotsky, A. & Coons, W. E., 1976. Thermochemistry of some pyroxenes and related compounds. *Geochimica et Cosmochimica Acta*, **40,** 1281–1288.

Navrotsky, A., Hon, R., Weill, D. F. & Henry, D. J., 1980. Thermochemistry of glasses and liquids in the systems $CaMgSi_2O_6$-$CaAl_2Si_2O_8$-$NaAlSi_3O_8$, SiO_2-$CaAl_2Si_2O_8$-$NaAlSi_3O_8$ and SiO_2-Al_2O_3-CaO-Na_2O. *Geochimica et Cosmochimica Acta*, **44,** 1409–1423.

Nell, J. & Wood, B. J., 1989. Thermodynamic properties in a multicomponent solid solution involving cation disorder: Fe_3O_4-$MgFe_2O_4$-$FeAl_2O_4$-$MgAl_2O_4$ spinels. *American Mineralogist*, **74,** 1000–1015.

Nelson, D. O. & Guggenheim, S., 1993. Inferred limits to the oxidation of Fe in chlorites: a high-temperature single-crystal X-ray study. *American Mineralogist*, **78,** 1197–1207.

Newton, R. C. & Harlov, D. E., 1993. Standard thermodynamic properties of almandine. *Canadian Mineralogist*, **31,** 391–399.

Nicholls J., 1980. A simple thermodynamic model for estimating the solubility of H_2O in magmas. *Contributions to Mineralogy and Petrology*, **74,** 211–220.

Olinger, B. W., 1977. Compression of forsterite (Mg_2SiO_4) and enstatite ($MgSiO_3$). In: *High-pressure Research. Applications in Geophysics* (eds Manghnani, M. H. & Akimoto, S. I.), pp. 325–334. Academic Press, New York.

O'Neill, H. St. C., 1987a. Free energies of formation of NiO, CoO, Ni_2SiO_4, and Co_2SiO_4. *American Mineralogist*, **72,** 280–291.

O'Neill, H. St. C., 1987b. Quartz-fayalite-iron and quartz-fayalite-magnetite equilibria and the free energy of formation of fayalite (Fe_2SiO_4) and magnetite (Fe_3O_4). *American Mineralogist*, **72,** 67–75.

O'Neill, H. St. C., 1988. Systems Fe-O and Cu-O: thermodynamic data for the equilibria Fe-"FeO", Fe-Fe_3O_4, Fe_3O_4-Fe_2O_3, Cu-Cu_2O, and Cu_2O-CuO from emf measurements. *American Mineralogist*, **73,** 470–486.

O'Neill, H. St. C. & Wood, B. J., 1979. An experimental study of Fe-Mg partitioning between garnet and olivine and its calibration as a geothermometer. *Contributions to Mineralogy and Petrology*, **70,** 59–70.

O'Neill, H. St. C., Pownceby, M. I. & Wall, V. J., 1988. Ilmenite-rutile-iron and ulvospinel-ilmenite-iron equilibria and the thermochemistry of ilmenite ($FeTiO_3$) and ulvospinel. *Geochimica et Cosmochimica Acta*, **52,** 2065–2072.

Oelkers, E. H. & Helgeson, H. C., 1988. Calculation of the thermodynamic and transport properties of aqueous species at high pressures and temperatures: Dissociation constants for supercritical alkali metal halides at temperatures from 400 °C to 800 °C and pressures from 500 to 4000 bars. *Journal of Physical Chemistry*, **92,** 1631–1639.

Ostrovsky, I. A., 1966. PT-diagram of the system SiO_2-H_2O. *Geological Journal*, **5,** 127–134.

Palmer, D. C., Salje, E. K. H. & Schmahl, W. W., 1989. Phase transitions in leucite: X-ray diffraction studies. *Physics and Chemistry of Minerals*, **16,** 714–719.

Pawley, A. R., 1994. The pressure and temperature stability limits of lawsonite: Implications for H_2O recycling in subduction zones. *Contributions to Mineralogy and Petrology*, **118,** 99–108.

Pawley, A. R. & Wood, B. J., 1995. The high pressure stability of talc and 10Åphase: potential storage sites for H_2O in subduction zones. *American Mineralogist*, **80,** 998–1003.

Pawley, A. R. & Wood, B. J., 1996. The low-pressure stability of phase A, $Mg_7Si_2O_8(OH)_6$. *Contributions to Mineralogy and Petrology*, **124,** 90–97.

Pawley, A. R., Redfern, S. A. T. & Holland, T. J. B., 1996. Volume behaviour of hydrous minerals at high pressure and temperature: 1. Thermal expansion of lawsonite, zoisite, clinozoisite and diaspore. *American Mineralogist*, **81,** 335–340.

Pawley, A. R., Redfern, S. A. T. & Wood, B. J., 1995. Thermal expansivities and compressibilities of hydrous phases in the system MgO-SiO_2-H_2O: talc, phase A and 10-Åphase. 340. *Contributions to Mineralogy and Petrology*, **122,** 301–307.

Perchuk, L. L. & Lavrent'eva, I. V., 1983. Experimental investigation of exchange equilibria in the system cordierite-garnet-biotite. In: *Kinetics and Equilibrium in Mineral Reactions*, (ed. Saxena, S. K.), pp. 199–240. Springer Verlag.

Perkins, D. & Vielzeuf, D., 1992. Reinvestigation of fayalite + anorthite = garnet. *Contributions to Mineralogy and Petrology*, **111,** 260–263.

Perkins, D., Westrum, E. F. & Essene, E. J., 1980. The thermodynamic properties and phase relations of some minerals in the system CaO-Al_2O_3-SiO_2-H_2O. *Geochimica et Cosmochimica Acta*, **44,** 61–84.

Peterson, J. W. & Newton, R. C., 1990. Experimental biotite-quartz melting in the KMASH-CO_2 system and the role of CO_2 in the petrogenesis of granites and related rocks. *American Mineralogist*, **75,** 1029–1042.

Plummer, L. N. & Busenberg, E., 1982. The solubilities of calcite, aragonite and vaterite in CO_2–H_2O solutions between 0 and 90 °C, and an evaluation of the aqueous model for $CaCO_3$–CO_2–H_2O. *Geochimica et Cosmochimica Acta*, **46,** 1011–1040.

Poirier, J.-P., 1991. *Introduction to the Earth's Interior*. Cambridge University Press, Cambridge.

Popp, R. K. & Frantz, J. D., 1979. Mineral solution equilibria – II. An experimental study of mineral solubilities and the thermodynamic properties of aqueous $CaCl_2$ in the system CaO-SiO_2-H_2O-HCl. *Geochimica et Cosmochimica Acta*, **43,** 1777–1790.

Powell, R. & Holland, T. J. B., 1985. An internally consistent thermodynamic dataset with uncertainties and correlations: 1. Methods and a worked example. *Journal of Metamorphic Geology*, **3,** 327–342.

Powell, R. & Holland T. J. B., 1988. An internally consistent thermodynamic dataset with uncertainties and correlations: 3. Application methods, worked examples and a computer program. *Journal of Metamorphic Geology*, **6,** 173–204.

Powell, R. & Holland, T. J. B., 1993a. On the formulation of simple mixing models for complex phases. *American Mineralogist*, **78,** 1174–1180.

Powell, R. & Holland, T. J. B., 1993b. The applicability of least squares in the extraction of thermodynamic data from experimentally bracketed mineral equilibria. *American Mineralogist*, **78,** 107–112.

Powell, R., Holland, T. J. B. & Worley, B., 1998. Calculating phase diagrams with THERMOCALC: methods and examples. *Journal of Metamorphic Geology*, **16,** (in press).

Pownceby, M. I., Wall, V. J. & O'Neill, H. St. C., 1987. Fe-Mn partitioning between garnet and ilmenite: experimental calibration and applications. *Contributions to Mineralogy and Petrology*, **97,** 116–126.

Putnis, A., 1992. *Introduction to Mineral Sciences*. Cambridge University Press, Cambridge.

Quist, A. S. & Marshall, W. D., 1968. Electrical conductances of aqueous sodium chloride solutions from 0 to 800 °C and at pressures to 4000 bars. *Journal of Physical Chemistry*, **72,** 684–703.

Ralph, R. L., Finger, L. W., Hazen, R. M. & Ghose, S., 1984. Compressibility and crystal structure of andalusite at high pressure. *American Mineralogist*, **69,** 513–519.

Rao, B. & Johannes, W., 1979. Further data on the stability of staurolite + quartz. *Neues Jahrbuch für Mineralogie Monatshefte*, 437–447.

Reeder, R. J. & Markgraf, S. A., 1986. High-temperature crystal chemistry of dolomite. *American Mineralogist*, **71,** 775–804.

Redfern, S. A. T., Salje, E. & Navrotsky, A., 1989. High-temperature enthalpy at the orientational order-disorder transition in calcite: implications for the calcite/aragonite phase equilibrium. *Contributions to Mineralogy and Petrology*, **101,** 479–484.

Redfern, S. A. T., Wood, B. J. & Henderson, C. M. B., 1993. Static compressibility of magnesite to 20 GPa: implications for MgCO3 in the lower mantle. *Geophysical Research Letters*, **20,** 2099–2102.

Rice, M. H. & Walsh, J. M., 1957. Equation of state of water to 250 kilobars. *Journal of Chemical Physics*, **26,** 824–830.

Richardson, S. W., 1968. Staurolite stability in a part of the system Fe-Al-Si-O-H. *Journal of Petrology*, **9,** 467–488.

Richardson, S. W., Bell, P. M. & Gilbert, M. C., 1968. Kyanite-sillimanite equilibrium between 700 and 1500 °C. *American Journal of Science*, **266,** 513–541.

Richardson, S. W., Gilbert, M. C. & Bell, P. M. 1969. Experimental determination of kyanite-andalusite and andalusite-sillimanite equilibria; the aluminium silicate triple point. *American Journal of Science*, **267,** 259–272.

Richet, P. & Fiquet, G., 1991. High-temperature heat capacity and premelting of minerals in the system MgO-CaO-Al_2O_3-SiO_2. *Journal of Geophysical Research*, **96,** 445–456.

Richet, P., Gillet, P. & Fiquet, G., 1992. Thermodynamic properties of minerals: macroscopic and microscopic approaches. In: *Thermodynamic Data* (ed. Saxena, S.): *Advances in Physical Geochemistry*, **10,** 98–131.

Richet, P., Robie, R. A. & Hemingway, B. S., 1991. Thermodynamic properties of wollastonite, pseudowollastonite and $CaSiO_3$ glass and liquid. *European Journal of Mineralogy*, **3,** 475–484.

Rimstidt, J. D., 1997. Quartz solubility at low temperatures. *Geochimica et Cosmochimica Acta*, **61,** 2553–2538.

Robie, R. A. & Hemingway, B. S., 1995. Thermodynamic properties of minerals and related substances at 298.15 K and 1 bar (10^5 Pascals) pressure and at higher temperatures. *United States Geological Survey Bulletin* No. 2131.

Robie, R. A., Bethke, P. E. & Beardsley, K. M., 1967. Selected X-ray crystallographic data, molar volumes, and densities of minerals and related substances. *United States Geological Survey Bulletin* No. 1248.

Robie, R. A., Hemingway, B. S. & Fisher, J. R., 1978. Thermodynamic properties of minerals and related substances at 298.15 K and 1 bar (10^5 Pascals) pressure and at higher temperatures. *United States Geological Survey Bulletin* No. 1452.

Robie, R. A., Hemingway, B. S. & Takei, H., 1982. Heat capacities and entropies of Mg_2SiO_4, Mn_2SiO_4, and Ca_2SiO_4 between 5 and 380 K. *American Mineralogist*, **67,** 470–482.

Robie, R. A., Zhao, B., Hemingway, B. S. & Barton, M. S., 1987. Heat capacity and thermodynamic properties of andradite garnet, $Ca_3Fe_2Si_3O_{12}$, between 10 and 1000K and revised values for $\Delta_f G^\circ$m (298,15K) of hedenbergite and wollastonite. *Geochimica et Cosmochimica Acta*, **51,** 2219–2224.

Rosenberg, P. E., 1967. Subsolidus relations in the system $CaCO_3$-$MgCO_3$-$FeCO_3$ between 350 and 550 °C. *American Mineralogist*, **52,** 787–797.

Ross, N. L. & Reeder, R. J., 1992. High-pressure structural study of dolomite and ankerite. *American Mineralogist*, **77,** 412–421.

Ruaya, J. D., 1988. Estimation of instability constants of metal chloride complexes in hydrothermal solutions up to 300 °C. *Geochimica et Cosmochimica Acta*, **52,** 1983–1996.

Ruaya, J. D. & Seward, T. M., 1987. The ion-pair constant and other thermodynamic properties of HCl up to 350 °C. *Geochimica et Cosmochimica Acta*, **51,** 121–130.

Sato, Y., Akaogi, M. & Akimoto, S., 1978. Hydrostatic compression of the synthetic garnets pyrope and almandine. *Journal of Geophysical Research*, **83,** 335–338.

Schiffman, P. & Liou, J. G., 1980. Synthesis and stability relations of Mg–Al pumpellyite, $Ca_4Al_5MgSi_6O_{21}(OH)_7$. *Journal of Petrology*, **21,** 441–474.

Schlenker, J. L., Gibbs, G. V., Hill, E. G., Crews, S. S. & Myers, R. H., 1977. Thermal expansion coefficients for indialite, emerald and beryl. *Physics and Chemistry of Minerals*, **1,** 243–255.

Schmidt, M. W. & Poli, S., 1994. The stability of lawsonite and zoisite at high pressures: Experiments in CASH to 92 kbar and implications for the presence of hydrous phases in subducted lithosphere. *Earth and Planetary Science Letters*, **124,** 105–118.

Schreyer, W. & Seifert, F., 1969. High pressure phases in the system MgO-Al_2O_3-SiO_2-H_2O. *American Journal of Science*, **267A,** 407–443.

Seidel, E. & Okrusch, M., 1977. Chloritoid-bearing metapelites associated with glaucophane rocks in western Crete, Greece. *Contributions to Mineralogy and Petrology*, **60,** 321–324.

Seifert, F., 1974. Stability of sapphirine: A study of the aluminous part of the system MgO-Al_2O_3-SiO_2-H_2O. *Journal of Geology*, **82,** 173–204.

Sharma, A., 1995. Experimentally derived thermochemical data for pargasite and reinvestigation of its stability with quartz in the system Na_2O-CaO-MgO-Al_2O_3-SiO_2-H_2O. *Contributions to Mineralogy and Petrology*, **125,** 263–275.

Sharp, Z. D., Essene, E. J., Anovitz, L. M., Metz, G. W., Westrum, E. F., Hemingway, B. S. & Valley, J. W., 1986. The heat capacity of a natural monticellite and phase equilibria in the system CaO-MgO-SiO_2-CO_2, *Geochimica et Cosmochimica Acta*, **50,** 1475–1484.

Shearer, J. A., 1973. Thermochemistry of the garnets and some related compounds. *Unpublished PhD thesis, Department of Chemistry, University of Chicago, USA*.

Shock, E. L. & Helgeson, H. C., 1988. Calculations of the thermodynamic and transport properties of aqueous species at high pressures and temperatures: correlation algorithms for

ionic species and equation of state predictions to 5 kb and 1000 °C. *Geochimica et Cosmochimica Acta*, **52,** 2009–2036.
Skinner, B. J., 1966. Thermal expansion. In: *Handbook of Physical Constants* (ed. Clark, S. P.): *Geological Society of America Memoir*, **97,** 75–96.
Skippen, G. B. & Gunter, A. E., 1996. The thermodynamic properties of H_2O in magnesium and iron cordierite. *Contributions to Mineralogy and Petrology*, **124,** 82–89.
Smyth, J. R., 1975. High-temperature crystal chemistry of fayalite. *American Mineralogist*, **60,** 1092–1097.
Skrok, V., Grevel, K. D. & Schreyer, W., 1994. Die Stabilität von Lawsonit, $CaAl_2(OH)_2.H_2O$, bei Drücken bis zu 50 kbar. *European Journal of Mineralogy*, **6,** 270.
Stebbins, J. F., Carmichael, I. S. E. & Moret, L. H., 1984. Heat capacities and entropies of silicate liquids and glasses. *Contributions to Mineralogy and Petrology*, **86,** 131–148.
Sterner, S. M. & Pitzer, K. S., 1994. An equation of state for carbon dioxide valid from zero to extreme pressures. *Contributions to Mineralogy and Petrology*, **117,** 362–374.
Striefler, M. E. & Barsch, G. R., 1976. Elastic and optical properties of stishovite. *Journal of Geophysical Research*, **81,** 2453.
Sueno, S., Cameron, M., Papike, J. J. & Prewitt, C. T., 1973. The high-temperature crystal chemistry of tremolite. *American Mineralogist*, **58,** 649–664.
Sueno, S., Cameron, M. & Prewitt, C. T., 1976. Orthoferrosilite: High temperature crystal chemistry. *American Mineralogist*, **61,** 38–53.
Sverjensky, D. A., Hemley, J. J. & D'Angelo, W. M., 1991. Thermodynamic assessment of hydrothermal alkali feldspar-mica-aluminosilicate equilibria. *Geochimica et Cosmochimica Acta*, **55,** 989–1004.
Sverjensky, D. A., Shock, E. L. & Helgeson, H. C., 1997. Prediction of the thermodynamic properties of aqueous metal complexes to 1000 °C and 5 kbar. *Geochimica et Cosmochimica Acta*, **61,** 1359–1412.
Takeda, H. & Morosin, B., 1975. Comparison of observed and predicted structural parameters of mica at high temperatures. *Acta Crystallographica*, **B.31,** 2444–2452.
Tequi, C., Robie, R. A., Hemingway, B. S., Neuville, D. R. & Richet, P., 1991. Melting and thermodynamic properties of pyrope ($Mg_3Al_2Si_3O_{12}$). *Geochimica et Cosmochimica Acta*, **55,** 1005–1010.
Theye, T., Seidel, E. & Vidal, O., 1992. Carpholite, sudoite, and chloritoid in low-grade high-pressure metapelites from Crete and the Peloponnese, Greece. *European Journal of Mineralogy*, **4,** 487–507.
Theye, T., Chopin, C., Grevel, K.-D. & Ockenga, E., 1997. The assemblage diaspore + quartz in metamorphic rocks: a petrological, experimental and thermodynamic study. *Journal of Metamorphic Geology*, **15,** 17–28.
Thompson, A. B., 1970. Laumontite equilibria and the zeolite facies. *American Journal of Science*, **269,** 267–275.
Thompson, A. B., 1971. Analcite-albite equilibria at low temperatures. *American Journal of Science*, **271,** 79–92.
Trommsdorff, V. & Connolly, J. A. D., 1990. Constraints on phase diagram topology in the system $CaO\text{-}MgO\text{-}SiO_2\text{-}CO_2\text{-}H_2O$. *Contributions to Mineralogy and Petrology*, **104,** 1–7.
Vaidya, S. N., Bailey, S., Pasternak, T. & Kennedy, G. C., 1973. Compressibility of fifteen minerals to 45 kilobars. *Journal of Geophysical Research*, **78,** 6893–6898.
Velde, B., 1965. Phengite micas: synthesis, stability, and natural occurrence. *American Journal of Science*, **263,** 886–913.
Vidal, O., Goffé, B. & Theye, T., 1992. Experimental study of the stability of sudoite and magnesiocarpholite and calculation of a new petrogenetic grid for the system $MgO\text{-}Al_2O_3\text{-}SiO_2\text{-}H_2O$. *Journal of Metamorphic Geology*, **10,** 603–614.
Vidal, O., Theye, T. & Chopin, C., 1994. Experimental study of chloritoid stability at high pressure and various f_{O2} conditions. *Contributions to Mineralogy and Petrology*, **118,** 256–270.
Viswanathan, K. & Seidel, E., 1979. Crystal chemistry of Fe-Mg Carpholites. *Contributions to Mineralogy and Petrology*, **70,** 41–47.
Voigt, R. & Will, G., 1981. Das System Fe_2O_3–H_2O unter hohen Drucken. *Neues Jahrbuch für Mineralogie Monatshefte*, 89–96.
von Seckendorff, V. & O'Neill, H. St. C., 1993. An experimental study of Fe-Mg partitioning between olivine and orthopyroxene at 1173, 1273 and 1423 K and 1.6 GPa. *Contributions to Mineralogy and Petrology*, **113,** 196–207.
Walther, J. V. & Helgeson, H. C., 1977. Calculation of the thermodynamic properties of aqueous silica and the solubility of quartz and its polymorphs at high pressures and temperatures. *American Journal of Science*, **277,** 1315–1351.
Walther, J. V. & Orville, P. M., 1983. The extraction-quench technique for determination of the thermodynamic properties of solute complexes: application to quartz solubility in fluid mixtures. *American Mineralogist*, **68,** 731–741.
Waters, D. J., 1986. Metamorphic history of sapphirine-bearing and related magnesian gneises from Namaqualand, South Africa. *Journal of Petrology*, **27,** 541–565.
Wechsler, B. A. & Prewitt, C. T., 1984. Crystal structure of ilmenite ($FeTiO_2$) at high temperature and at high pressure. *American Mineralogist*, **69,** 176–185.
Weill, D. F., 1966. Stability relations in the $Al_2O_3\text{-}SiO_2$ system calculated from solubilities in the $Al_2O_3\text{-}SiO_2\text{-}Na_3AlF_6$ system. *Geochimica et Cosmochimica Acta*, **30,** 223–237.
Welch, M. D., Barras, J. B. & Klinowski, J., 1995. A multinuclear NMR study of clinochlore. *American Mineralogist*, **80,** 441–447.
Westrich, H. R. & Navrotsky, A., 1981. Some thermodynamic properties of flourapatite, fluorpargasite and fluorphlogopite. *American Journal of Science*, **281,** 1091–1103.
Williams-Jones, A. E. & Seward, T. M., 1989. The stability of calcium chloride ion pairs in aqueous solutions at temperatures between 100 and 360 °C. *Geochimica et Cosmochimica Acta*, **53,** 313–318.
Winter, J. K. & Ghose, S., 1979. Thermal expansion and high-temperature crystal chemistry of the Al_2SiO_5 polymorphs. *American Mineralogist*, **64,** 573–586.
Winter, J. K. Okamura, F. P. & Ghose, S., 1979. A high-temperature structural study of high albite, monalbite and the albite-monalbite phase transition. *American Mineralogist*, **64,** 409–423.
Wood, B. J., 1976. The reaction phlogopite + quartz = enstatite + sanidine + H_2O. Progress in Experimental Petrology, *3rd NERC report*, **6,** 17–19.
Wood, B. J., Hackler, R. T. & Dobson, D. P., 1994. Experimental determination of Mn-Mg mixing properties in garnet, olovine and oxide. *Contributions to Mineralogy and Petrology*, **115,** 438–448.
Wunder, B., Rubie, D. C., Ross II, C. R., Medenbach, O., Seifert, F. & Schreyer, W., 1993. Synthesis, stability and properties of $Al_2SiO_4(OH)_2$: a fully hydrated analogue of topaz. *American Mineralogist*, **78,** 285–297.
Xu, J., Hu, J., Ming, L., Huang, E. & Xie, H., 1994. The compression of diaspore, AlO(OH) at room temperature up to 27 GPa. *Geophysical Research Letters*, **21,** 161–164.
Zhang, L., Ahsbahs, H., Kutoglu, A. & Hafner, S., 1992. Compressibility of grunerite. *American Mineralogist*, **77,** 480–483.
Zharikov, V. A. & Shmulovich, K. I., 1969. High temperature mineral equilibria in the system $CaO\text{-}SiO_2\text{-}CO_2$. *Geochemistry International*, **6,** 853–869.
Zheng, J., Li, B., Utsumi, W. & Liebermann, R. C., 1996. In situ X-ray observations of the coesite-stishovite transition: reversed phase boundary and kinetics. *Physics and Chemistry of Minerals*, **23,** 1–10.
Zhu, H., Newton, R. C. & Kleppa, O. J., 1994. Enthalpy of formation of wollastonite ($CaSiO_3$) and anorthite ($CaAl_2Si_2O_8$) by experimental phase equilibrium measurements and high-temperature solution calorimetry. *American Mineralogist*, **79,** 134–144.

Received 31 January 1997; revision accepted 18 September 1997.

APPENDICES

Appendix 1. Summary of notation used

T	temperature
P	pressure
R	gas constant (0.0083144 kJ K^{-1})
α	thermal expansion
a°	thermal expansion parameter
V	molar volume
G	molar Gibbs free energy
H	molar enthalpy
S	molar entropy
A_T	molar property A at temperature of interest
A_{298}	molar property A at 298K
ΔA	change in molar property A for a reaction
$\Delta_f H$	molar enthalpy of formation from the elements
$\Delta_f G$	molar Gibbs energy of formation from the elements
σ_i	standard deviation of i
V_{vir}	volume contribution from a virial-like EOS
V_{MRK}	volume contribution from the Modified Redlich Kwong EOS
K	equilibrium constant
κ	bulk modulus
κ'	pressure derivative of the bulk modulus
ρ	density of H_2O
β	compressibility of H_2O
f_{H_2O}	fugacity of H_2O
C_p	heat capacity at constant pressure
C_v	heat capacity at constant volume
T_c	critical temperature in the Landau model
T_c°	critical temperature in the Landau model at 1 bar
Q	order parameter in the Landau model
S_{max}	maximum entropy of disorder in the Landau model
V_{max}	maximum volume of disorder in the Landau model
G_{excess}	excess Gibbs free energy
G_{equil}	equilibrium Gibbs free energy
h'_{298}	excess enthalpy at 298K from Landau model disordering
s'_{298}	excess entropy at 298K from Landau model disordering
v'_T	excess volume from Landau model disordering at the temperature of interest
X_j^k	mole fraction of element i on site k in a crystal
y	compositional parameter for an end-member in a solid solution
p_i	molar proportion of end-member species i in a solid solution
a_i	activity of component i in a solution
a_i^{ideal}	ideal activity of component i in a solution
γ_i	activity coefficient of component i
w_{ij}	macroscopic interaction energy in the ij binary
m_i	molality of component i in an aqueous solution

Appendix 2. Table A1

Table A1. Sources for molar volume (V), entropy (S), heat capacity (C_p), thermal expansion (a°) and incompressibility (κ) data. Numbers refer to references at the foot of the table.

End-member	V	S	C_p	a°	κ
Ortho- & ring silicates					
akermanite	41	41	41	41	0
almandine	20	2	0	12	14
andalusite	2	2,1	2	21	22
andradite	2	2,1	16	17	15
clinohumite	10	0	0	0	0
clinozoisite	35	0	0	33	34
cordierite	2	2	2	43	44,45
epidote	37	2	0	0,33	34
fayalite	2	2,1	2	6	7
Fe–chloritoid	31	0	0	0	0
Fe–cordierite	47	0	0	0	0
Fe–epidote	0	0	0	0	0
Fe–osumilite	18	18,1	18	18	18
Fe–staurolite	27	0	0	0	25
forsterite	2	2	3	4	5
gehlenite	27	40,1	2	12	0
grossular	2	1	0	12	15
hydrous cordierite	0	0	46	0,43	0,44,45
hydroxy topaz	24	0	0	0	0
kyanite	2	2,1	2	21	23
larnite	2	2	2	0	0
lawsonite	2	2	2,1	33	38
merwinite	32	2	2	12	0
Mg–chloritoid	28	0	0	29	30
Mg–staurolite	26	0	0	0	25
Mn–chloritoid	0	0	0	0	0
Mn–cordierite	0	0	0	0	0
Mn–staurolite	0	0	0	0	0
monticellite	2	2	2	8	9
osumilite(1)	18	18	18	18	18
osumilite(2)	18	18	18	18	18
phaseA	48	0	0	48	48
pumpellyite	39	0	0	0	0
pyrope	2	2	11	12	13
rankinite	2	2,1	0	0	0
sillimanite	2	2,1	2	21	23
spessartine	49	0	0	12	15
sphene	2	2	2,1	0	0
spurrite	2	2,1	0	0	0
tephroite	2	2	2	0	0
tilleyite	42	0	0	0	0
vesuvianite	19	0	0	0	0
zircon	2	2	2	12	25
zoisite	36,1	2,1	2,1	33	34
Pyroxenes & pyroxenoids					
acmite	27	2	2	0	50
Ca–tschermak pyroxene	51	51,1	51	51	0
diopside	55	2	2	56	57
enstatite	2	2	2,1	12	52
ferrosilite	53	2,1	2,1	53	50
hedenbergite	58	58	58,1	0,56	50
jadeite	2	2	2	12	25
Mg–tschermak pyroxene	54	0	0	0,12	0,52
pseudowollastonite	2	2,1	0,59	12	0
pyroxmangite	2	2,1	2	0	0
rhodonite	2	2	2	0	0
wollastonite	27	2,1	59	0,12	60
Amphiboles					
anthophyllite	2	2,1	2,1	0	0
cummingtonite	70	0	0	0	0
Fe–anthophyllite	0	0	0	0	0
Fe–glaucophane	68	0	0	0	0,64
ferroactinolite	65	0	0	0	0
gedrite	0	0	0	0	0
glaucophane	68	68	68	0	64
grunerite	70	0,1	0	0	71
pargasite	67	0	0	0	64
riebeckite	69	0	0	0	0,64
tremolite	61	2,1	62,1	63	64
tschermakite	66	0	0	0,63	0,64
Other chain silicates					
deerite	75	0	0	0	75
Fe–carpholite	74	0	0	0	0
Fe–sapphirine	0	0	0	0	0
Mg–carpholite	28	0	0	0	0
sapphirine(221)	72,73	0	0	0	0
sapphirine(793)	72,73	0	0	0	0
Micas					
annite	27	2,1	0	0,80	0,81
celadonite	0	0	0	76	77
eastonite	82	0	0	0	0
Fe–celadonite	0	0	0	0,76	0,77
margarite	2	2,1	2,1	79	0
Mn–biotite	0	0	0	0	0
muscovite	2	2,1	2,1	76	77
Na–phlogopite	83	0	0	0	0
paragonite	2	2,1	2,78	0,76	77
phlogopite	2	2,1	2,1	80	81
Chlorites					
Al-free chlorite	85	0	0	0,85	0,81
amesite	85	0	0	0,85	0,81

clinochlore	85	0	0	85	81
daphnite	47	0	0	0	0
Fe–sudoite	0	0	0	0	0
Mn–chlorite	0	0	0	0	0
sudoite	86	0	0	0	0
Other sheet silicates					
antigorite	89	0	90	0	0
chrysotile	2	2	2,1	0	0
Fe–talc	0	0	0	0,87	0,87
kaolinite	2	2,1	2,1	0	0
prehnite	88	88	88,1	0	0
pyrophyllite	2	2	2,1	79	0
talc	2	2,1	2,1	87	87
tschermak talc	0	0	0	0,87	0,87
Framework silicates					
albite	2	2,1	2	104	91
analcite	2	2,1	2,1	0	25
anorthite	2,1	2,1	93	94	91
coesite	2	2,1	2	12	96
cristobalite (high)	2,1	2,1	0,2	1	1
heulandite	124	0	0	0	0
high albite	2,1	2,1	2	104	91
kalsilite	99	2	99	100	0
laumontite	125	0	0	0	0
leucite	2	2	2,1	101	0
meionite	102	102,1	0	127	103
microcline	92	2,1	2	12	91
nepheline	2	2	2,1	12	25
quartz	2	2	2,1	95	95
sanidine	2,1	2,1	2	12	91
stilbite	126	0	0	0	0
stishovite	2	2,1	2	97	98
tridymite (high)	92,1	92,1	0	1	1
wairakite	2	0	0	0	0
Oxides					
baddeleyite	2	2	2	12	0
corundum	2	2	106	12	107
geikielite	2	2	2,1	0	0
hematite	92	2	2,1	108	109
hercynite	2	92,1	0	12	0
ilmenite	2	2	2,1	110	110
lime	92	2	2	12	25
magnesioferrite	2	2,1	2	0	0
magnetite	2	2	2,1	12	111
manganosite	2	2	2	0	0
nickel oxide	2	2	2,1	0	0
periclase	2	2	2	4	25
pyrophanite	109	2	2	0	0
rutile	2	2	2	12	105
spinel	92	2,1	0	12	111
ulvospinel	2	92,1	2	0	0
Hydroxides					
brucite	2	2,1	2,1	123,1	112
diaspore	2	2	2,1	33	114
goethite	2	2	0	0,33	0,114
Carbonates					
ankerite	121	0	0	119	120
aragonite	92	2,1	0,1	117	117
calcite	92	2,1	2,1	115	116
dolomite	2	2,1	2	119	120
magnesite	92	2	2,1	115	118
rhodochrosite	2	2	2	0	25
siderite	2	2,1	2	0	25
Elements					
diamond	2	2,1	2	12	25
graphite	2	2,1	2	12	25
iron	2	122	2	12	25
nickel	2	2	2	12	25
Gas species					
methane	–	2	2	–	–
carbon monoxide	–	2	2	–	–
carbon dioxide	–	92	2	–	–
ydrogen	–	2	2	–	–
water	–	2	2	–	–
oxygen	–	2	2	–	–

0 Estimated; 1 Adjusted in this study; 2 Robie & Hemingway (1995); 3 Robie *et al.* (1982); 4 Hazen (1976); 5 Downs *et al.* (1996); 6 Smyth (1975); 7 Isaak *et al.* (1993); 8 Lager & Meagher (1978); 9 Sharp *et al.* (1986); 10 Duffy & Greenwood (1979); 11 Tequi *et al.* (1991); 12 Skinner (1966); 13 Hazen *et al.* (1994); 14 Sato *et al.* (1978); 15 Bass (1986, 1989); 16 Robie *et al.* (1987); 17 Hazen & Finger (1989); 18 Holland *et al.* (1996a); 19 Hochella *et al.* (1982); 20 Chatillon-Colinet *et al.* (1983); 21 Winter & Ghose (1979); 22 Ralph *et al.* (1984); 23 Brace *et al.* (1969); 24 Wunder *et al.* (1993); 25 Birch (1966); 26 Schreyer & Seifert (1969); 27 Robie *et al.* (1967); 28 Chopin & Schreyer (1983); 29 Ivaldi *et al.* (1988); 30 Comodi *et al.* (1991b); 31 Rao & Johannes (1979); 32 Moore & Araki (1972); 33 Pawley *et al.* (1996); 34 Comodi & Zanazzi (1997); 35 Jenkins *et al.* (1983); 36 Chatterjee (1976); 37 Helgeson *et al.* (1978); 38 Comodi & Zanazzi (1996); 39 Schiffman & Liou (1980); 40 Hemingway & Robie (1984); 41 Hemingway *et al.* (1986); 42 Harker (1959); 43 Mirwald *et al.* (1984); 44 Mirwald (1981); 45 Schlenker *et al.* (1977); 46 Carey (1993); 47 Holdaway & Lee (1977); 48 Pawley & Wood (1995); 49 Hsu (1968); 50 Kandelin & Weidner (1988); 51 Haselton *et al.* (1984); 52 Olinger (1977); 53 Sueno *et al.* (1976); 54 Gasparik & Newton (1984); 55 Krupka *et al.* (1985a); 56 Finger & Ohashi (1976); 57 McCormick *et al.* (1989); 58 Haselton *et al.* (1987); 59 Richet *et al.* (1991); 60 Vaidya *et al.* (1973); 61 Hewitt (1975); 62 Krupka *et al.* (1985b); 63 Sueno *et al.* (1973); 64 Comodi *et al.* (1991a); 65 Ernst (1966); 66 Jenkins (1994); 67 Lykins & Jenkins (1993); 68 Holland (1988); 69 Ernst (1962); 70 Evans & Ghiorso (1995); 71 Zhang *et al.* (1992); 72 Seifert (1974); 73 Chatterjee & Schreyer (1972); 74 Viswanathan & Seidel (1979); 75 Lattard & LeBreton (1994); 76 Guggenheim *et al.* (1987); 77 Comodi & Zanazzi (1994); 78 Holland (1979); 79 Symmes (1986) quoted in Berman (1988); 80 Takeda & Morosin (1975); 81 Hazen & Finger (1978); 82 Hewitt & Wones (1975); 83 Carman (1974); 84 Baker & Holland (1996); 85 Nelson & Guggenheim (1993); 86 Vidal *et al.* (1992); 87 Pawley *et al.* (1995); 88 Perkins *et al.* (1980); 89 Mellini *et al.* (1987); 90 King *et al.* (1967); 91 Angel *et al.* (1988); 92 Robie *et al.* (1978); 93 Richet & Fiquet (1991); 94 Grundy & Brown (1974); 95 Dorogokupets (1995); 96 Levien & Prewitt (1981); 97 Ito *et al.* (1974); 98 Striefler & Barsch (1976); 99 Lange *et al.* (1986); 100 Henderson & Taylor (1988); 101 Palmer *et al.* (1989); 102 Baker & Newton (1994); 103 Hazen & Sharp (1988); 104 Winter *et al.* (1979); 105 Hazen & Finger (1981); 106 Richet *et al.* (1992); 107 Finger & Hazen (1978); 108 Finger & Hazen (1980); 109 Powneby *et al.* (1987); 110 Wechsler & Prewitt (1984); 111 Finger *et al.* (1986); 112 Catti *et al.* (1995); 113 Pawley (1994); 114 Xu *et al.* (1994); 115 Markgraf & Reeder (1985); 116 Martens *et al.* (1982); 117 Martinez *et al.* (1996); 118 Redfern *et al.* (1993); 119 Reeder & Markgraf (1986); 120 Ross & Reeder (1992); 121 Davidson *et al.* (1993); 122 Khodakovsky *et al.* (1990); 123 Karpinskaya & Ostrovsky (1982); 124 Cho *et al.* (1987); 125 Liou (1971a); 126 Liou (1971b); 127 Baker (1995).

Appendix 3. Additional notes

- The bulk modulus of margarite (ma) has been raised to agree better with the experiments of Jenkins (1984) and Chatterjee *et al.* (1984).
- The Landau C_p data for iron (iron), hematite (hem) and magnetite (mt) have been refitted since HP90.
- Heat capacity of almandine (alm) has been adjusted to fit the heat content measurements of Newton & Harlov (1993).
- Landau formalism is used for C_p of calcite (cc) and aragonite (arag) following Redfern *et al.* (1989); also for dolomite (dol), and ankerite (ank) to allow for disordering.
- Spinel (sp) C_p has been estimated from the sum of periclase + corundum with a Landau excess added, following Carpenter & Salje (1994a). This has enabled agreement with the experiments of Chamberlin *et al.* (1995) for free energy of formation of spinel from the oxides.
- Hercynite (herc) C_p has been estimated from the sum of FeO + corundum (Robie & Hemingway, 1995), with a Landau excess added from Harrison (1997).
- The erroneously high entropy of magnesium staurolite (mst) in HP90 has been corrected down to the estimate (910 J K^{-1}) from Holland (1989).
- A typographic error in the heat capacity of rankinite (rnk) in HP90 has been corrected ($a = 0.3723$ not 0.6723). Derived enthalpies for rnk, spurrite (spu) and tilleyite (ty) are therefore very different (Table 3).
- A Landau excess has been added to anorthite (an) with $T_c =$ 2300K (Carpenter, 1992), $S_{max} = 11$ J K^{-1} to fit the high T heat contents.
- A Landau excess has been added to sillimanite (sill) with $T_c =$ 2200K, $S_{max} = 4$ J K^{-1} to fit high T experiments of Richardson *et al.* (1968).
- A Landau excess has been added to cordierite (crd) with $T_c =$ 1800K, $S_{max} = 25$ J K^{-1}. So long as the data are not used above this temperature this will simulate the disorder below the first order transition. All cordierite end-members are assumed to disorder similarly.
- A Landau excess has been added to gehlenite (geh) with $T_c =$ 700K, $S_{max} = 11$ J K^{-1}.
- A Landau excess has been added to ilmenite (ilm) with $T_c =$ 1900K, $S_{max} = 11$ J K^{-1} to allow for Fe–Ti disordering and to fit the high T heat contents.